

**CHARACTERISATION AND HANDLING OF  
UNCERTAINTIES IN EMC/EMI MEASUREMENTS**

**SONG JIAN**

**NATIONAL UNIVERSITY OF SINGAPORE**

**2016**

**CHARACTERISATION AND HANDLING OF  
UNCERTAINTIES IN EMC/EMI MEASUREMENTS**

**SONG JIAN**

*(B. Tech., Hons., National University of Singapore, Singapore)*

**A THESIS SUBMITTED  
FOR THE DEGREE OF DOCTOR OF PHILOSOPHY**

**DEPARTMENT OF ELECTRICAL  
AND COMPUTER ENGINEERING  
NATIONAL UNIVERSITY OF SINGAPORE**

**2016**

## **DECLARATION**

I hereby declare that this thesis is my original work and it has been written by me in its entirety. I have duly acknowledged all the sources of information which have been used in the thesis.

This thesis has also not been submitted for any degree in any university previously.

---

Song Jian

05/08/2016

## ACKNOWLEDGEMENTS

I would like to express my appreciation to my supervisor Prof. Guo Yongxin who had given me constant support and encouragement in my last two years' research work. He provided valuable comments in my research directions and guided me with his patience, expertise and experiences. Also, I want to thank my late professor, Dr. Hui Hontat, who supervised me in my first two years of research and study. I'm thankful for all the effort he contributed to establish the Industrial Ph.D. Program (IPP) with Economic and Development Board (EDB) and Rohde & Schwarz Asia (R&S). His guidance and help will be memorized forever.

It is always difficult to achieve a balance between research study and work related assignments in IPP. Fortunately in my four years with R&S, my fellow colleagues have offered numerical help towards my research and work assignments. I would like to thank the board of R&S for giving me the opportunity to pursue a Ph.D. in the organization. Thanks to my industrial supervisor, Mr. Kuah Anntat and Mr. Thomas Wong for their kind and prompt arrangements for all my academic needs. I'm grateful to my team members, Mr. Sim Zhiwei, Dr. Wang Hang and Ms. Bek Shiauchin for their helpful suggestions and recommendations in my data collection, simulation and measurement works. I would also like to thank Mr. Albert Lee and Mr. Li Shuwen for the selfless sharing of their experiences dealing with measurement uncertainties as project engineers. Their decades' of experiences in dealing with EMC systems, measurement uncertainty definition and treatments are always valuable for researchers to understand the real problem which the industry is facing. I have also received great help from both Application and System Engineering group for the training of using various instrumentations, e.g. signal generators, test receivers, VNA, etc.

I want to thank Ms. Lynn Chong and Ms. Bernadette Gian from HR department of R&S, Mdm. Lee Siewchoo from Microwave & RF lab of NUS for helping me with all

the administration works. I would also like to express my gratefulness to my classmates for the helpful discussions in the research study.

Last but not least, I'm grateful to have the utmost support from my family in pursuing the degree. Without their understanding, trust and encouragement, I would not have come this far.

“The world owes all its onward impulses to men ill at ease. The happy man inevitably confines himself within ancient limits.” - Nathaniel Hawthorne

## **DECLARATION**

## **ACKNOWLEDGEMENTS**

## **TABLE OF CONTENTS**

## **SUMMARY**

## **LIST OF TABLES**

## **LIST OF FIGURES**

## **NOMENCLATURE**

## **ACRONYMS**

<b>1</b>	<b>CHAPTER 1 INTRODUCTION .....</b>	<b>1</b>
1.1	Background .....	1
1.2	Measurement Uncertainty in the Standards.....	6
1.3	Motivation of the Research .....	8
1.4	Original Contributions of This Thesis.....	9
1.5	Outline of the Thesis .....	12
<b>2</b>	<b>CHAPTER 2 REVERBERATION CHAMBERS FOR EMC APPLICATIONS.....</b>	<b>13</b>
2.1	Background .....	13
2.2	Cavity Mode Theory .....	15
2.3	Q Factor.....	18
2.4	EMC Measurement in RCs.....	20
2.4.1	EMC Standards Using Reverberation Chambers.....	20
2.4.2	Working Volume .....	22
2.4.3	Lowest Usable Frequency.....	22
2.4.4	Field Uniformity .....	22
2.4.5	Chamber Loading Effects .....	24
2.5	Chamber Validation .....	25
2.5.1	Unloaded Calibration.....	25
2.5.2	Loaded Calibration .....	27
2.5.3	Q Factor and Time Constant.....	31
2.6	Conclusion.....	34

<b>3</b>	<b>CHAPTER 3 INVESTIGATION OF FIELD UNIFORMITY AND UNCERTAINTIES IN A REVERBERATION CHAMBER AT LOWEST USABLE FREQUENCY .....</b>	<b>35</b>
3.1	Intrinsic Field Uncertainty.....	35
3.2	Investigation of Field Uniformity at Lowest Usable Frequency .....	36
3.2.1	Geometry and Test Set-up .....	38
3.2.2	Results and Discussions.....	40
3.2.2.1	Simulation Results.....	40
3.2.2.2	Measurement Results and Discussion .....	52
3.3	Conclusion.....	55
<b>4</b>	<b>CHAPTER 4 CHARACTERISATION OF MEASUREMENT UNCERTAINTY IN A RADIATED EMISSION SYSTEM .....</b>	<b>56</b>
4.1	Background .....	56
4.2	RF Adapter .....	58
4.3	Pre-Amplifier Gain Variation.....	61
4.4	Impedance Mismatch .....	66
4.5	Measurement Uncertainty Calculation Software.....	70
4.5.1	AMN Impedance Uncertainty Calculation .....	71
4.5.2	Mismatch Uncertainty Calculation .....	78
4.6	Conclusion.....	79
<b>5</b>	<b>CHAPTER 5 MEASUREMENT UNCERTAINTY AND ACCURACY USING TIME DOMAIN SCAN METHOD IN RADIATED SPURIOUS EMISSION MEASUREMENT .....</b>	<b>81</b>
5.1	Background .....	81
5.2	FFT-Based TD Scan.....	82
5.3	Test Set Up and Methodology.....	83
5.4	Results and Discussions .....	86
5.4.1	GSM 900 Test Result .....	86
5.4.2	GSM 1800 Test Result .....	91
5.4.3	Result Verification using Stable Noise Source.....	93
5.4.4	Uncertainty through Repeatability Study .....	95
5.5	Conclusion.....	97
<b>6</b>	<b>CHAPTER 6 CONCLUSION AND FUTURE WORK .....</b>	<b>99</b>
6.1	Conclusion.....	99
6.2	Future Work .....	101

<b>REFERENCES.....</b>	<b>103</b>
<b>APPENDIX: Calibration Reports of Instrumentation Used in the Thesis .....</b>	<b>109</b>
<b>LIST OF PUBLICATIONS .....</b>	<b>117</b>



## SUMMARY

Measurement uncertainty (MU) is one of the most important topics in Electromagnetic Compatibility (EMC) field. MU calculation has been discussed specifically in many technical articles. However, due to the complexity of MU characterisation, the way of obtaining a correct and meaningful MU quantity together with its handling may cause confusion in the industry.

The characterisation of MU aims to provide an appropriate tolerance/budget to the test laboratories, which is considered as a supplement to the measurement results of the equipment under test (EUT). The purpose is to make sure the test results of the same EUT, which are obtained in different laboratories are correlated. Thus, the EUT which passes the test at one laboratory will not fail at another. It is often time-consuming to identify MU budget as comprehensive measurements are required to obtain the individual instrumentation's uncertainty. Regulatory authorities have taken the effort to set the MU budgets for commercial product testing standards. Both Electromagnetic Interference (EMI) and Electromagnetic Susceptibility (EMS) tests have their respective guidelines to determine the MU budgets for different frequency ranges. However, not all the testing laboratories have the technical know-hows in interpreting the standards. Furthermore, some important areas where measurement errors and MU may seriously affect the measurement results are not clearly defined in the standards.

It is the purpose of this thesis to propose new approaches to further clarify the areas where not all detailed procedures on characterising MU contributions are available; and to provide additional knowledge to the existing measurement standards used in the industry. The main contributions of this thesis include (1) the proposed use of non-equidistant stirrer positions to improve field uniformity and measurement uncertainty in the lowest usable frequency region when performing tests in a reverberation chamber, (2) new findings in EMI test systems where errors and MU are not explained in detail

in the standards, and (3) the proposed use of FFT-based time domain scan method for radiated spurious emission test and the finding of its accuracy and consistency.

The results presented in this dissertation provide additional knowledge to the existing measurement standards used in the industry. They also have important implications for practical measurements in seeking to fulfill industrial measurement standards.

## LIST OF TABLES

Table 1.1 Measurement uncertainty status update for CISPR standards .....	8
Table 2.1 Field uniformity tolerance requirements [36] .....	22
Table 2.2 Sampling requirements [36].....	24
Table 3.1 Non-equidistant tuner positions selected in the investigation.....	40
Table 3.2 Comparison of number of independent samples for equidistant and non-equidistant methods .....	52
Table 4.1 The measured insertion loss, standard deviation and standard uncertainty of an N-type to N-type RF adapter.....	60
Table 4.2 The maximum gain variations at different temperatures with reference to the values at room temperature .....	64
Table 4.3 Maximum gain variation of pre-amplifiers of different frequency ranges with reference to room temperature .....	65
Table 4.4 An example of the evaluation of AMN impedance magnitude and phase with consideration of uncertainty at 30 MHz.....	76
Table 4.5 Summary of MU contributions, their impact and treatments discussed in this section .....	80
Table 5.1 R&S® FSV40 parameter specifications in sweep mode .....	85
Table 5.2 R&S® ESR26 parameter specifications in TD mode .....	85
Table 5.3 Measurement data for GSM 900 RSE TX Mode .....	87
Table 5.4 Measurement data for GSM 1800 RSE TX Mode .....	92
Table 5.5 Average peak value for ten repeated measurements for GSM 900 test .....	96
Table 5.6 Standard deviation of peak value for ten repeated measurements for GSM 900 test.....	96
Table 5.7 Average peak value for ten repeated measurements for GSM 1800 test ....	97
Table 5.8 Standard deviation of peak value for ten repeated measurements for GSM 1800 test.....	97

## LIST OF FIGURES

Fig. 1.1 The main EMC tests .....	2
Fig. 1.2 System and random errors .....	3
Fig. 1.3 Graphical illustration of probability for (a) normal distribution (b) triangular distribution (c) rectangular distribution (d) U-shape distribution .....	5
Fig. 1.4 The hierarchy illustration of different CISPR standards .....	7
Fig. 2.1 Reverberation chamber illustration.....	14
Fig. 2.2 Mode density against frequency for RC used in R&S.....	17
Fig. 2.3 Typical reverberation chamber facility [36] .....	21
Fig. 2.4 Mean-normalised data for $x$ -component of eight probes [36] .....	23
Fig. 2.5 R&S reverberation chamber .....	25
Fig. 2.6 Standard deviation for E-field components of eight probe positions for $x$ , $y$ , $z$ and total data set with (a) 5% frequency step 400 MHz -1000 MHz (b) 5% frequency step 1 GHz - 8 GHz (c) 9% frequency step from 8 GHz - 18 GHz for unloaded condition .....	26
Fig. 2.7 Chamber with maximum loading material .....	27
Fig. 2.8 Standard deviation for E-field components of eight probe positions for $x$ , $y$ , $z$ axes and the total data set with: (a) 5% frequency step 400 MHz - 1000 MHz; (b) 5% frequency step 1 GHz - 8 GHz; and (c) 9% frequency step 8 GHz - 18 GHz, for loaded condition.....	28
Fig. 2.9 Maximum chamber loading of: (a) 400 MHz - 1 GHz; (b) 1 GHz - 8 GHz; and (c) 8 GHz - 18 GHz .....	30
Fig. 2.10 Measured chamber $Q$ factor of: (a) 400 MHz - 1 GHz; (b) 1 GHz - 8 GHz; and (c) 8 GHz - 18 GHz .....	32
Fig. 2.11 Measured chamber time constant of: (a) 400 MHz - 1 GHz; (b) 1 GHz - 8 GHz; and (c) 8 GHz - 18 GHz. ....	34
Fig. 3.1 RC simulation model in CST 2015.....	39

Fig. 3.2 Simulation results of the electric field distribution using: (a) equidistant tuner positions; (b) non-equidistant Set 1 positions; and (c) non-equidistant Set 2 positions, at 400 MHz with transmitting antenna parallel to $x$ - $y$ plane. ....	41
Fig. 3.3 Simulation results of the electric field distribution using: (a) equidistant tuner positions; (b) non-equidistant Set 1 positions; and (c) non-equidistant Set 2 positions, at 400 MHz with transmitting antenna rotated 45 degrees clockwise. ....	43
Fig. 3.4 Equidistant and non-equidistant positions (Set 1) comparison of standard deviations for E-field components of eight probes for: (a) $x$ -axis; (b) $y$ -axis; (c) $z$ -axis; and (d) total data set, with transmitting antenna parallel to $x$ - $y$ plane. ....	45
Fig. 3.5 Equidistant and non-equidistant positions (Set 2) comparison of standard deviations for E-field components of eight probes for: (a) $x$ -axis; (b) $y$ -axis; (c) $z$ -axis; and (d) total data set, with transmitting antenna parallel to the $x$ - $y$ plane. ....	47
Fig. 3.6 Equidistant and non-equidistant positions (Set 1) comparison of standard deviations for E-field components of eight probes for: (a) $x$ -axis; (b) $y$ -axis; (c) $z$ -axis; and (d) total data set, with transmitting antenna rotated 45 degrees clockwise. ....	49
Fig. 3.7 Equidistant and non-equidistant positions (Set 2) comparison of standard deviations for E-field components of eight probes for: (a) $x$ -axis; (b) $y$ -axis; (c) $z$ -axis; and (d) total data set, with transmitting antenna rotated 45 degrees clockwise. ....	50
Fig. 3.8 Measurement results of standard deviation for E-field components of eight probes for: (a) $x$ -axis; (b) $y$ -axis; (c) $z$ -axis; and (d) total data set, with transmitting antenna rotated 45 degrees clockwise. ....	55
Fig. 4.1 Measurement uncertainty contributions in a typical radiated emission system .....	56
Fig. 4.2 The measurement set up: (a) overview; and (b) inside the temperature chamber, for the characterisation of the measurement uncertainty associated with the pre-amplifier gain under different environmental temperatures. ....	62
Fig. 4.3 The measured pre-amplifier gains at different temperatures from 0 to 40 °C	63
Fig. 4.4 Block diagram of a typical radiated emission test system with external pre-amplifier.....	66
Fig. 4.5 The measured input VSWR of the pre-amplifier at different temperatures from 0 °C to 40 °C.....	67
Fig. 4.6 The measured output VSWR of the pre-amplifier at different temperatures from 0 °C to 40 °C.....	68
Fig. 4.7 Illustration of main user interface of MUCS .....	71

Fig. 4.8 Circuit illustration of EUT and ideal AMN connection .....	72
Fig. 4.9 AMN impedance uncertainty calculator main GUI (Microsoft Excel-based).....	73
Fig. 4.10 Actual impedance magnitude and phase deviation calculation .....	75
Fig. 4.11 Complete AMN impedance uncertainty presentation with actual impedance deviation and calibration uncertainty .....	76
Fig. 4.12 Prototype GUI of AMN impedance calculator plug-in .....	77
Fig. 4.13 Prototype GUI of automated impedance mismatch calculator .....	78
Fig. 5.1 Block diagram of using FFT-based TD scan for a test receiver [95].....	82
Fig. 5.2 Concept of FFT-based TD scan [79] .....	83
Fig. 5.3 Actual investigation set-up in a semi-anechoic chamber.....	84
Fig. 5.4 RSE preview measurement for GSM 900 TX Mode (30 MHz to 3 GHz) ....	86
Fig. 5.5 RSE preview measurement for GSM 900 TX Mode (3 GHz to 6 GHz) .....	87
Fig. 5.6 RSE preview measurement for GSM 900 TX Mode (zoom at first harmonics of uplink frequency: 1804.8 MHz) .....	88
Fig. 5.7 RSE preview measurement for GSM 900 TX Mode (zoom at second harmonics of uplink frequency: 2707.2 MHz).....	89
Fig. 5.8 RSE preview measurement for GSM 900 TX Mode (zoom at third harmonics of uplink frequency: 3609.6 MHz) .....	89
Fig. 5.9 RSE preview measurement for GSM 900 TX Mode (zoom at fourth harmonics of uplink frequency: 4512.0 MHz).....	90
Fig. 5.10 RSE preview measurement for GSM 900 TX Mode (zoom at fifth harmonics of uplink frequency: 5414.4 MHz).....	90
Fig. 5.11 RSE preview measurement for GSM 1800 TX Mode (30 MHz to 3 GHz) .....	91
Fig. 5.12 RSE preview measurement for GSM 1800 TX Mode (3 GHz to 12.75 GHz) .....	92
Fig. 5.13 RSE measurement using stable noise source based on IFBW of 1 MHz – zoom in measurement at 4850 MHz .....	93
Fig. 5.14 RSE measurement using stable noise source based on IFBW of 1 MHz – zoom in measurement at 5700 MHz .....	94

## NOMENCLATURE

$E$	Electric field
$\delta G_p$	Maximum gain variation
$k$	Wave number
$Q$	Quality factor
$\eta_0$	Intrinsic impedance of free space
$\sigma$	Standard deviation

## ACRONYMS

ADC	Analog to Digital Converter
CLF	Chamber Loading Factor
EMC	Electromagnetic Compatibility
EMI	Electromagnetic Interference
EMS	Electromagnetic Susceptibility
EUT	Equipment under Test
FFT	Fast Fourier Transform
IFBW	Intermediate Frequency Bandwidth
IFU	Intrinsic Field Uncertainty
GUI	Graphical User Interface
LUF	Lowest Usable Frequency
MIU	Measurement Instrumentation Uncertainty
MU	Measurement Uncertainty
PRF	Pulse Repetition Frequency
RBW	Resolution Bandwidth
RC	Reverberation Chamber
RSE	Radiated Spurious Emission
RX	Receive

TD	Time Domain
TE	Transverse Electric
TM	Transverse Magnetic
TX	Transmit



## CHAPTER 1 INTRODUCTION

### 1.1 Background

Electromagnetic Compatibility (EMC) is considered as an important test for modern electrical and electronics products [1, 2]. The test is to make sure the equipment under test (EUT) shall be satisfactorily functional in the electromagnetic environment where it is exposed, without introducing substantial amount of electromagnetic emissions which may affect other products. In general, two main issues are considered in EMC tests which are emission (Electromagnetic Interference / EMI) and susceptibility (Electromagnetic Susceptibility / EMS) of the particular product. Emission is the generation of disturbance signal by the electrical and electronic product to the environment, whether intentionally or unintentionally. Susceptibility is the tendency of the equipment to be malfunctioned in the presence of any unwanted interferences. EMC tests focus on these two issues and verify whether the electrical and electronic product is compatible, with reference to the respective product standards [3].

Both EMI and EMS activities are categorised into two tests: conducted test and radiated test. For these two cases, the tests focus on conducting paths and radiating paths respectively. Thus, as shown in Fig. 1.1, each EMC test can be categorised into below aspects:

- conducted emission test
- conducted susceptibility test
- radiated emission test
- radiated susceptibility test

Since conducted part is referred as cable paths, the testing frequency range is often targeted from 9 kHz to 30 MHz, whereas for radiated part, the testing frequency is normally from 30 MHz to 18 GHz. However, it is worth noting that, different product

standards may have different frequency range requirements. For instance, military and automotive applications have wider frequency test ranges as compared to residential and industrial test standards. This thesis focuses on the residential and industrial product standards. Thus the aforementioned frequency ranges apply.

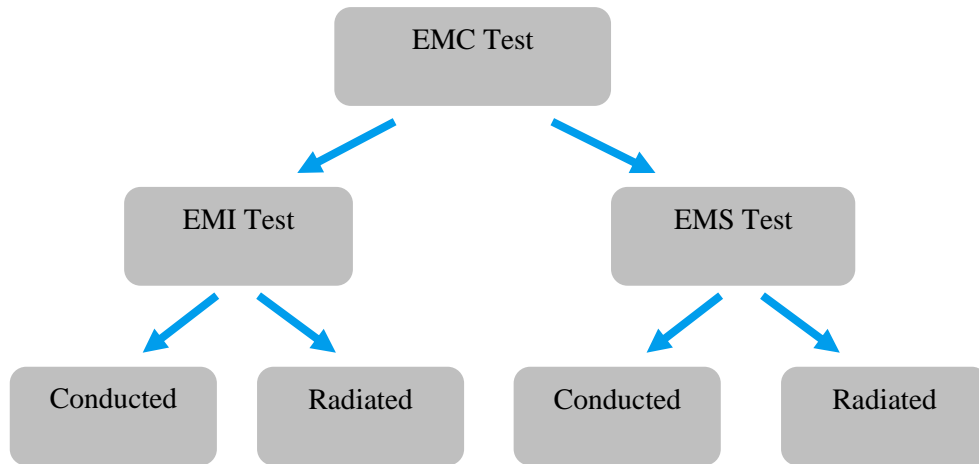


Fig. 1.1 The main EMC tests

Each EMC measurement is associated with numerous uncertainties in different parts of the system. The results obtained are never exactly correct. For most of the time, the measurement result is only an estimated value of the real quantity which is subjected to the uncertainty of the measurement equipment. Thus, the measured value is only meaningful when it is associated with an appropriate quantitative margin of uncertainty. In ISO Guide to the Expression of Uncertainty in Measurement (GUM) [4], measurement uncertainty (MU) is defined as a parameter, associated with the result of a measurement that characterises the dispersion of the values that could reasonably be attributed to the measurement.

Measurement uncertainties may be divided into two classes: random errors and systematic errors, which depend on the precision and accuracy of the measurement apparatus. A random error is caused by unpredictable variation or fluctuation of the readings from repeated measurements, and it can be statistically analysed. A systematic

error is often referred as a fixed value for a discrepancy and shall be compensated when conducting a measurement. Fig. 1.2 shows the graphical illustration of the systematic and random errors. All measurement systems are prone to systematic errors. They could arise from imperfect calibration of measurement apparatus, improper observation methods, etc. For instance, the clock signal used in different measurement apparatus may vary from one another, causing a slight discrepancy in measurement frequency. Practically, all systematic errors shall be corrected. Thus the uncertainty related to a systematic error shall only be considered as the uncertainty of the correction itself. This correction uncertainty and its contribution to the uncertainty budget may be either Type A or Type B depending on the evaluation methods used [2].

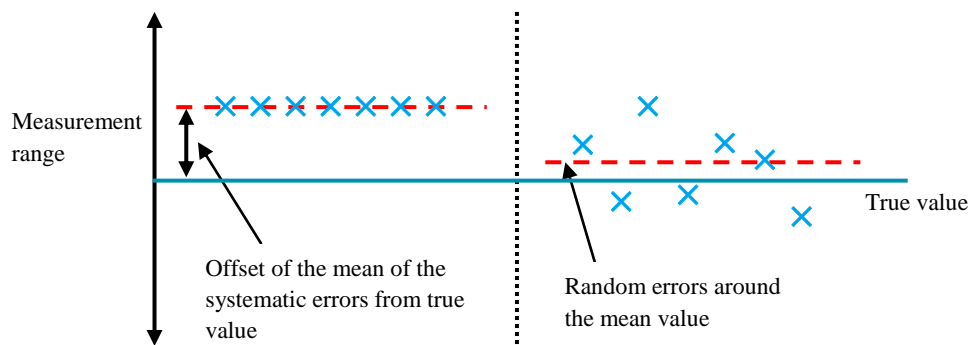


Fig. 1.2 System and random errors

Type A and Type B uncertainty evaluations provide similar information. The uncertainty contributions are categorised differently to indicate the procedures with which the data are obtained. Type A uncertainties are often introduced by unpredictable variation in the readings from the measurement apparatus, or in the interpretation of such readings by the experimenters. The evaluation method is based on statistical analysis of a series of independent observations. In another word, they should be evaluated statistically over repeated physical measurements. Type B uncertainties are those evaluated by other methods, such as information quoted with manufacturer's specifications, calibration reports, data from previous measurements or scientific judgment, etc. The quoted information is normally stated to be a particular multiple of

a standard uncertainty. The standard uncertainties are simply the quoted values divided by the multiplier [4]. However, the quoted information may not always be given as a multiple of standard uncertainties, but associated with an interval of confidence level such as 95%. Unless otherwise specified, a normal distribution is always assumed and used to convert the quoted uncertainty to its standard uncertainty. The dividing factor in such a case will be corresponding to 1.96 for a 95% confidence interval. As shown in Fig. 1.3, there are four types of typical distributions used in deriving Type B uncertainty:

- normal distribution
- triangular distribution
- rectangular distribution
- U-shaped distribution

Other than normal distribution, the triangular distribution states that the probability of the true value lying in the region between two limits which increase linearly to the maximum towards the center. The best estimation of the value of true quantity will be quoted information divided by square root of six [4]. For rectangular distribution, the true value lying between the lower and upper limits is equally probable. U-shape is applicable when the measured value is unlikely to be the real value. These probability distributions describe the variations in probability where the measured value is likely to be the real value. Often, the assumption has to be made based on the prior knowledge and experiences, to determine which probability is more appropriate to be applied.

To further process the uncertainty contributions, all individual uncertainty contributions are characterised into their respective standard uncertainties, which are statistically equivalent to standard deviations. After the standard uncertainty contributions are obtained, these components shall be combined, by applying root-sum-

square of both Type A and Type B uncertainties. Equation (1) can be used to describe the combined standard uncertainty [4]:

$$u(y) = \sqrt{\sum_{i=1}^n \left( \frac{\partial y}{\partial x_i} \right)^2 u^2(x_i)} \quad (1)$$

where  $u^2(x_i)$  is the square of standard uncertainty of the input quantity  $x_i$  and the partial derivatives are the weighting factors and often referred as sensitivity coefficients.

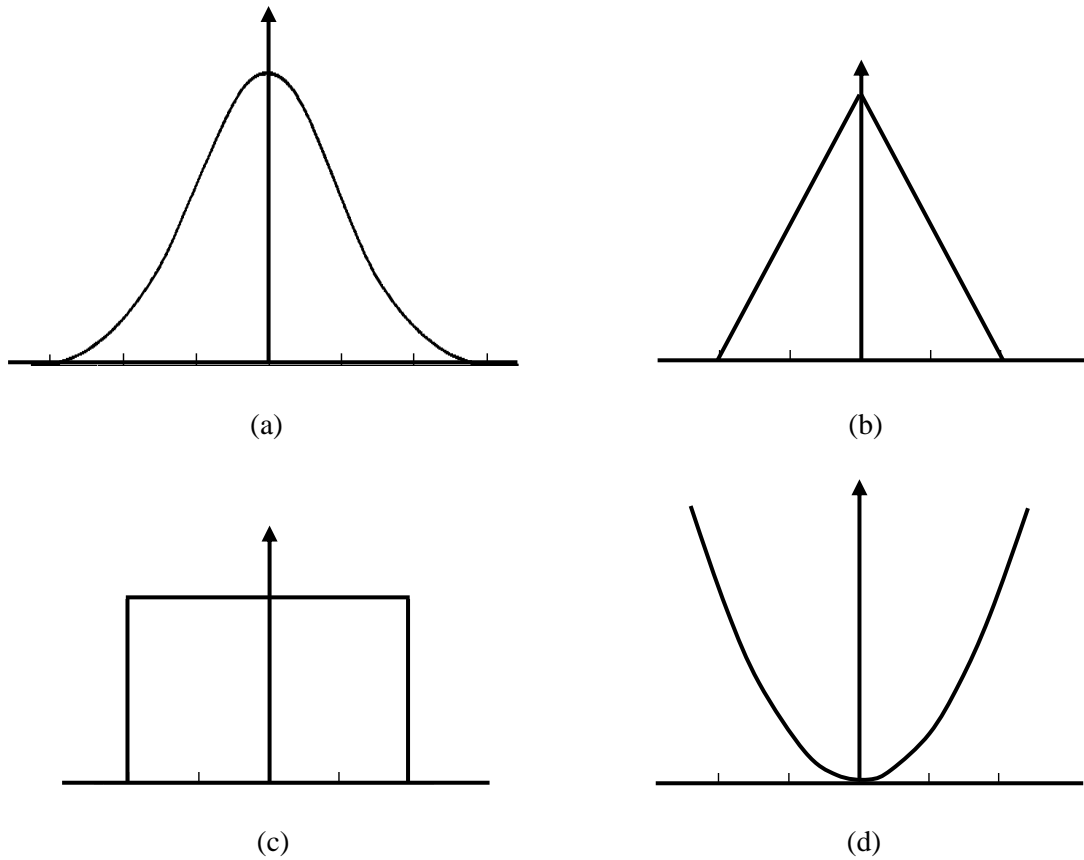


Fig. 1.3 Graphical illustration of probability for (a) normal distribution (b) triangular distribution (c) rectangular distribution (d) U-shape distribution

It is worth noting that, the combined standard uncertainty evaluation procedures described above assume that the input standard uncertainties are not correlated with each other. It is further described in GUM, Section 5.2, that if the input quantities ( $x_1$  and  $x_2$ ) are correlated with each other, equation (1) will be modified and correlation coefficient  $r$  shall be introduced [4]:

$$u(y) = \sqrt{\left(\frac{\partial y}{\partial x_1}\right)^2 u^2(x_1) + \left(\frac{\partial y}{\partial x_2}\right)^2 u^2(x_2) + 2r_{x_1, x_2} \left(\frac{\partial y}{\partial x_1}\right) \left(\frac{\partial y}{\partial x_2}\right) u(x_1) u(x_2)} \quad (2)$$

It clearly shows that when the inputs are uncorrelated, where  $r = 0$ , equation (2) will be reverted to the same as equation (1). It is rather complicated when dealing with input quantities which are correlated. For brevity, the procedures are not shown in this thesis. A “coverage factor” is often used to multiply the combined standard uncertainty which indicates the level of confidence of the measurement results. As a common practice, the multiplying factor of 2 which defines a confidence interval of  $\approx 95\%$  is mostly used. With the coverage factor determined, the final expanded uncertainty can be obtained as twice of the value of the combined standard uncertainty.

## 1.2 Measurement Uncertainty in the Standards

CISPR (Comité International Spécial des Perturbations Radioélectriques) is a technical committee of the International Electrotechnical Commission (IEC) established in 1933 to protect radio reception from interference. The CISPR standards are structured in three levels, which are basic standards, generic standards and product standards. These standards are drafted and nominated by CISPR subcommittees which have different roles in basic and product standards. At the basic level, 16 parts of CISPR 16 series define the measurement apparatus, MU, test methods and facilities. Generic standards, referring to IEC 61000-6 series, comprise two parts for both emission and susceptibility measurements. The standards are applicable for both residential and industrial environment. Product standards are often more specific and in detail, describing the test requirements for certain product family. They provide detailed requirements such as allowable limits, EUT arrangement and test methods for specific product or EUT. The hierarchy illustration of different CISPR standards is shown in Fig. 1.4.

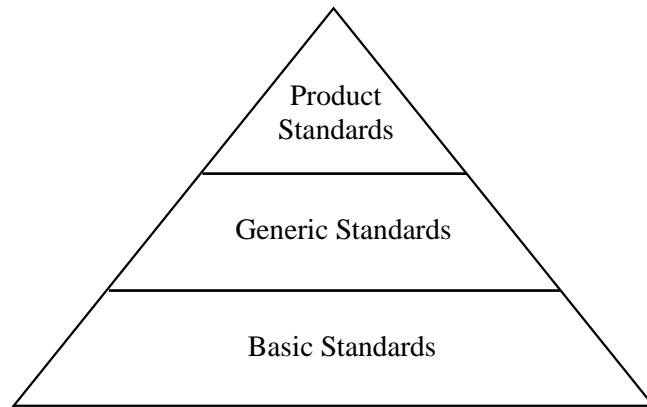


Fig. 1.4 The hierarchy illustration of different CISPR standards

Among the basic standards, CISPR 16-4-1 and CISPR 16-4-2 [5, 6] illustrate the uncertainties, statistics and limit modelling. CISPR 16-4-2 was first published in year 2003. It serves as a specification of the methods for applying Measurement Instrumentation Uncertainty (MIU, same as MU in this thesis for brevity) when determining compliance with CISPR disturbance limits. The material is also relevant to any EMC test when the interpretation of the results and conclusions reached will be impacted by the uncertainty of the measurement instrumentation used during the test [6]. The possible MU contributions for both conducted and radiated disturbance measurements are identified in the standard.

A system level of measurement uncertainty characterisation is always important, especially those associated with test setup and measurement equipment. CISPR 16-4-2 states that measurement uncertainty should be taken into account when determining compliance or non-compliance of an EUT with a disturbance limit. This is also mentioned in the IEC 61000-4-3 [7] and IEC 61000-4-6 [8] standards for EMS testing. In the latest product standards update in 2015, a few standards have already started to adopt the full approach for the MU specified in [6]. Therefore, MU needs to be taken into account in the determination of compliance. On the other hand, MU is not required to be accounted for in some product standards during the product compliance determination; however, it is still required to be calculated and presented in the final

report together with the measurement results. The latest updates on measurement uncertainty requirements by CISPR/IEC product standards are shown in Table 1.1 [9].

Table 1.1 Measurement uncertainty status update for CISPR standards

<b>CISPR Standard</b>	<b>Status of Implementation</b>	<b>CISPR Standard</b>	<b>Status of Implementation</b>
CISPR 11:2015 (Ed. 6.0) [10]	Full approach for MIU in accordance with CISPR 16-4-2:2011.	CISPR 22:2008 (Ed. 6.0)	Only calculation and documentation in the test report is required. Implementation of full approach not planned.
CISPR 12:2009 (Ed. 6.1)	New normative Annex H will be added on the consideration of MIU in edition 7, publication expected in 2016	CISPR 25:2008 (Ed. 3.0)	No requirement to consider MIU. Implementation is under consideration.
CISPR 13:2015 (Ed. 5.1)	In amendment 1 to Edition 5, both the measurement results and the calculated uncertainty shall appear in the test report. But MIU need not be taken into account in the determination of compliance.	CISPR 32:2015 (Ed. 2.0)	Only calculation and documentation in the test report is required.
CISPR 14-1:2009 (Ed. 5.1)	MIU not to be taken into account in the determination of compliance, only calculation, and documentation in the test report is required. Implementation of full approach will be part of Edition 6. Publication expected in 2016	IEC 61000-6-3:2010 (Ed. 2.1)	Full approach in accordance with CISPR 16-4-2:2011.
CISPR 15:2013 (Ed. 8.0)	Full approach for MIU in edition 8, amendment1, in accordance with CISPR 16-4-2:2011	IEC 61000-6-4:2010 (Ed. 2.1)	Full approach in accordance with CISPR 16-4-2:2011.

### 1.3 Motivation of the Research

The Industrial Postgraduate Programme (IPP) is introduced by the Economic Development Board (EDB) Singapore to build up a pool of postgraduate manpower with critical R&D skill-sets for roles in industry through providing postgraduate training in a corporate R&D environment. The objective of the IPP is to establish a link between research study and industrial application. Rohde & Schwarz Asia (R&S) is a leading EMC solution provider in the region, and measurement uncertainty characterisation in EMC test is one of the important topics to the organization. The



motivation of the research is to provide an insight into the characterisation of the uncertainties which are not well defined in the standards. Meanwhile, the results obtained in the research are expected to have important implications for practical measurements and for the proper interpretation of measurement standards.

#### **1.4 Original Contributions of This Thesis**

Existing literature have provided certain additional knowledge to the generic standards, for instance, uncertainties related to measuring apparatus [11-13], uncertainties associated with conducted tests [14-17], antenna related uncertainties [18, 19] and uncertainties related to the entire test system [20-22]. However, not all detailed procedures on characterising MU contributions are available. There are still areas which require further clarification, especially the way to characterise an instrument's MU when the necessary information is not available in the manufacturing datasheet. Furthermore, a system level MU characterisation is always desired in the industry to supplement the generic standards and provide a clear picture for the test houses to carry out uncertainty identification, and subsequently its handling and treatment.

Uncertainty study of the reverberation chamber (RC) has attracted more attention for EMC test in the past decade. It is of interest in this thesis to improve the electric field uniformity and reduce the measurement uncertainties in the reverberation chamber especially at lowest usable frequency range. The characterisation of some important uncertainty contributions in EMI test systems are conducted and additional knowledge is provided to the existing measurement standards used in the industry. Furthermore, the accuracy and consistency of the measurement results using the newly adopted Fast Fourier Transform (FFT)-based time domain (TD) scan method for radiated spurious emission (RSE) test has also been investigated in this thesis. The original contributions of this thesis are as follows:

It is known that at the lowest usable frequency range, the reverberation chamber is often working at under-mode regime. The performance of the chamber is greatly affected since not enough independent samples can be collected during one complete stirrer/tuner rotation. In this thesis, a new mechanical stirring technique using non-equidistant stirrer/tuner positions is proposed. By applying the new technique, the reverberation chamber performance can be improved at the lowest usable frequency range as compared to the conventional method. Better electric field uniformity is achieved with a smaller standard deviation of electric field of total data set (the average of three orthogonal electric field components  $E_x$ ,  $E_y$  and  $E_z$ ), thus the intrinsic field uncertainty is reduced and overall MU is improved.

Some of the important MU contributions in a typical radiated emission test system have been characterised in this thesis. These areas have not been investigated in depth either in the current standards or in the existing literature. For instance, the detailed methods and procedures to obtain pre-amplifier gain variation due to temperature change are not clearly defined in CISPR 16-4-2 or in other literature. Therefore, further consideration and characterisation of this MU contribution is necessary to avoid confusions and measurement discrepancies in the industry. The results obtained in this thesis have significant contributions to the industry in the MU identifications and treatments by providing additional knowledge to the existing standards.

The use of FFT-based time domain scan method for RSE measurement is getting more and more popular in the industry. However, the comparison of accuracy and consistency using the TD scan method and the conventional sweep method is not reported in the literature. In this thesis, the performance of both methods is compared for GSM 900 and GSM 1800 tests. Theoretical background of achieving the comparable accuracy using TD scan method compared to sweep method has been provided. The result of standard deviation of repeated measurements is also calculated and presented. It serves a purpose to provide additional knowledge to the industry on

the reliability and measurement uncertainty (through repeatability study) of the TD scan method for RSE measurement.

Some of my research results have been adopted by Rohde & Schwarz Asia and the development of “Measurement Uncertainty Calculation Software” (MUCS) has been proposed to the software development team. The purpose of this software is to enable EMC labs which follow commercial EMC standards to calculate their MU, without the need for additional manpower from the labs. It will ensure that the test reports adhere to the standards’ requirements by appending the MU calculation to the EMC measurement results as a separate chapter or appendix. Important findings in my research work have been incorporated into the software, such as the preamplifier gain variation due to temperature change, Artificial Mains Network (AMN) impedance and the in-depth interpretation of the MU contributions from the standard.

For instance, the AMN used in the conducted emission test is associated with a few MU contributions, and one of the important uncertainty contributions is AMN impedance uncertainty  $\delta Z_{AMN}$ . It is often time consuming and computation-intensive to obtain AMN impedance uncertainty, and some test houses even do not have the technical know-hows to obtain this value.

Furthermore, the consideration of the MU associated with the AMN impedance calibration is also missing in the current standard or literature. A specific model has been developed to consider the MU associated with the AMN impedance calibration by evaluating a selected number of combinations of different calibration MU impedance amplitude and angle with a proper step size. The worst case AMN impedance uncertainty can be obtained by comparing the results from these combinations within MUCS. With this work, I hope to continue to contribute to the industry in the MU field.

## **1.5 Outline of the Thesis**

The remaining of the thesis is organised into five parts. Chapter 2 introduces theoretical aspects of the reverberation chamber and establishes the link between theory and actual EMC measurement in a reverberation chamber. In Chapter 3, the electric field uniformity and intrinsic field uncertainty in a reverberation chamber is addressed. Non-equidistant tuner positions as a new mechanical stirring technique is proposed to improve the reverberation chamber performance when the measurement is carried out at the lowest usable frequency (LUF) range. Simulation and measurement results have been obtained and compared, and the good agreement proves that the method proposed has superior performance compared to the conventional methods mentioned in the standard at the under-mode regime. Chapter 4 presents new findings on the MU characterisation in some important areas which have not been addressed in the existing literature or the standards. Information about the proposed software MUCS which incorporates some of the results mentioned in this chapter is also briefly introduced. The comparison of the accuracy and consistency for the use of the TD scan method and conventional sweep method in RSE measurement is discussed in Chapter 5. Finally, results presented in this thesis are summarised in Chapter 6, and some suggestions for future work are given.

## CHAPTER 2 REVERBERATION CHAMBERS FOR EMC APPLICATIONS

### 2.1 Background

Reverberation chambers (RCs) are often referred to as enclosures with conducting and electromagnetic reflective surfaces. A transmitting antenna is used as the excitation source within the chamber, and an arbitrarily-shaped metallic paddle with a function of “stirring” electromagnetic fields is used to continuously change the chamber's boundary conditions [23-26]. The chamber behaves like a multi-mode resonator in which the modes create interference with each other due to the conductive walls, which results in interference of the electric field within the chamber. By rotating the paddle, different modes of the resonances are “stirred” and a statistical environment is created to achieve a time-averaged, spatially homogeneous field distribution within the chamber [27]. An illustration of a typical RC is provided in Fig. 2.1.

During one stirrer rotation, samples of electric field strength (in volts) or power (in watts) can be collected. The samples collected are used for statistical analysis and the number of samples required is determined by the stirrer step size. Typically, the samples collected are not always independent from each other. It is desirable, however, to obtain more independent samples, as the uniformity of the electric field in the chamber is directly affected by the number of independent samples. Only when electric field uniformity is achieved, the average of the power measured at any position within the working volume can be considered constant (within a certain tolerance) [28].

The concept of using RCs for EMC testing was first proposed in 1968 [28], and it has taken some time for the industry to accept such a concept. During the 1990s, the use of RCs increased rapidly, and their use in various aspects of EMC testing was studied and established [29-35].

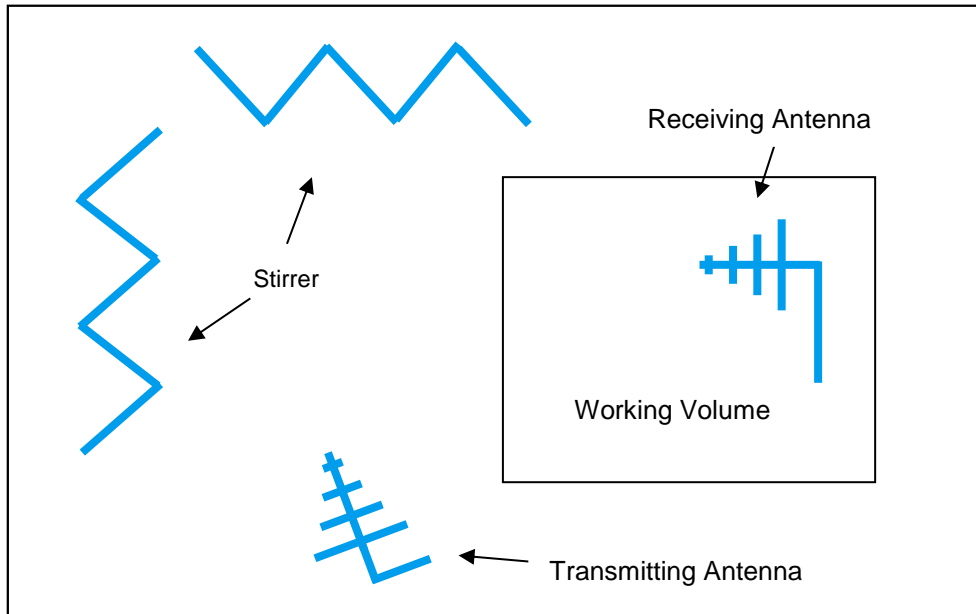


Fig. 2.1 Reverberation chamber illustration

In 2003, an international standard was published on the use of RCs for conducting EMC tests and measurements [36]. RCs are used for both EMI and EMS tests, and have several important advantages for performing EMS test as compared to the anechoic chambers. These advantages include:

- low chamber building cost;
- the capability of achieving high electric field strength (often required in military or automotive test standards) with relatively low input power, which is typically preferred by the industry as high power amplifiers are very costly;
- a broad operating frequency range (above the lowest usable frequency);
- no requirement for rotation of the EUT; and
- suitable isolation/shielding from the external environment.

RCs, however, also have disadvantages when compared to anechoic chambers, such as the loss of polarisation information from the EUT, and difficulties in interpreting measurement results. Nonetheless, despite their disadvantages, RCs remain as attractive alternatives for performing EMC tests.

This chapter discusses some of the important theoretical background and concepts which argue well that RCs can be used as EMC measurement facilities. The concepts discussed will provide the basic guideline for Chapter 3, which investigates RC performance at the lowest usable frequency range. Prior to the experiment mentioned in Chapter 3, the actual chamber used for practical measurement in this thesis has been validated with respect to loaded/unloaded calibrations, the quality factor, and time constant. The results are presented and discussed in this chapter.

The cavity mode theory is discussed in Section 2.2 of this chapter, including how it can be applied to the RC for electromagnetic field calculation. The definition of quality factor and time constant of the RC is introduced in Section 2.3. In Section 2.4, the important parameters and characteristics of RCs are discussed and presented for a better understanding of using RCs for EMC applications. The actual chamber validation is discussed in Section 2.5. Finally, the conclusions are presented in Section 2.6.

## 2.2 Cavity Mode Theory

Cavity mode theory has been studied in depth in previous literature [37-39]; and some of the important RC-related results are summarised in this section. In the industry, most RCs are rectangular-shaped. Thus, this section will focus only on the electromagnetic properties of a rectangular cavity. For a rectangular metallic cavity, as shown in Fig. 2.1, the wave numbers (eigenvalues) can be derived from:

$$k_{lmn}^2 = \omega_{lmn}^2 \mu \epsilon = \left( \frac{l\pi}{a} \right)^2 + \left( \frac{m\pi}{b} \right)^2 + \left( \frac{n\pi}{d} \right)^2 \quad (3)$$

where  $k_{lmn}$  is the eigenvalue;  $l$ ,  $m$  and  $n$  are integer numbers, referred to as mode coefficients; and  $a$ ,  $b$  and  $d$  are the width, height and length of the chamber, respectively. In the mode counting, Transverse Electric (TE) or Transverse Magnetic (TM) modes are always considered for each eigenvalue. In the consideration of the non-evanescent

components, when  $lmn$  are non-zero values, each eigenvalue will have two types of modes: the  $TE_{lmn}$  and  $TM_{lmn}$  modes. When  $l = 0$ , only a  $TE_{0mn}$  mode exists for each eigenvalue. When  $m = 0$ , only a  $TE_{l0n}$  mode exists for each eigenvalue. When  $n = 0$ , only a  $TM_{lm0}$  mode exists for each eigenvalue [40]. In general, for TE modes, the mode coefficients  $l$ ,  $m$  and  $n$  are integers, and either  $l$  or  $m$  can have a value of 0; however  $l = m = 0$  is not allowed. For TM modes, the mode coefficients  $l$ ,  $m$  and  $n$  are integers where  $n$  can have a value of 0.

When the number of modes are assessed in the cavity using the mode counting method, the total number of modes with eigenvalues  $k_{lmn}$  of less than or equal to  $k$  (a practical limit for the propagation of modes) [41] can be described as:

$$N = N_1 + N_2 + N_3 + N_4 + N_5 \quad (4)$$

where  $N_1$  represents  $TM_{lmn}$  modes,  $N_2 (= N_1)$  represents  $TE_{lmn}$  modes,  $N_3$  represents  $TM_{lm0}$  modes,  $N_4$  represents  $TE_{0mn}$  modes, and  $N_5$  represents  $TE_{l0n}$  modes. Equation (4) can be numerically evaluated; however the computation is intensive. Another method of mode counting [28] is stated in (5), which is an improved version of the original Weyl's approximation:

$$N = \frac{8\pi}{3}abd\frac{f^3}{c^3} - (a + b + d)\frac{f}{c} + \frac{1}{2} \quad (5)$$

where  $a$ ,  $b$  and  $d$  represent the length, width and height of the cavity. The choice of chamber length, width and height will affect the degeneracy of the modes – the fluctuating part of the total number of modes. In a practical design consideration, the ratio of  $a^2$ :  $b^2$ :  $d^2$  should not be too mutually rational in order to reduce the degeneracy of the modes and hence increase the uniformity in the resonant modes distribution.



A further important chamber design parameter which must be assessed is mode density, which determines the number of modes which could be presented in a small bandwidth about a given frequency [28]. By differentiating equation (5) with respect to  $f$ , the mode density can be obtained as:

$$D_s(f) = 8\pi abd \frac{f^2}{c^3} - \frac{a+b+d}{c} \quad (6)$$

A graph showing mode density against frequency (from 400 MHz to 1 GHz) is presented in Fig. 2.2. It indicates that, from around 500 MHz onwards, the Rohde & Schwarz Asia RC, with dimensions of  $a = 2.25$  m,  $b = 1.95$  m, and  $d = 2.03$  m, has a mode density greater than 1. This implies that spatial field uniformity may be difficult to achieve below 500 MHz.

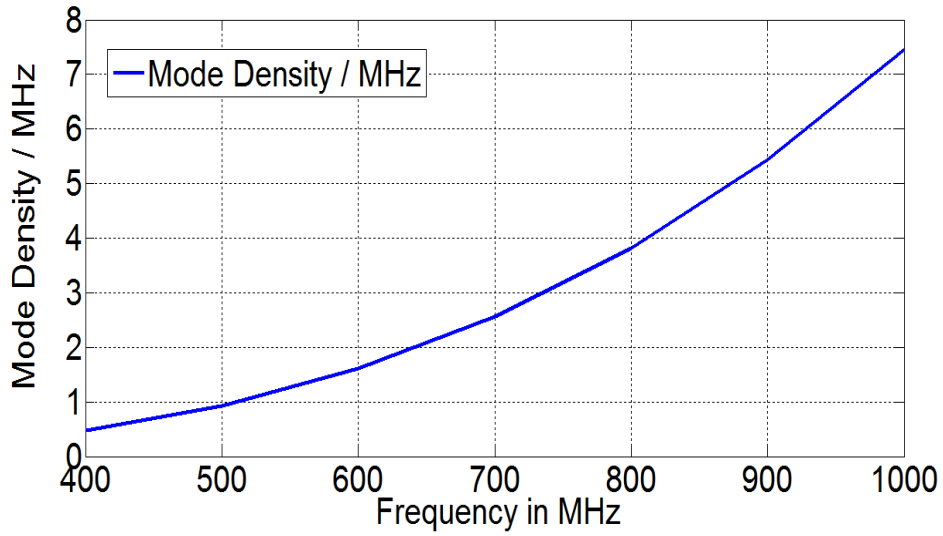


Fig. 2.2 Mode density against frequency for RC used in R&S

The mode count in the cavity has been discussed; and the resonance frequencies existing in the cavity shall be investigated. For the aforementioned RC, the resonance frequencies can be obtained based on [28]:

$$f_{lmn} = \frac{1}{2\sqrt{\mu\epsilon}} \sqrt{\left(\frac{l}{a}\right)^2 + \left(\frac{m}{b}\right)^2 + \left(\frac{n}{d}\right)^2} \quad (7)$$

where  $\mu$  and  $\varepsilon$  are the permeability and permittivity of the medium inside the cavity. It should be noted that equation (7) is a transformation of equation (3). It is always important to be aware of the modal condition inside the RC. Practically, in order to achieve spatial field uniformity, different modes need to be excited within the chamber.

### 2.3 Q Factor

Another important parameter to be considered in the design of an RC is the quality factor ( $Q$  factor), which is intrinsic to the chamber dimensions and chamber construction material (wall loss).  $Q$  factor has been defined in [42]:

$$Q = \frac{\omega U}{P_d} \quad (8)$$

where  $\omega$  is the angular frequency,  $U$  is the energy stored in the cavity, and  $P_d$  is the power dissipated in the cavity.  $U$  can be determined by:

$$U = WV \quad (9)$$

where  $V$  is the volume of the chamber, and  $W$  is the energy density. The energy density depends on the electric fields in the cavity:

$$W = \varepsilon_0 E^2 \quad (10)$$

where  $\varepsilon_0$  is the permittivity of the medium in the cavity (free space), and  $E$  is the root mean square of the electric field. For steady-state condition, the transmitted power  $P_t$  and the power dissipated in the loss mechanisms  $P_d$  are equal [42]:

$$P_t = P_d \quad (11)$$

If the result shown in (11) is substituted into (8), (9) and (10), then the mean squared electric field can be obtained as:

$$E^2 = \frac{Q}{\omega \epsilon_0 V} P_t \quad (12)$$

The average received power is determined by the product of the scalar power density  $E^2/\eta$  and the effective area  $\lambda^2/4\pi$  of an isotropic antenna, multiplied by a polarisation mismatch factor of one half [43]. Thus, the final representation of the averaged received power is:

$$\langle P_r \rangle = \frac{1}{2} \frac{E^2}{\eta} \frac{\lambda^2}{4\pi} \quad (13)$$

To further relate the average received power to the transmitted power, the result of (12) is substituted into (13). The average received power can now be deduced as a function of the transmitted power, as presented in (14):

$$\langle P_r \rangle = \frac{Q \lambda^3}{16\pi^2 V} P_t \quad (14)$$

where  $\eta = 1/c_0 \epsilon_0$ ,  $c_0$  is the speed of light in free space, and  $\epsilon_0$  is the permittivity of the free space. It is worth noting that the presence of the receiving antenna will not affect the validity of equation (11), as power dissipated in the loads of the receiving antenna has been accounted for as one of the power loss in the cavity in evaluating  $P_d$ ; and no additional power is introduced into or removed from the cavity. Thus, to obtain the chamber  $Q$  factor, equation (14) can be re-arranged as:

$$Q = \frac{16\pi^2 V}{\lambda^3} \frac{\langle P_r \rangle}{P_t} \quad (15)$$

Equation (15) is applicable to an impedance-matched, lossless receiving antenna; however dissipative or mismatch losses can be accounted for by modifying the effective area of the receiving antenna [40].

Another assessment of  $Q$  factor concluded in [23] has shown that, besides the frequency domain method described in (15), the  $Q$  factor can also be derived from the chamber time constant  $\tau$  [41]:

$$Q = 2\pi f\tau \quad (16)$$

In comparison to (15), this method of obtaining the  $Q$  factor could diminish the contribution of the antennas involved, leaving just the effect of the chamber alone.

## 2.4 EMC Measurement in RCs

The basic cavity mode theories have been introduced in Section 2.2, and the modes and resonance frequencies which can be excited in an RC have been discussed.  $Q$  factor-related information has been introduced in Section 2.3. These theories and information are necessary in understanding the basic RC working principles. The typical RC facility used for EMC applications is presented in Fig. 2.3.

This section introduces further important parameters in carrying out EMC testing in the RC. Detailed chamber validation methods using RCs are also discussed with respect to IEC61000-4-21 [36]. The main purpose of this section is to discuss the important parameters of an RC for EMC applications.

### 2.4.1 EMC Standards Using Reverberation Chambers

As mentioned earlier, the basic standard for the use of RCs in EMC applications is IEC61000-4-21 [36]. The standard was first published in 2003 and was later updated in 2011. It provides a comprehensive coverage of chamber validation, radiated immunity, and radiated emission applications. It is the most widely adopted standard across the industry. There are, however, other standards for EMC measurement using RCs. For example, the manufacturer-specific standards covering radiated immunity testing of automotive and military applications in RCs are [41]:

- J551-16: Vehicle-level radiated immunity tests
- J1113-27: Component-level radiated immunity tests
- J1113-28: Component-level radiated immunity tests
- GMW3097 / Ford ES-XW7T-1A278-AC: Vehicle-level radiated immunity tests
- MIL-STD-461F: Military EMC tests

It is worth noting that, at present, RCs have not been widely accepted. With the development of further technology, however, it is likely that RCs will become more accepted within the industries.

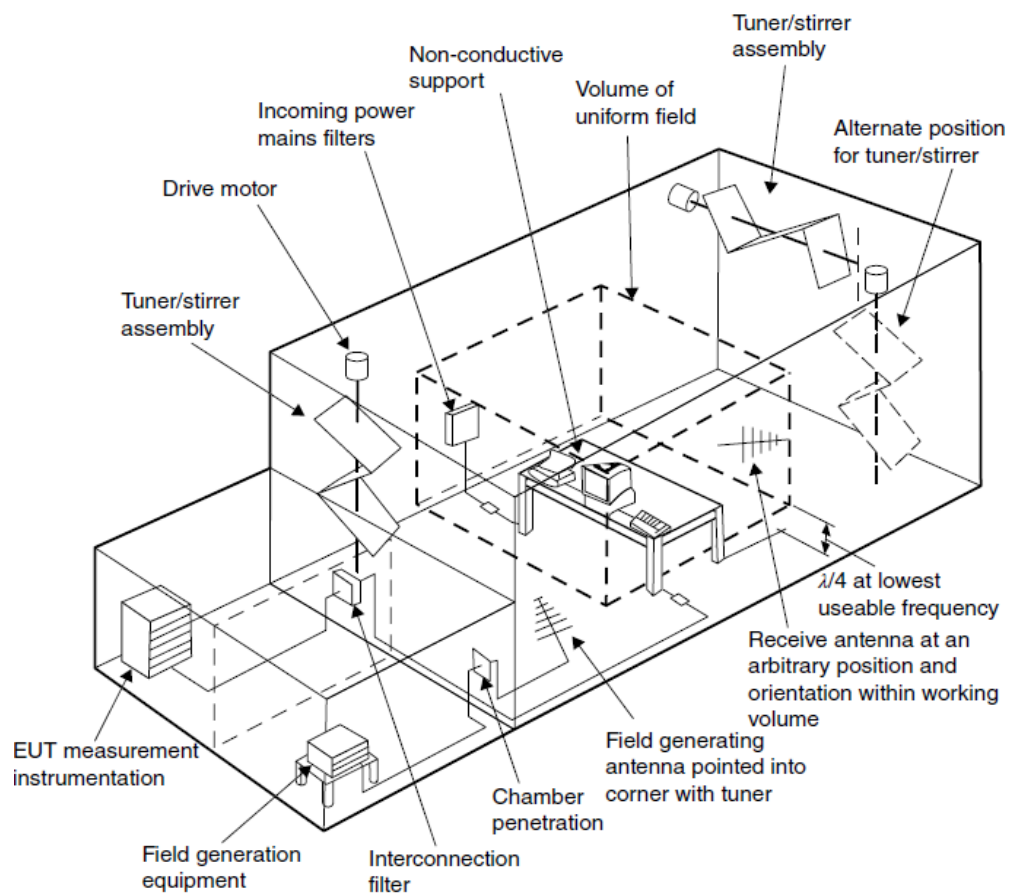


Fig. 2.3 Typical reverberation chamber facility [36]

### 2.4.2 Working Volume

The chamber working volume is bounded by eight points within the chamber, which are of sufficient distance from the walls to avoid boundary effects [36]. Typically, the working volume is defined by a cubic region at  $\lambda/4$  from the walls, and the EUT is placed in such a working volume during the actual test.

### 2.4.3 Lowest Usable Frequency

Lowest usable frequency (LUF) is often referred to as the minimum operational frequency of the RC. It is determined by several parameters, including chamber size, shape, and  $Q$  factor. In practical consideration, LUF is often defined as  $3f_s$  where  $f_s$  is the first resonance frequency of the chamber. For the definition provided in the standard, LUF is the lowest frequency at which the specified field uniformity can be achieved within the chamber's working volume [36].

### 2.4.4 Field Uniformity

For this thesis, the field uniformity shall be validated for the first decade from the LUF in the working volume. An electric field probe shall be placed at the eight corner locations of the working volume to capture the electric field strength (V/m). At each location, three orthogonal electric field components ( $E_x$ ,  $E_y$  and  $E_z$ ) shall be recorded

Table 2.1 Field uniformity tolerance requirements [36]

Frequency range MHz	Tolerance requirements for standard deviation
80 to 100	4 dB <sup>a</sup>
100 to 400	4 dB at 100 MHz decreasing linearly to 3 dB at 400 MHz <sup>a</sup>
Above 400	3 dB <sup>a</sup>
<sup>a</sup> A maximum of three frequencies per octave may exceed the allowed standard deviation by an amount not to exceed 1 dB of the required tolerance.	

over the frequency band for each stirrer step. The data shall then be further processed. Maximum and average received power, maximum field strength for each axis, and average input power over the tuner rotation shall be recorded [36]. For brevity, the detailed procedures for handling the data are not presented in this thesis. The tolerance requirements of the standard deviation of the individual components  $E_x$ ,  $E_y$  and  $E_z$ , and the total data combination of the three axes, are specified in Table 2.1. For ease of data processing, the minimum number of samples to be collected is summarised in [36]. A typical set of probe data, which is normalised to the mean of the eight maximum probe readings ( $x$ -axis data for clarity) at each frequency, is presented in Fig. 2.4 [36]. The number of steps used to collect the data shown in Fig. 2.4 was set prior to determining the values in Table 2.2, and it is shown that the entire validation is conducted through four frequency subranges, and the minimum number of samples from the lowest usable frequency is twelve.

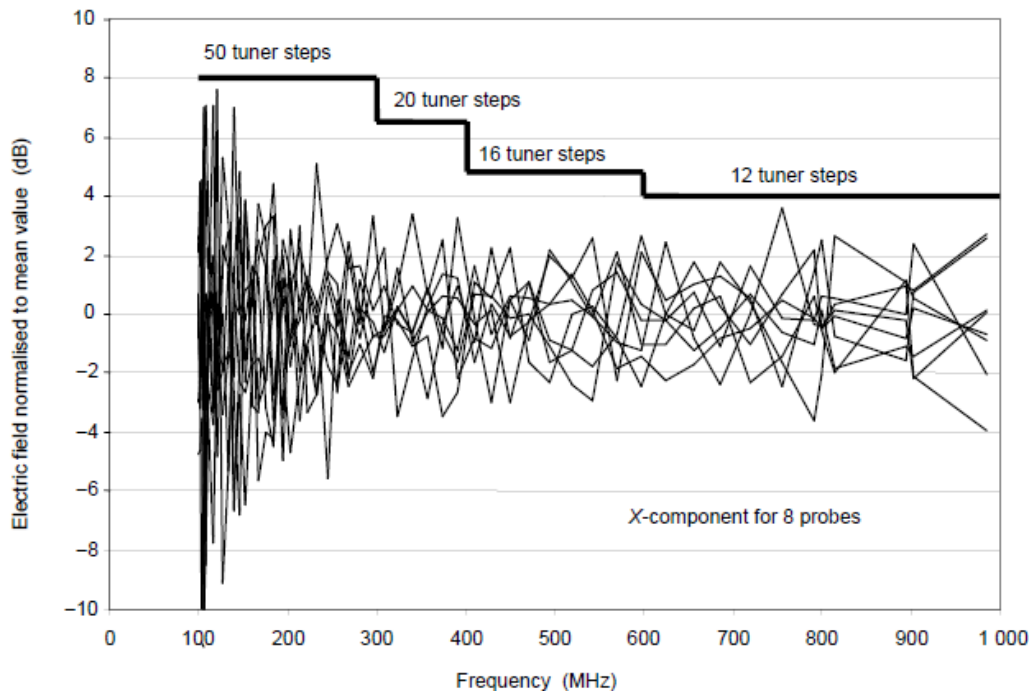


Fig. 2.4 Mean-normalised data for  $x$ -component of eight probes [36]

Table 2.2 Sampling requirements [36]

Frequency range	Minimum number of samples <sup>a</sup> required for validation and test <sup>d</sup>	Number of frequencies <sup>b</sup> required for validation
$f_s$ to $3f_s$ <sup>c</sup>	12	20
$3f_s$ to $6f_s$	12	15
$6f_s$ to $10f_s$	12	10
Above $10f_s$	12	20/decade

<sup>a</sup> The minimum number of tuner steps is 12 for all frequencies. For many chambers the number of tuner steps will need to be increased at the lower frequencies. The maximum number of tuner steps is the number of independent samples that a given tuner can produce. This number varies with frequency and needs to be verified when commissioning the chamber. In the event that the chamber fails to meet the uniformity requirement, the number of tuner steps may be increased up to the number of independent tuner samples.

<sup>b</sup> Log spaced.

<sup>c</sup>  $f_s$  = Start frequency (see A.1.3 for LUF)

<sup>d</sup> The tuner sequencing used for validation of the chamber shall be the same as for subsequent testing.

#### 2.4.5 Chamber Loading Effects

The impact of chamber loading on field uniformity shall be checked, and the maximum acceptable loading of the RC must be determined. The EUT is said to load the chamber when the energy absorbed by the EUT is no longer able to maintain the chamber field uniformity. The checking of loaded chamber validation shall be carried out before the chamber can be used for EMC tests. Chamber loading is verified using the ratio below:

$$Loading = \frac{AVF_{\text{empty chamber}}}{AVF_{\text{loaded chamber}}} \quad (17)$$

where  $AVF$  (antenna validation factor) is the ratio of the average received power to input power, and  $AVF = \langle \frac{P_{\text{AvgRec}}}{P_{\text{input}}} \rangle$ . Chamber loading has been practically discussed in

Section 2.5.2, in addition, the detailed information can also be found in [36].



## 2.5 Chamber Validation

### 2.5.1 Unloaded Calibration

The experimental investigations for this chapter were carried out in the R&S RC, as shown in Fig. 2.5. Prior to the investigations, the chamber was validated in both unloaded and loaded conditions. For the unloaded validation, the chamber working volume was cleared, and a receiving antenna was placed at an arbitrary position and orientation within the working volume of the chamber. The E-field probe was placed in the eight corner locations of the working volume to capture the E-field strength. The standard deviation is calculated using data from each probe axis as well as from the total data set [36]:

$$\sigma(\text{dB}) = 20 \log_{10} \left( \frac{\sigma + \langle \vec{E} \rangle}{\langle \vec{E} \rangle} \right) \quad (18)$$

where  $\sigma$  is the standard deviation, and  $\langle \vec{E} \rangle$  represents the arithmetic mean of the normalised vectors for each probe axis as well as for the total data set.

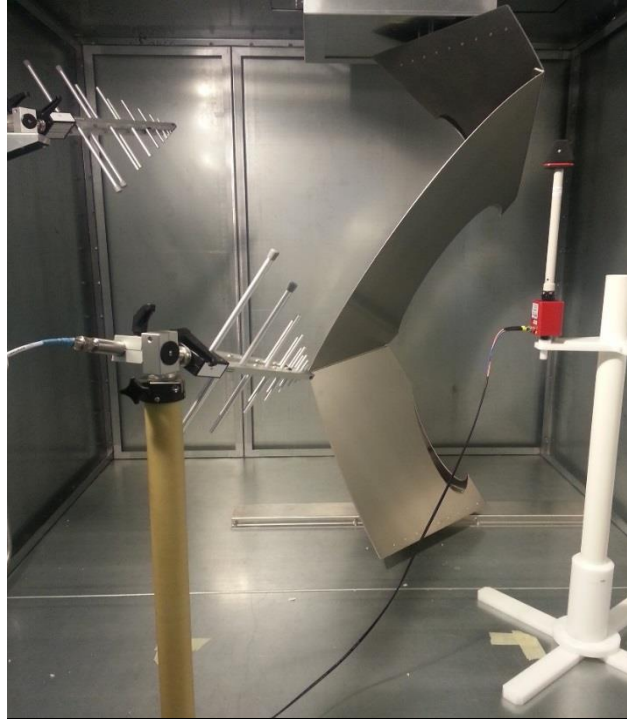
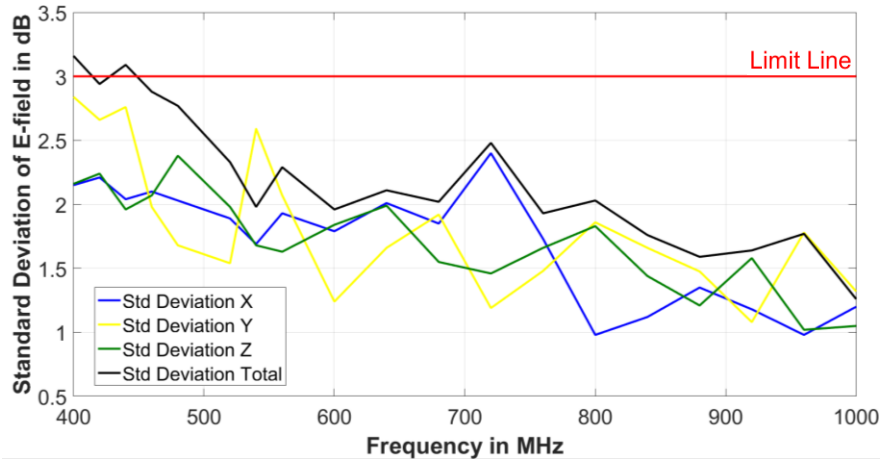


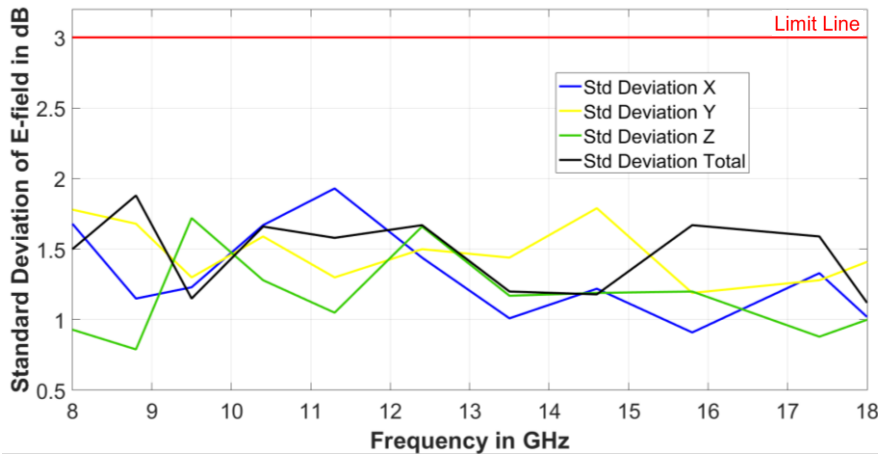
Fig. 2.5 R&S reverberation chamber



(a)



(b)



(c)

Fig. 2.6 Standard deviation for E-field components of eight probe positions for  $x$ ,  $y$ ,  $z$  and total data set with (a) 5% frequency step 400 MHz -1000 MHz (b) 5% frequency step 1 GHz - 8 GHz (c) 9% frequency step from 8 GHz - 18 GHz for unloaded condition

The calculated standard deviation of the measured maximum E-field strength in the eight probe positions for the  $x$ ,  $y$ , and  $z$  axes and total data set have been presented in Fig. 2.6 (a), (b), and (c). Due to the limitations of single power amplifier operating frequency, the testing was performed in three frequency ranges: 400 MHz - 1 GHz; 1 GHz - 8 GHz; and 8 GHz - 18 GHz. Referring to Table 2.1, the standard deviation of all axes and the total data set passed the field uniformity requirement.

### 2.5.2 Loaded Calibration

A one-time check of the chamber's field uniformity is required in order to determine if the chamber is adversely loaded by EUT, as stated in [36]. A sufficient amount of absorber material must be placed at random locations within the chamber working volume, as shown in Fig. 2.7. The absorbing materials typically used are charcoal, ferrite, and foam.

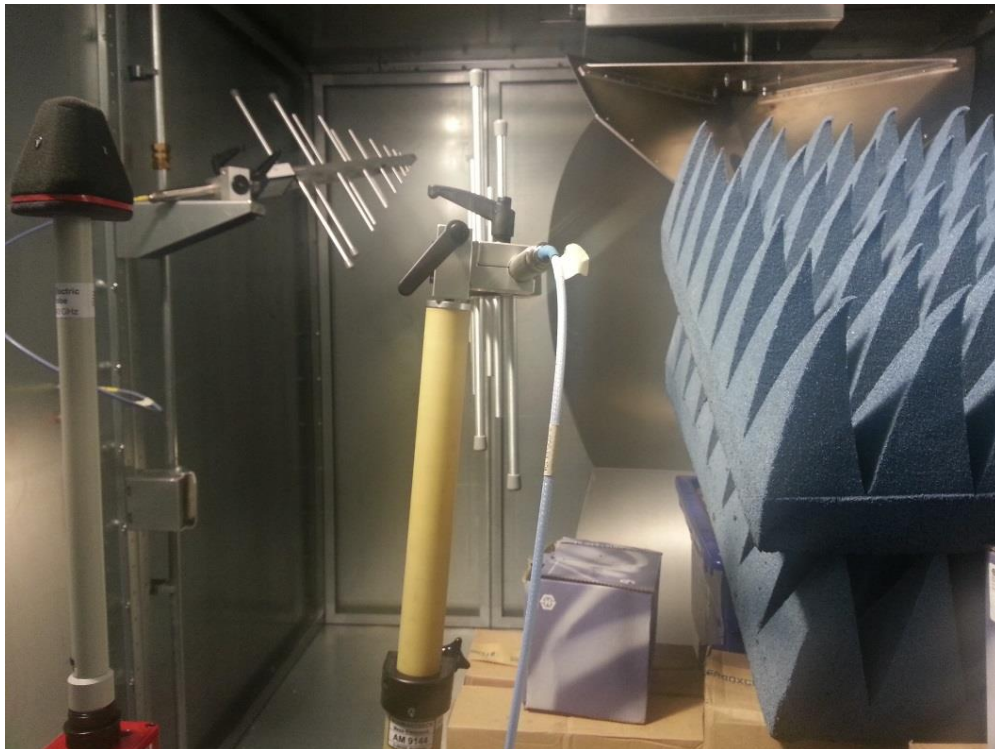
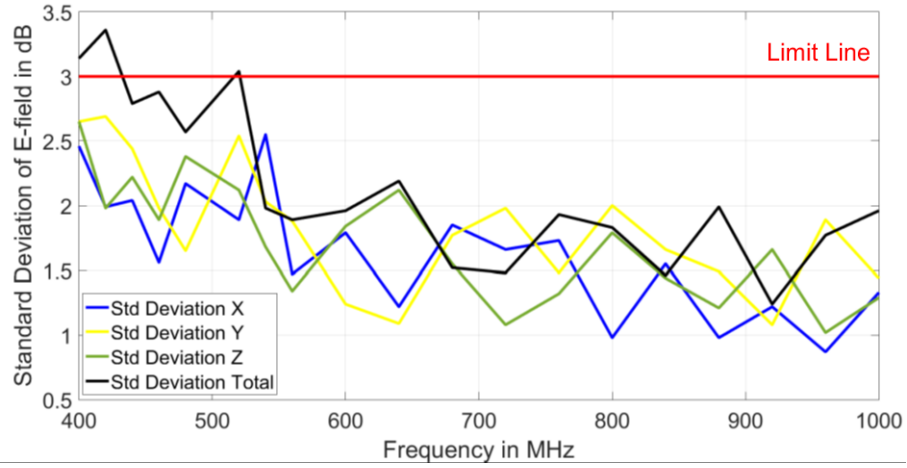
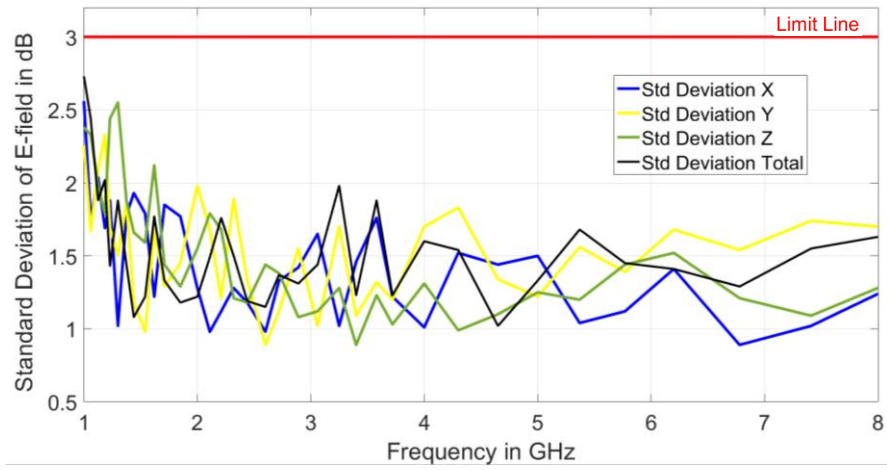


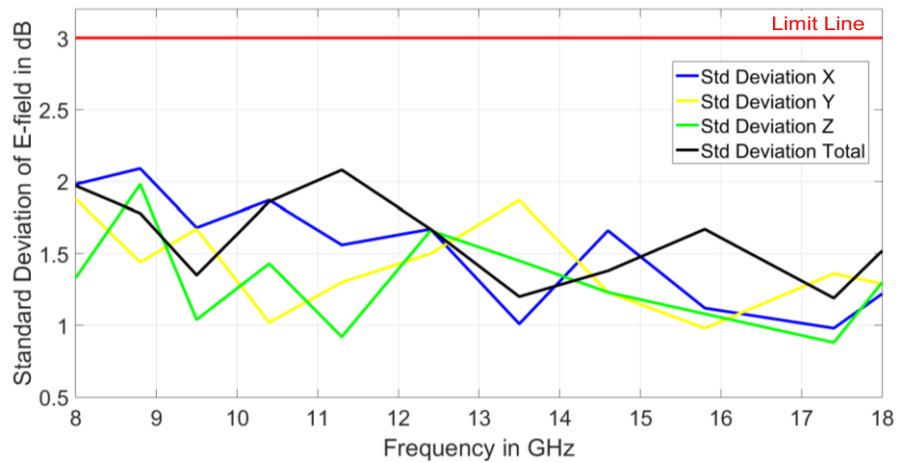
Fig. 2.7 Chamber with maximum loading material



(a)



(b)

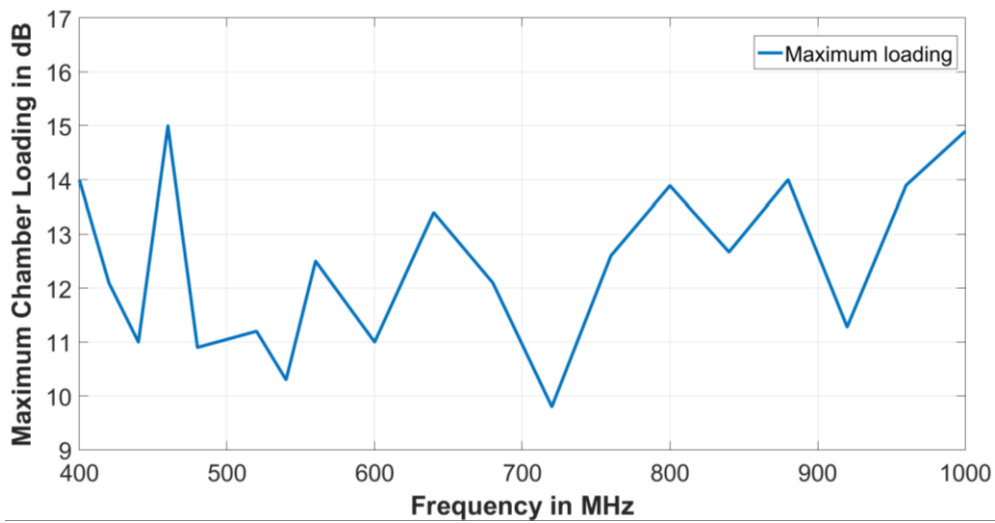


(c)

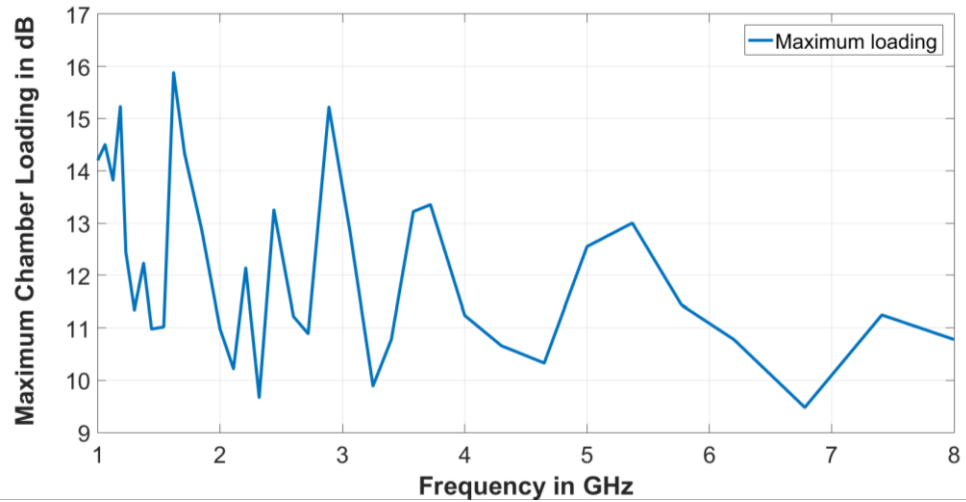
Fig. 2.8 Standard deviation for E-field components of eight probe positions for  $x$ ,  $y$ ,  $z$  axes and the total data set with: (a) 5% frequency step 400 MHz - 1000 MHz; (b) 5% frequency step 1 GHz - 8 GHz; and (c) 9% frequency step 8 GHz - 18 GHz, for loaded condition.

Similar procedures as outlined in Section 2.5.1 are followed, with field probe and receiving antenna maintained at a distance of greater than one quarter wavelength from any absorber. The field uniformity is calculated using the data from the eight locations of the E-field probe. If the standard deviation exceeds the allowable limits as stated in Table 2.1, the chamber is said to be loaded to an unacceptable point [36]. The amount of the absorbing material should then be reduced and the calibration procedure repeated until the maximum loading is found.

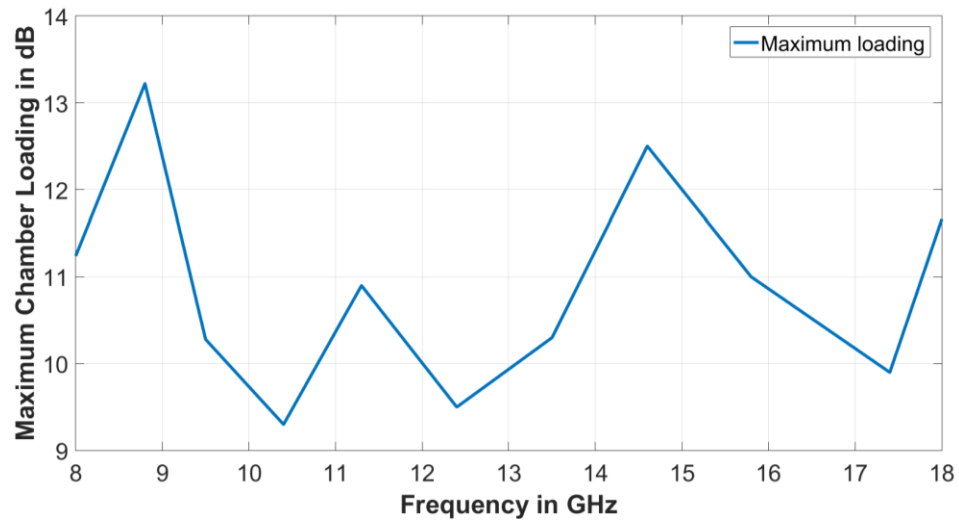
After many trial tests and adjustments to the amount of absorbing material, the maximum loading condition was achieved for the frequency ranges of 400 MHz - 1 GHz, 1 GHz – 8 GHz and 8 GHz – 18 GHz of R&S RC. Similar to the field uniformity evaluation mentioned in Section 2.5.1, the standard deviation for E-field components of eight probe positions for  $x$ ,  $y$ ,  $z$  and total data set has been calculated and presented in Fig. 2.8 (a), (b) and (c). It is shown that with the given amount of the loading material, the standard deviation of the  $x$ ,  $y$ ,  $z$  and total data set fulfil the field uniformity requirement referring to Table 2.1. The maximum chamber loading has also been calculated using equation (17) described in Section 2.4.5 for different frequency ranges and presented in Fig. 2.9.



(a)



(b)



(c)

Fig. 2.9 Maximum chamber loading of: (a) 400 MHz - 1 GHz; (b) 1 GHz - 8 GHz; and (c) 8 GHz - 18 GHz.

Maximum chamber loading verification is required only once during the life of the chamber, or after major modification to the chamber [36]. For this thesis, however, a load check with EUT and its supporting equipment in place shall be carried out prior to performing each test. The same procedure for finding the maximum chamber loading shall be used for the load check with EUT's presence.

The chamber loading factor (CLF) shall be obtained during the load check while EUT is in place, by taking the ratio between the average received power measured with

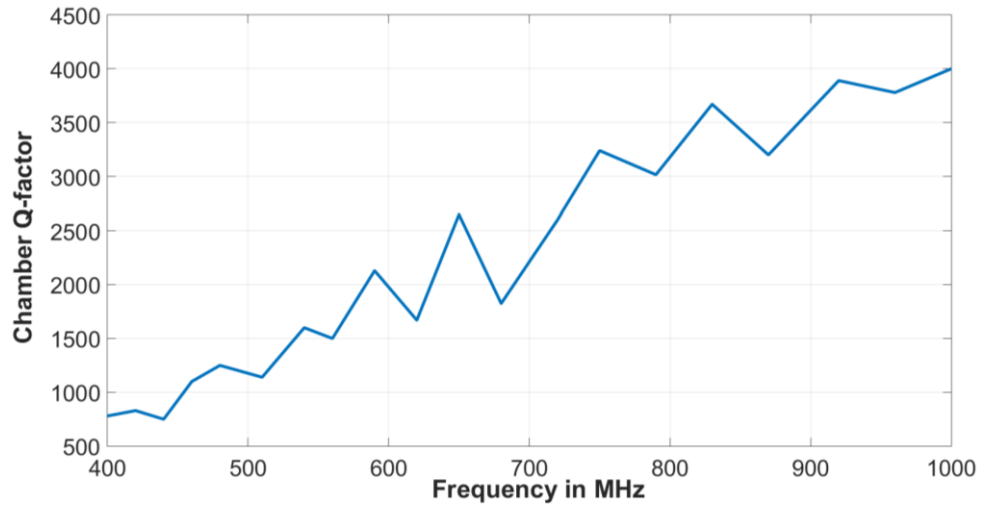
the EUT in place and with the empty chamber. The maximum chamber loading previously calculated is then used to compare with the CLF. If the CLF is greater than the maximum chamber loading, the chamber may have been loaded to the point where field uniformity is not achieved. In this case, chamber uniformity checks as described in Section 2.5.1 shall be repeated with EUT in place. It is also worth noting that the chamber loading effects will affect both radiated and immunity tests.

### 2.5.3 Q Factor and Time Constant

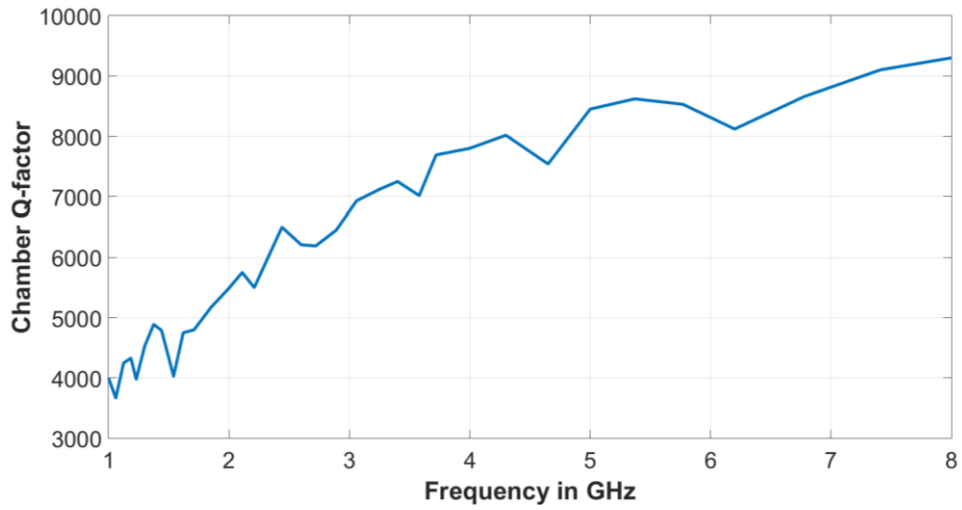
The above calibrations, as outlined in Sections 2.5.1 and 2.5.2, are based on continuous wave (CW) excitation. When using modulated waveforms, the  $Q$  factor must be taken into consideration. Referring to equation (15), when EUT is in place and taken into consideration with the antenna efficiency factors, the  $Q$  factor can be obtained using [36]:

$$Q = \left( \frac{16\pi^2 V}{\eta_{Tx} \eta_{Rx} \lambda^3} \right) \left\langle \frac{P_{AveRec}}{P_{Input}} \right\rangle \quad (19)$$

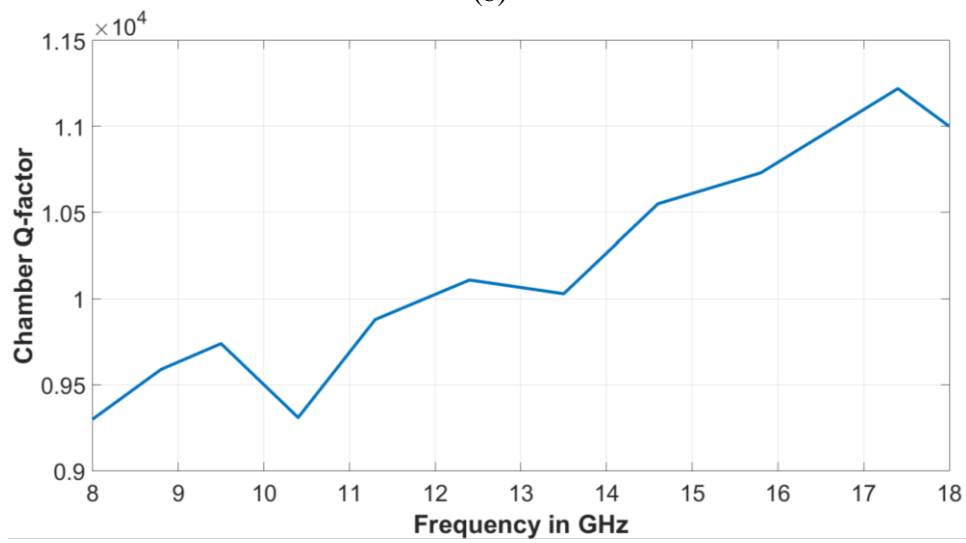
where  $\eta_{Tx}$  and  $\eta_{Rx}$  are the antenna efficiency factors for the transmitting and receiving antennas respectively, which can be assumed to be 0.75 for log periodic antennas and 0.9 for horn antennas.  $V$  is the chamber volume and  $\lambda$  is the free space wavelength at the specific frequency.  $P_{AveRec}$  is the average received power over one tuner rotation and  $P_{Input}$  is the forward power averaged over one tuner rotation. The measured  $Q$  factor of the R&S RC is provided in Fig. 2.10.



(a)



(b)



(c)

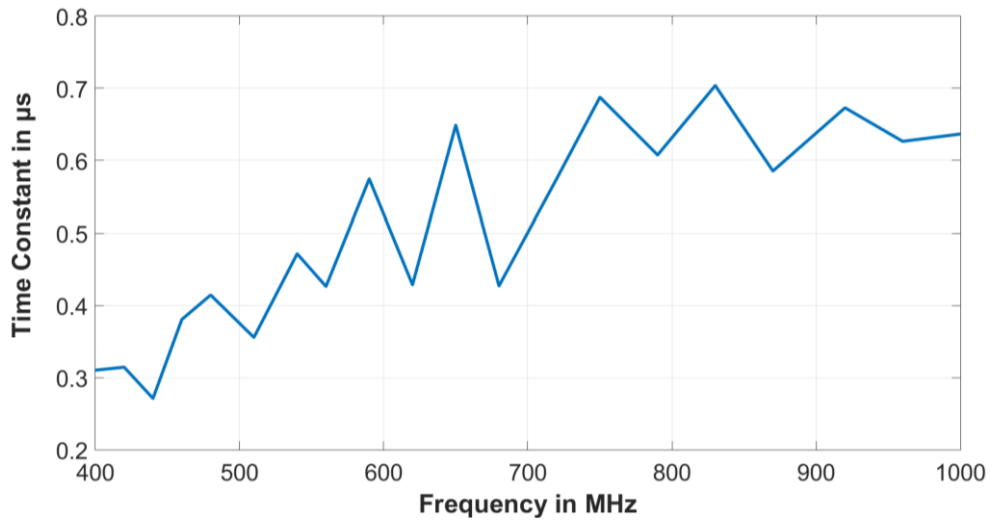
Fig. 2.10 Measured chamber  $Q$  factor of: (a) 400 MHz - 1 GHz; (b) 1 GHz - 8 GHz; and (c) 8 GHz - 18 GHz.



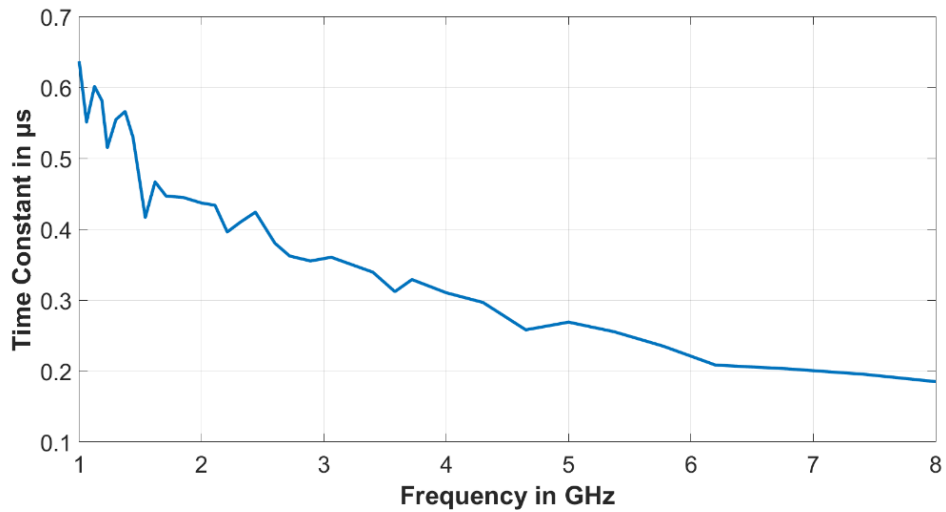
The time response of the chamber shall be fast enough to accommodate pulsed waveform testing. It corresponds to the time constant  $\tau$  of the chamber described in Section 2.3, and equation (16) can be rewritten as:

$$\tau = \frac{Q}{2\pi f} \quad (20)$$

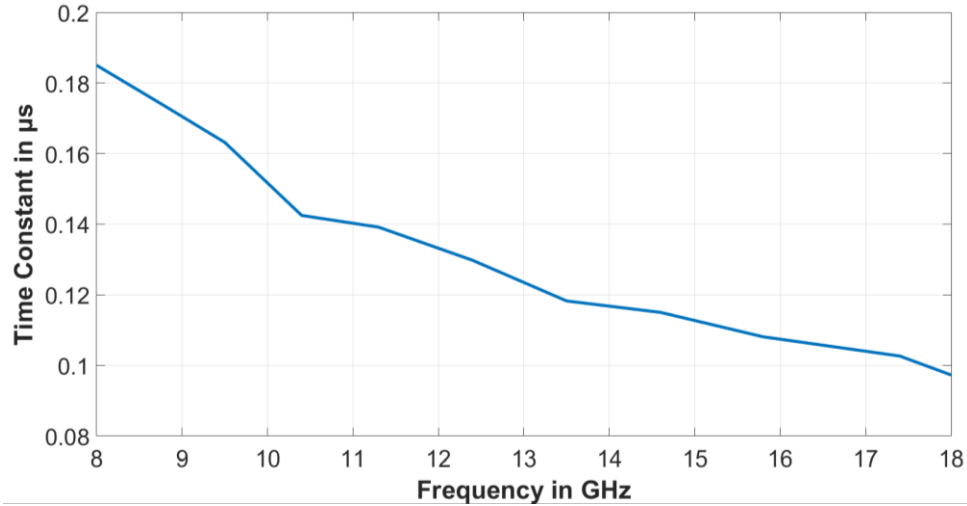
The measurement results of chamber time constant from 400 MHz to 18 GHz are presented in Fig. 2.11. It is mentioned in [36] that the chamber time constant should not be greater than 0.4 times any test waveform pulse width for more than 10% of the test frequencies; otherwise absorbers must be added to the chamber or the pulse width must be increased.



(a)



(b)



(c)

Fig. 2.11 Measured chamber time constant of: (a) 400 MHz - 1 GHz; (b) 1 GHz - 8 GHz; and (c) 8 GHz - 18 GHz.

## 2.6 Conclusion

This chapter has introduced the theoretical background of RCs which, as alternative facilities for EMC measurements, have important advantages over anechoic chambers. Such advantages include a low building cost and a capability to generate a high electric field with low input power. Chamber characteristics which are important for the actual EMC applications are discussed in Section 2.4. The chamber loading and unloading calibration, as well as the measured  $Q$  factor and time constant, are discussed in Section 2.5. The chamber validation works in this section are crucial to the investigation carried out in Chapter 3.

This chapter provides an important link between the theoretical background and the practical use of RCs for EMC measurements. It also provides the basic guideline for the work in Chapter 3 that investigates RC performance in the LUF range.

# **CHAPTER 3 INVESTIGATION OF FIELD UNIFORMITY AND UNCERTAINTIES IN A REVERBERATION CHAMBER AT LOWEST USABLE FREQUENCY**

Measurement uncertainty (MU) in an RC is generally contributed by the insertion loss of the chamber and the impedance mismatch between the EUT and the receiving antenna. A thorough research of MU in an RC has been discussed in [44]. Compared with other test methods, some MU contributions are also applied to an RC, such as antenna factor, site imperfection, and ambient (noise) aspects. The major MU contributions in an RC, however, are generally in respect to field properties and statistical aspects.

In this chapter, an analysis of field uniformity and uncertainties related to an RC in the lowest usable frequency (LUF) is discussed. In Section 3.1, the intrinsic field uncertainty (IFU) of the RC is introduced. An investigation of field uniformity and uncertainty at LUF is discussed in Section 3.2, where both simulated and measurement results are analysed and compared. Conclusions are drawn in Section 3.3.

## **3.1 Intrinsic Field Uncertainty**

In addition to the measurement instrumentation uncertainty outlined in [5, 6], intrinsic field uncertainty is specified as one of the largest MU contributions towards the total uncertainty budget of the RC. However, the evaluation of IFU is only meaningful when an RC is in its ideal working condition (over-mode regime). For typical operational conditions, the magnitude of the MU contributed from IFU is greater by one or more orders than the measurement instrumentation uncertainty [44]. In general, a characteristic of EMC/EMI testing in an RC is that the contribution of IFU to the MU is limited only by the number of independent stir states  $N$  that are generated [44]. The standard error of the average received power in the chamber decreases with

$N$  in accordance with  $1/\sqrt{N}$ . Thus, IFU can be reduced by improving the stirring mechanism or by increasing the number of stirrers for a more consistent averaging in the chamber.

### **3.2 Investigation of Field Uniformity at Lowest Usable Frequency**

Unlike the mode-stirred operation, an RC using the mode-tuned operation has a mechanical tuner rotating in a discrete stepwise manner [24, 45-47]. The number of independent samples which can be obtained during one tuner rotation has been considered as one important factor which may affect the chamber performance with respect to electric field uniformity and MU. As discussed in the previous section, MU in the reverberation chamber depends substantially on its IFU. IFU, however, is determined by the number of independent samples which the stirrer/tuner can generate in the RC. It has been revealed that, near the LUF, the RC is working in the under-mode regime. As a result, it is often difficult to achieve field uniformity and the samples collected in one tuner rotation may be correlated; therefore affecting the measurement accuracy and reproducibility.

A number of works have been conducted in attempts to improve chamber performance by analysing the uncorrelated field distributions in the RC. These works focus on:

- 1) tuner positions [48-50] and design parameters [51-55]. The effects of different tuner positions and design parameters have been discussed in the cited works. However, there is no significant improvement with these technique when the chamber is working in the under-mode regime.
- 2) measurement correlations. For instance, effective sample size estimation based on the spatial degrees of freedom method [56], autocovariance method [57], autoregressive method [58], and sample differences method [59]. These works

focus on the assessment of the measurement correlations using different approaches. The proposed methods are able to effectively estimate the number of independent samples; however there is no practical method for generating adequate independent samples as proposed in these works.

Currently, only a small number of works have concentrated on chamber performance at low frequencies [60, 61]. The method proposed in [60] of adding absorbing material inside the chamber ensures a better performance at the LUF range; however this method may increase the chamber loading and is not suitable for a small chamber. The work mentioned in [61] only provides the validation results in addition to the standard, and no significant improvement method is proposed.

Chamber validation for the mode-tuned operation has relatively flexible requirements at low frequencies, e.g., the tolerance requirement for the electric field standard deviation at 80 MHz is 4 dB and decreases linearly to 3 dB at 400 MHz. Furthermore, a maximum of three frequencies per octave is allowed to have a standard deviation exceeding the tolerance required by 1 dB [36]. However, despite the relaxation of the requirement at low frequencies, it is still desirable to achieve a low electric field standard deviation, as more accurate measurement results can be obtained closer to the LUF.

This section focuses on the electric field uniformity and measurement uncertainty investigation by improving the number of independent samples collected during one stirrer rotation, at LUF range, for both immunity and emission testing in an RC. The use of non-equidistant tuner positions is proposed, and compared with the conventional equal step size method. The main purpose is to reduce the impact of the tuner symmetries near the LUF. As the use of non-equidistant tuner positions acts as sample shuffling, periodicity will be disturbed, and fewer correlated samples can be obtained during one tuner rotation. The investigation is conducted through intensive simulations based on empirical study.

Test set up parameters (different transmitting antenna orientations as well as random sets of discrete, non-equidistant tuner positions), which offer significant improvements in electric field uniformity compared to conventional equidistant tuner positions, are selected and discussed. The results are then verified with actual measurements in the chamber.

### **3.2.1 Geometry and Test Set-up**

The RC performance using different transmitting antenna orientations and random sets of discrete tuner positions are simulated using CST STUDIO SUITE® 2015, and the model is shown in Fig. 3.1. The RC's dimensions are 2.25 m in length, 1.95 m in width, and 2.03 m in height. Only one tuner is used in the simulation model due to the chamber's relatively small size. The paddle size is 0.5 m x 0.6 m x 1.5 m, and three elliptical holes of different sizes are made in the paddle's upper, lower, and central elements for better stirring performance. The simulation model's LUF is 400 MHz. A log-periodic antenna is used as the transmitting antenna, with operating frequencies from 300 MHz to 7 GHz, and excited by the ideal power source. The transmitting antenna is placed in the chamber with two different orientations, as shown in Fig. 3.1, to observe the effects on the electric field uniformity with the use of different incident angles. Such orientations are: 1) parallel to the  $x$ - $y$  plane and pointed to the tuner; 2) and then, rotated 45 degrees clockwise with reference to the feeding point.

To study the performance of the RC near the LUF with the minimum required tuner positions stated in [36], twelve tuner positions are chosen in the experiment as the worst case scenario. In fact, it is not necessary to further increase the tuner steps since both simulation and measurement results of this investigation fulfil the uniformity requirement stated in [36].

As mentioned in the previous section, the choice of non-equidistant tuner positions is based on empirical study, and through intensive simulation of the electric field

uniformity within the chamber. An initial set of non-equidistant tuner positions is proposed based on:

$$P(n) = 2n(n + 3) \quad (21)$$

where  $n = 0, 1, 2, \dots, 11$ . The positions are then obtained as 0, 8, 20, 36, 56, 80, 108, 140, 176, 216, 260, and 308 degrees respectively (Set 1 positions). The differences between two adjacent steps are non-equal, with an increasing factor of 4 degrees. To further compare the effects of different step sizes, five other sets of non-equidistant positions are generated by randomly altering the differences between the adjacent steps of Set 1 positions. The chamber performance, in terms of electric field uniformity, using all five different sets of non-equidistant positions, is then simulated. Together with Set 1 positions, the set of non-equidistant positions (Set 2 positions) with the best performance among the other five sets of data is selected and compared with the conventional equidistant tuner positions. For brevity, only the simulation and measurement results of using equidistant and Sets 1 and 2 non-equidistant tuner positions (as shown in Table 3.1) are presented in this chapter. Since the LUF range is

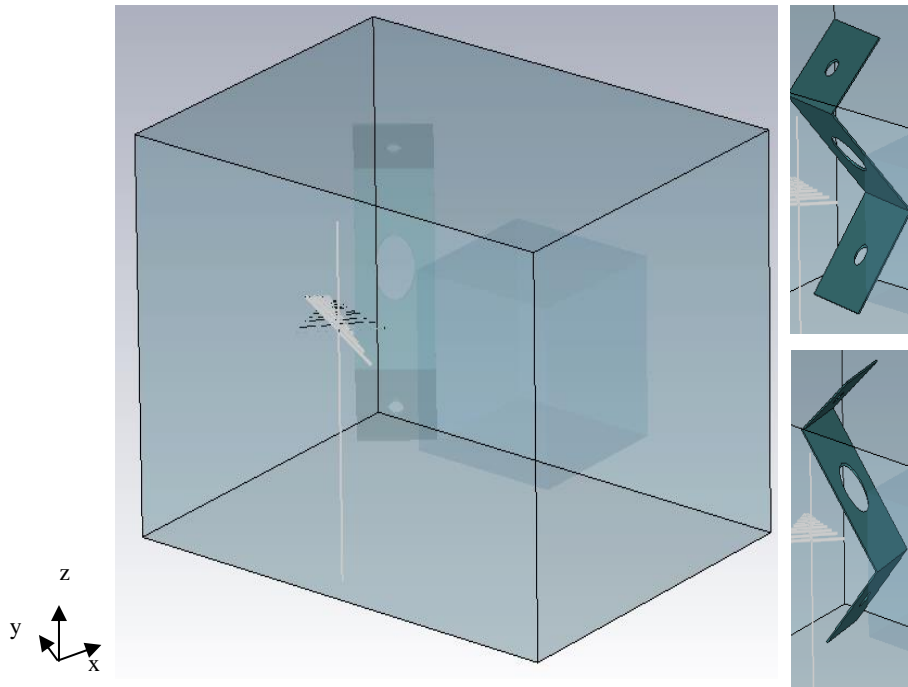


Fig. 3.1 RC simulation model in CST 2015

of interest, the investigation is conducted in the frequency range from 400 MHz to 800MHz, with a total of eleven frequency points.

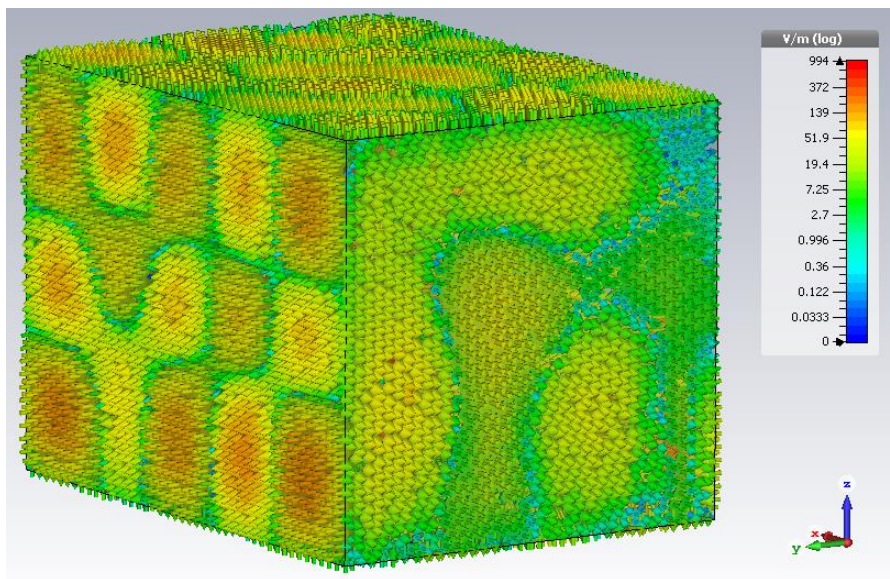
Table 3.1 Non-equidistant tuner positions selected in the investigation

Set 1 positions (degree)	0, 8, 20, 36, 56, 80, 108, 140, 176, 216, 260, 308
Set 2 positions (degree)	0, 27, 42, 66, 93, 116, 148, 176, 215, 236, 280, 328

It cannot be guaranteed that the selected non-equidistant tuner positions are the optimum solution; however it is of interest for this investigation to demonstrate the superiority of using non-equidistant tuner positions over equidistant tuner positions at the LUF. It is worth noting that the proposed set of tuner positions may not be generally applicable for all chambers of different size or with different stirrer structure, and additional empirical studies should be carried out for different chambers. Thus, the purpose of this investigation shall be fulfilled if a better electric field uniformity can be achieved using the proposed non-equidistant tuner positions.

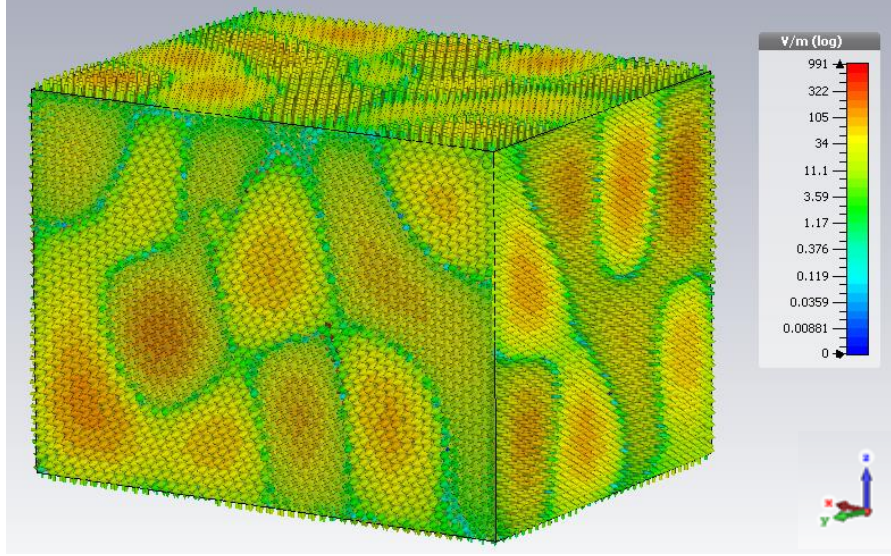
### 3.2.2 Results and Discussions

#### 3.2.2.1 Simulation Results

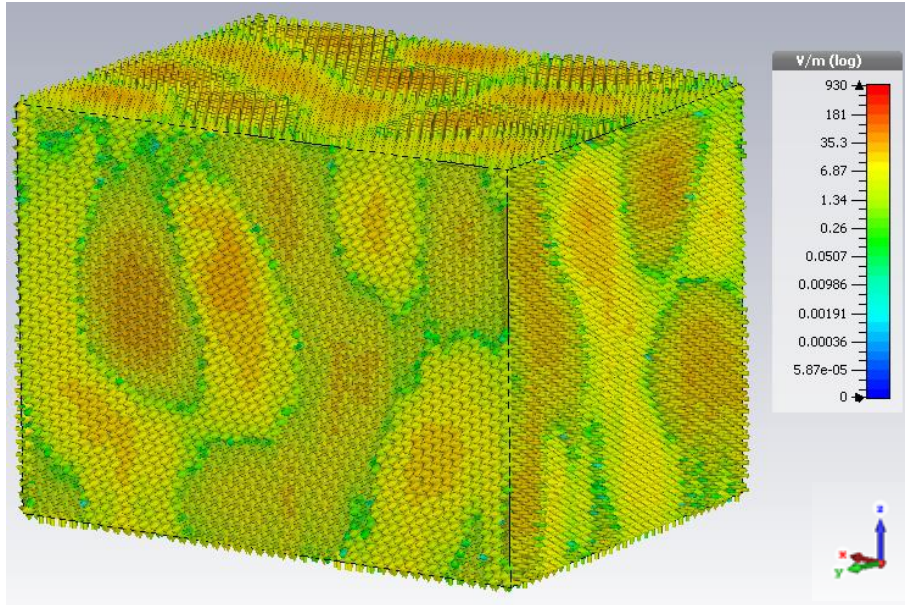


(a)





(b)

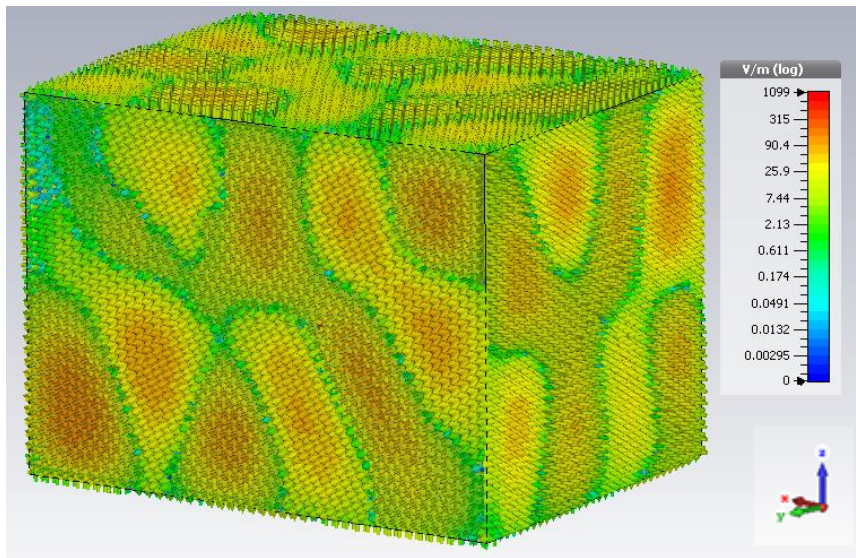


(c)

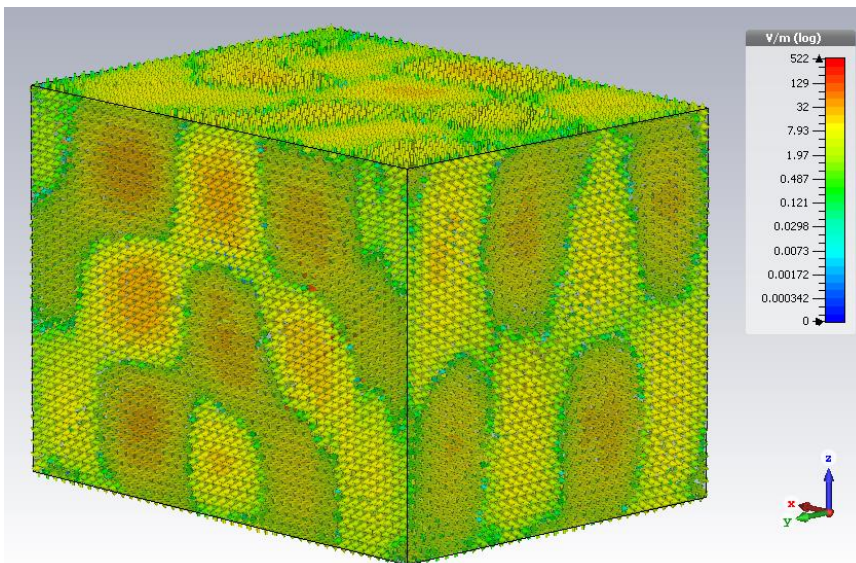
Fig. 3.2 Simulation results of the electric field distribution using: (a) equidistant tuner positions; (b) non-equidistant Set 1 positions; and (c) non-equidistant Set 2 positions, at 400 MHz with transmitting antenna parallel to  $x$ - $y$  plane.

The RC performance is first simulated to investigate the electric field distribution. Generally, the electric field uniformity can be observed and estimated by comparing field distribution using different tuner positions. Fig. 3.2 illustrates that, when the transmitting antenna is placed parallel to the  $x$ - $y$  plane and pointed to the tuner, better

electric field uniformity is achieved at 400 MHz (LUF) by using non-equidistant tuner positions (Set 1 and Set 2) than by using equidistant tuner positions. However, there is no significant difference observed between the use of Set 1 and Set 2 positions. The transmitting antenna is then rotated 45 degrees clockwise with reference to its feeding point. The electric field distributions are presented in Fig. 3.3. Similarly to the previous scenario, the field distributions are shown to be more uniform when using Set 1 and Set 2 positions than when using equidistant tuner positions.

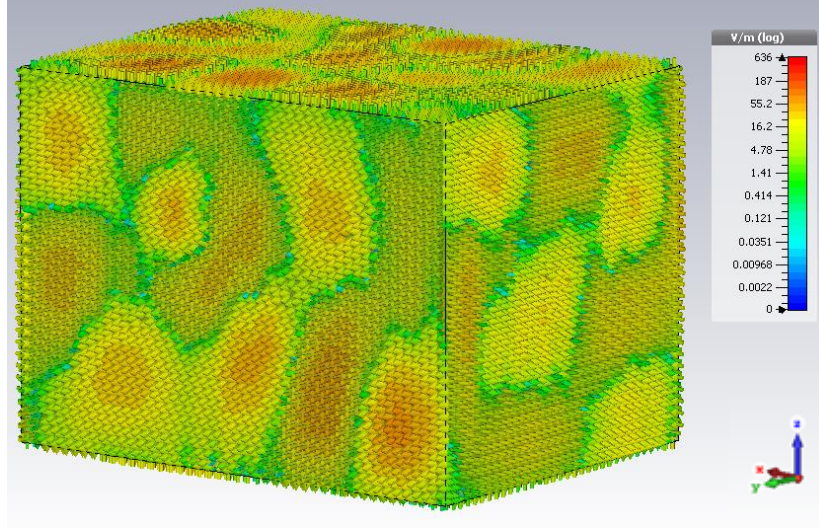


(a)



(b)





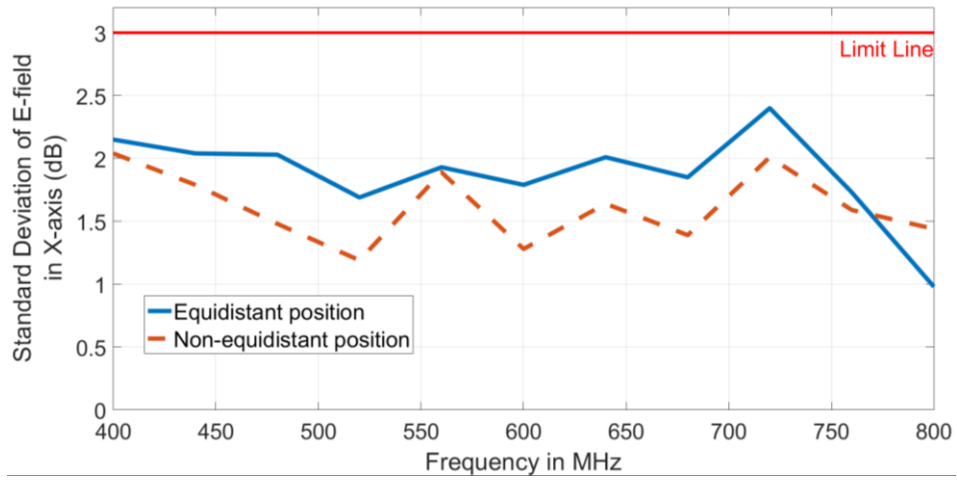
(c)

Fig. 3.3 Simulation results of the electric field distribution using: (a) equidistant tuner positions; (b) non-equidistant Set 1 positions; and (c) non-equidistant Set 2 positions, at 400 MHz with transmitting antenna rotated 45 degrees clockwise.

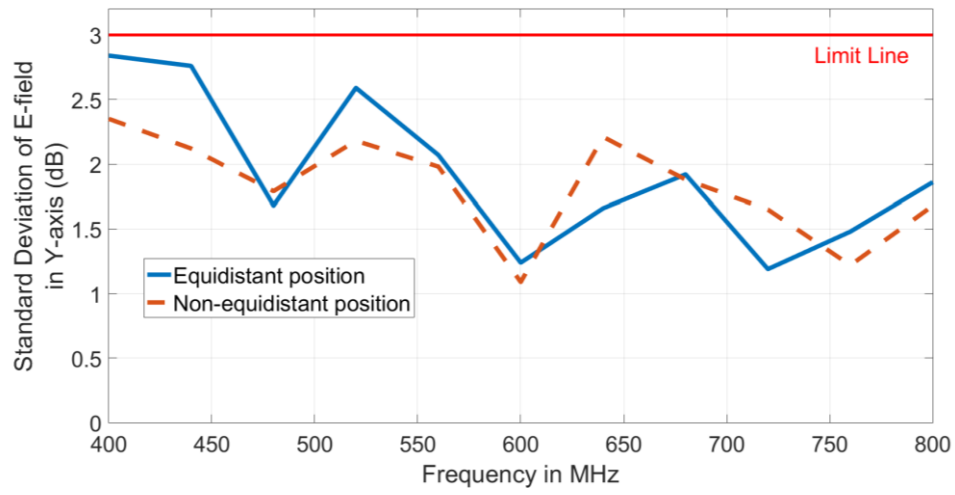
The advantage of using non-equidistant over equidistant tuner positions has been briefly illustrated in the simulated electric field distribution results. To further validate the observation, field uniformity is verified based on the standard deviation from the maximum normalised values obtained at each of the eight probe locations within the working volume during one tuner rotation using equation (18) described in Section 2.5.

For transmitting antenna parallel to the  $x$ - $y$  plane, the results of standard deviations of both equidistant and non-equidistant tuner positions (using Set 1 positions) from 400 MHz to 800 MHz are presented in Fig. 3.4. It is clear that, near the LUF, e.g., 400 MHz and 440 MHz, the standard deviations of all three axes are below the required value of 3 dB for both equidistant and non-equidistant tuner positions. However, the standard deviation of the total data sets (24 normalised maximum values) exceeds the limit of 3 dB using the equidistant method at both frequency points.

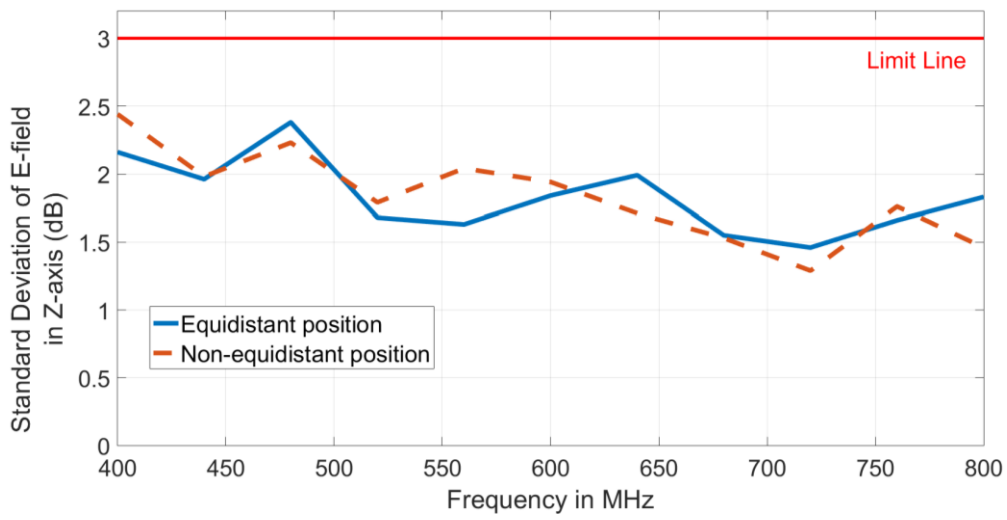
On the other hand, using non-equidistant tuner positions produces better results. At 440 MHz, the standard deviation of the total data set is less than 3 dB, and the value only exceeds the limit by 0.06 dB at 400 MHz, as illustrated in Fig. 3.4 (d). The



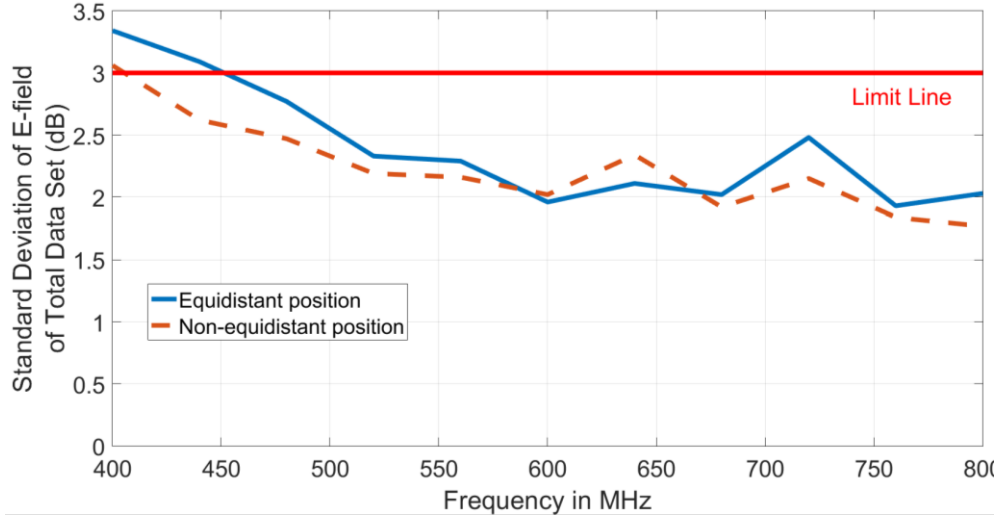
(a)



(b)



(c)

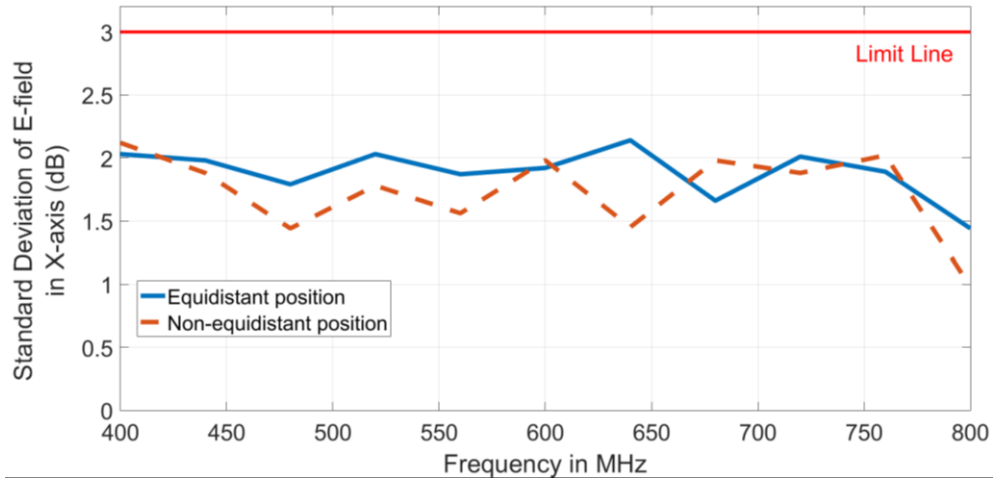


(d)

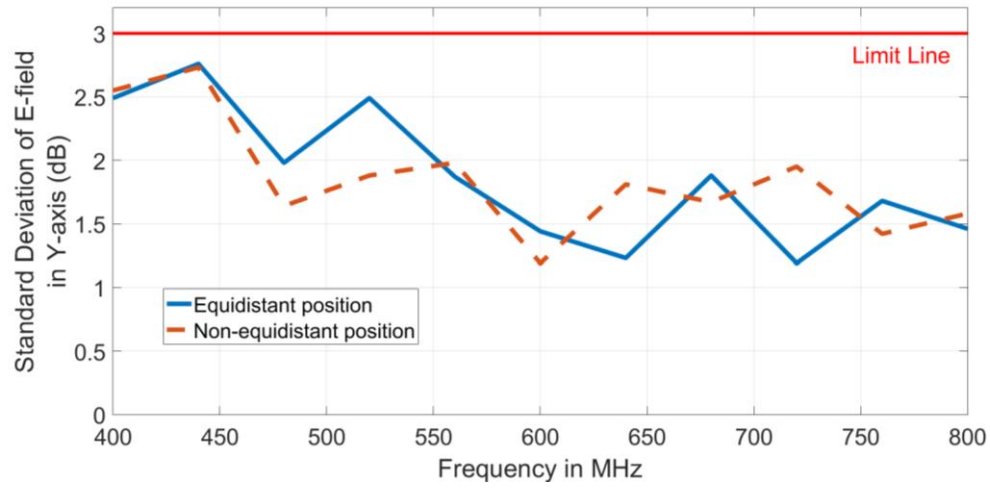
Fig. 3.4 Equidistant and non-equidistant positions (Set 1) comparison of standard deviations for E-field components of eight probes for: (a) x-axis; (b) y-axis; (c) z-axis; and (d) total data set, with transmitting antenna parallel to  $x$ - $y$  plane.

standard deviations when using non-equidistant positions are 0.3 dB and 0.47 dB lesser than those when using equidistant tuner positions, respectively, for the total data set at 400 MHz and 440 MHz. Meanwhile, the observation of less widely distributed electric field values across three axes also implies that the use of non-equidistant tuner positions is superior to the use of equidistant tuner positions.

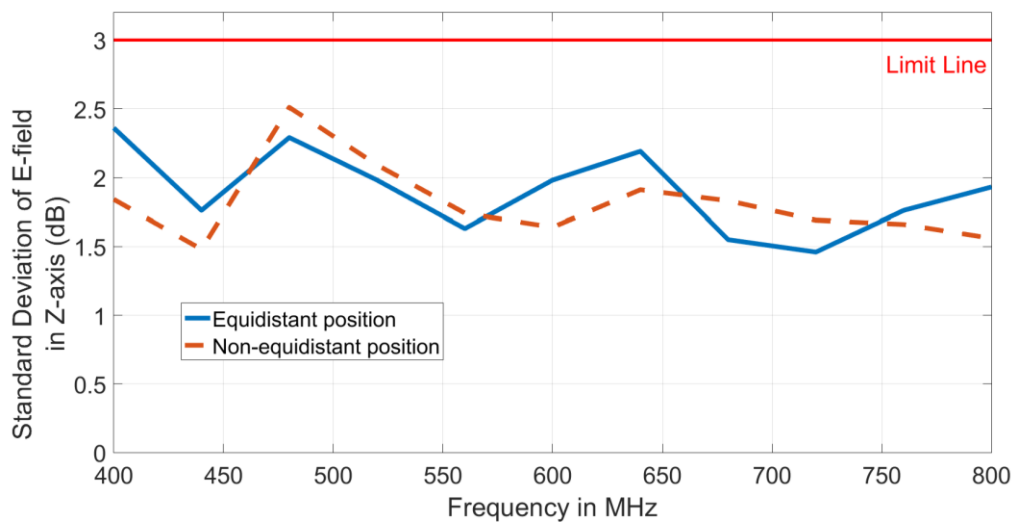
A further comparison has been carried out between equidistant positions and non-equidistant positions using Set 2 data. Similar to the observations using Set 1 positions, the standard deviations using non-equidistant positions are smaller than when using equidistant tuner positions for the total data set at 400 MHz and 440 MHz, as illustrated in Fig. 3.5 (d). Nonetheless, it can be seen that for non-equidistant tuner positions, the standard deviations for all three axes are comparable using Set 1 and Set 2 data. There is no significant difference between the two sets of tuner positions while the transmitting antenna remains parallel to the  $x$ - $y$  plane.



(a)



(b)



(c)

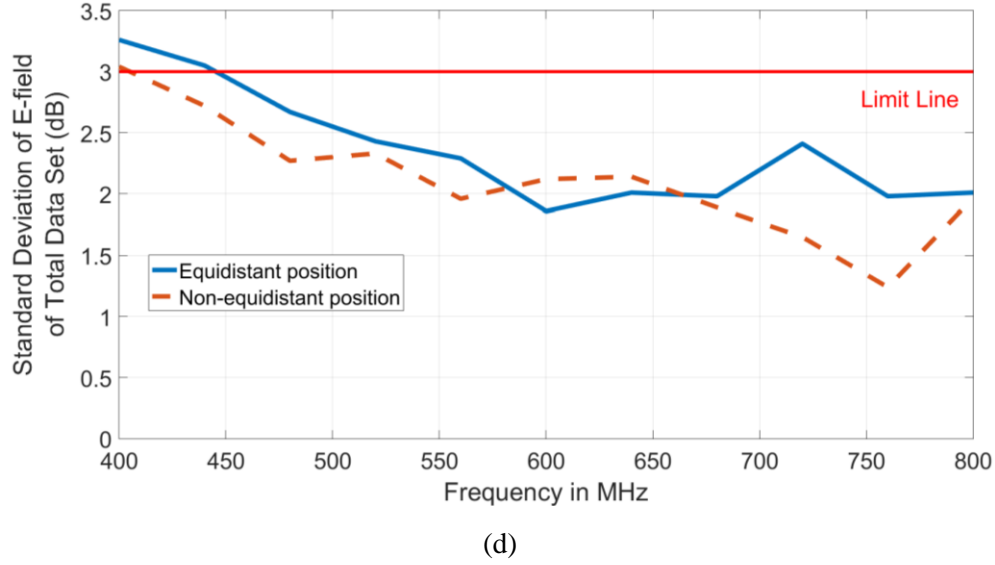
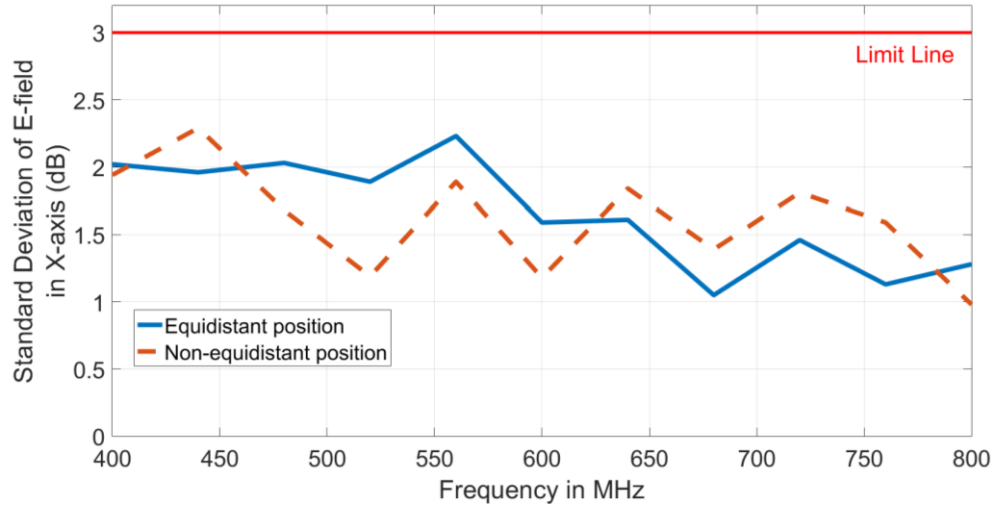


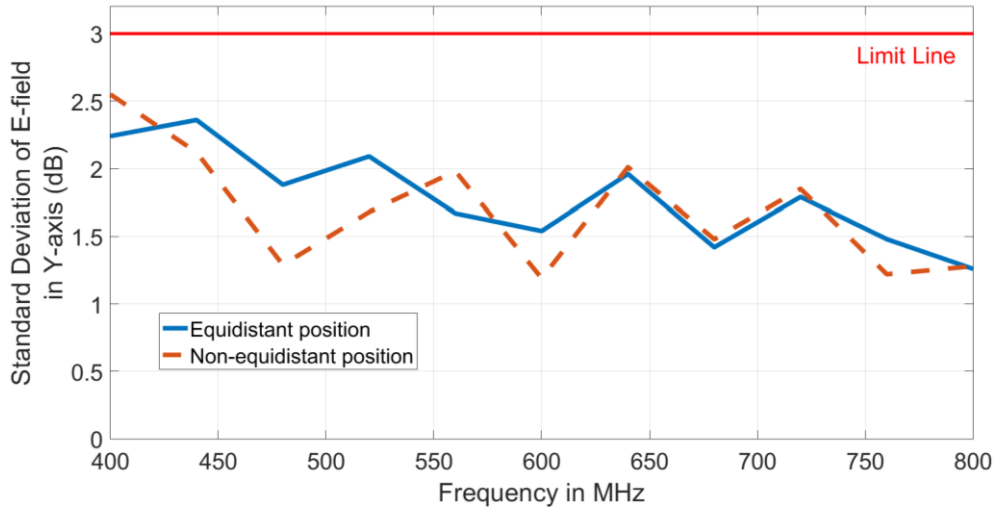
Fig. 3.5 Equidistant and non-equidistant positions (Set 2) comparison of standard deviations for E-field components of eight probes for: (a) x-axis; (b) y-axis; (c) z-axis; and (d) total data set, with transmitting antenna parallel to the  $x$ - $y$  plane.

The transmitting antenna is then rotated 45 degrees clockwise with reference to its feeding point. The same testing procedures are followed as aforementioned for both equidistant and non-equidistant tuner positions (using Set 1 and Set 2 positions respectively). The comparisons are plotted and presented in Fig. 3.6 and Fig. 3.7. It can be observed that, when the transmitting antenna is rotated 45 degrees clockwise and Set 2 positions are used, the standard deviation of the total data set is the smallest of all the combinations of parameters, as illustrated in Fig. 3.7 (d). The value only exceeds the limit by 0.03 dB at 400 MHz.

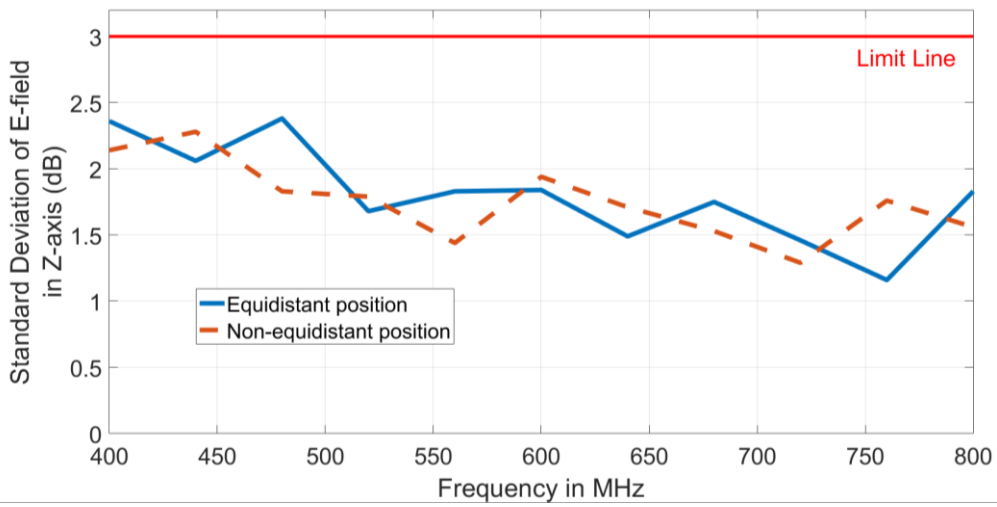
Furthermore, the lowest fluctuation in the standard deviation observed also implies a more stable averaging of the electric field of the three axes within the working volume. Thus, it is suggested that this set of parameters could be used as one of the optimal solutions to improve the chamber performance at the LUF range.



(a)

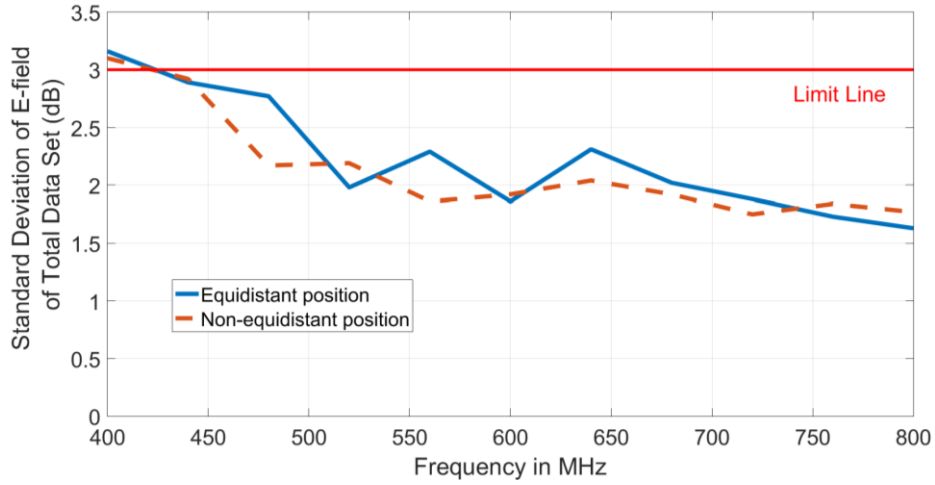


(b)



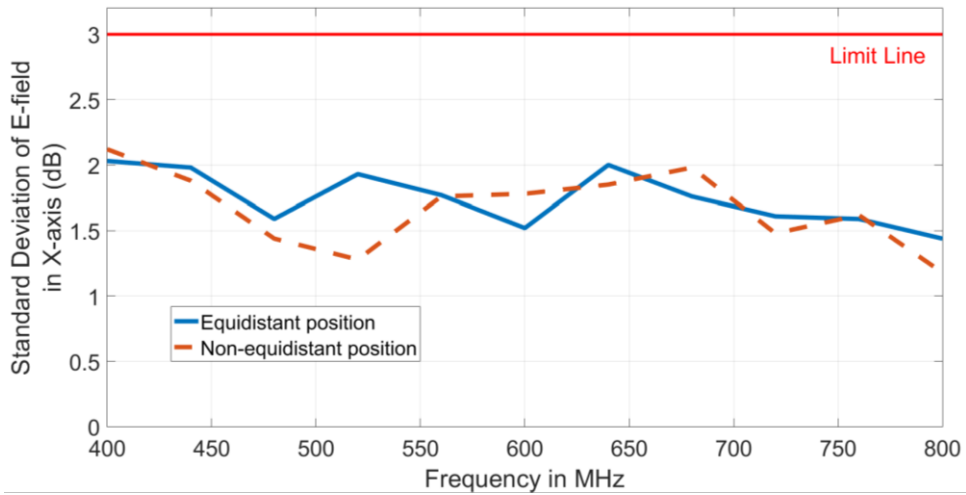
(c)



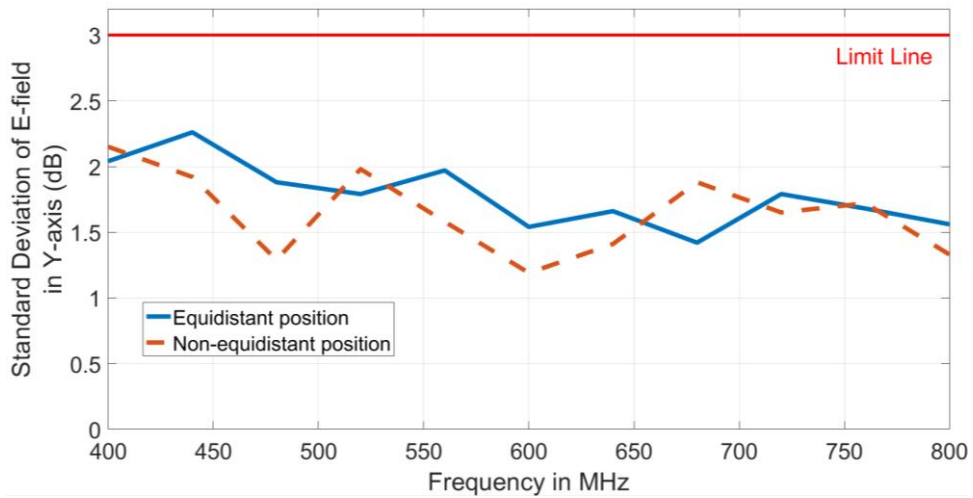


(d)

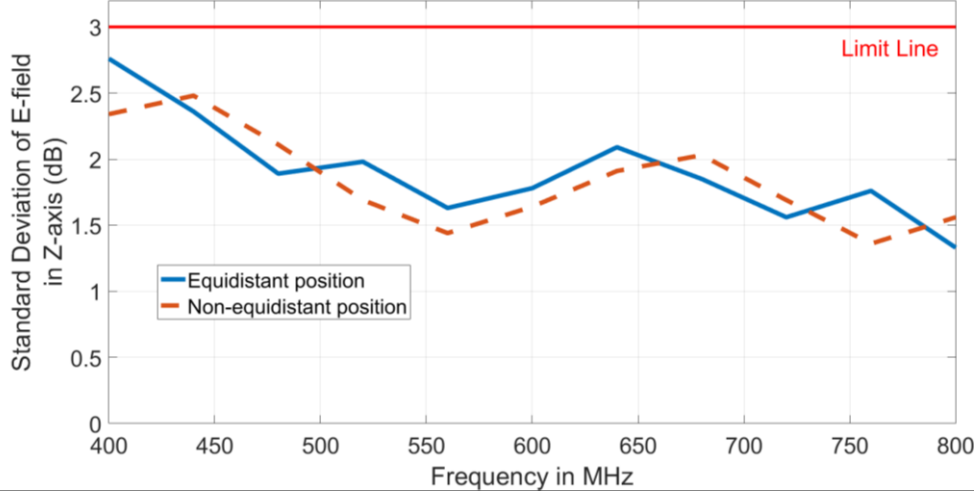
Fig. 3.6 Equidistant and non-equidistant positions (Set 1) comparison of standard deviations for E-field components of eight probes for: (a) x-axis; (b) y-axis; (c) z-axis; and (d) total data set, with transmitting antenna rotated 45 degrees clockwise.



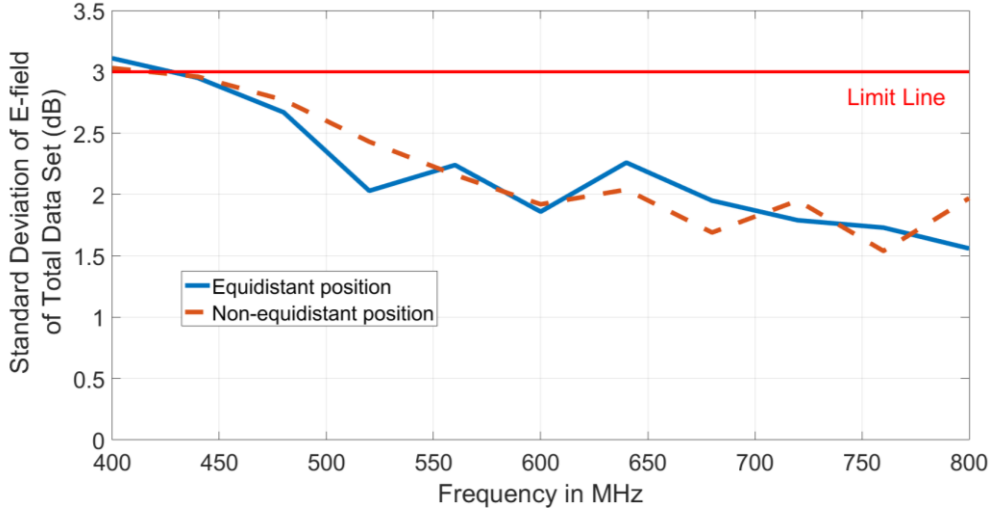
(a)



(b)



(c)



(d)

Fig. 3.7 Equidistant and non-equidistant positions (Set 2) comparison of standard deviations for E-field components of eight probes for: (a) x-axis; (b) y-axis; (c) z-axis; and (d) total data set, with transmitting antenna rotated 45 degrees clockwise.

The field uniformity has been verified using the aforementioned non-equidistant tuner positions. Furthermore, it is also important to observe the tuner efficiency when using the non-equidistant method. In [36], the tuner efficiency is assessed by the number of independent samples collected over one tuner rotation. From  $f_s$  (starting frequency) to  $3f_s$ , a minimum number of twelve independent samples are required. The independence of the samples is verified using the autocorrelation coefficient. In this investigation, the critical value  $\rho_0$  presented in [62] is employed.  $\rho_0$  is defined as the

upper bound of the integral of the probability density function of the correlation coefficient, given an error probability (5% for the purposes of this thesis). The value of the correlation coefficient lies between -1 to 1, where -1 and 1 correspond to completely correlated data, and 0 corresponds to completely uncorrelated data. The correlation coefficient is computed using the equation below:

$$r_{x,y} = \frac{\frac{1}{n-1} \sum_i^n (x_i - u_x)(y_i - u_y)}{\sqrt{\frac{1}{n-1} \sum_i^n (x_i - u_x)^2 \times \frac{1}{n-1} \sum_i^n (y_i - u_y)^2}} \quad (22)$$

where  $y_i$  is the same series of data as  $x_i$ , but is shifted by one sample to the right, e.g.,  $x_i = x_1, x_2, x_3, x_4, \dots, x_{n-1}, x_n$ ; and  $y_i = x_n, x_1, x_2, x_3, \dots, x_{n-2}, x_{n-1}$ .  $u_x$  and  $u_y$  are the mean of the original received power versus tuner position data set, and  $n$  is the number of samples collected during one tuner rotation. To obtain the result, the received power for equidistant and non-equidistant tuner positions is recorded, for twelve tuner steps. The number of independent samples is calculated for 400 MHz, 440 MHz, 480 MHz, and 520 MHz respectively. The correlation coefficients for both equidistant and non-equidistant methods are tabulated against the critical value (with 95% confidence interval in contrast to 5% error probability). Collected samples are considered to be independent if the correlation coefficient between two adjacent samples is smaller than the critical value. Results are calculated and presented in Table 3.2.

It can be observed that, at LUF (400 MHz), both methods are able to obtain only six independent samples instead of twelve. This provides an explanation for why the standard deviation of the total data set exceeds the limit at 400 MHz for both methods. At 440 MHz, the non-equidistant method is capable of obtaining twelve independent samples; whereas the equidistant method still has its data correlated, and only six independent samples can be obtained when the transmitting antenna is placed parallel to the  $x$ - $y$  plane. However, when the transmitting antenna is rotated 45 degrees clock

Table 3.2 Comparison of number of independent samples for equidistant and non-equidistant methods

Frequency	Number of independent samples using equidistant positions with transmitting antenna		Number of independent samples using equidistant positions with transmitting antenna			
	parallel to $x$ - $y$ plane	rotated 45 degrees clockwise	parallel to $x$ - $y$ plane		rotated 45 degrees clockwise	
			Set 1	Set 2	Set 1	Set 2
400 MHz	6	6	6	6	6	6
440 MHz	6	12	12	12	12	12
480 MHz	12	12	12	12	12	12
520 MHz	12	12	12	12	12	12

-wise from its original position, twelve independent samples can be collected using equidistant tuner positions. From 480 MHz, both methods are able to generate twelve independent samples. From the simulation results, it is observed that more independent samples at frequencies close to LUF range can be generated using the non-equidistant method, which implies that the samples collected are less correlated. Thus, MU is reduced since field uniformity is improved. Since a better result can be achieved using Set 2 non-equidistant positions with the transmitting antenna rotated 45 degrees clockwise with respect to its feeding point, practical measurement for result verification has been carried out in the chamber using the mentioned parameters.

### 3.2.2.2 Measurement Results and Discussion

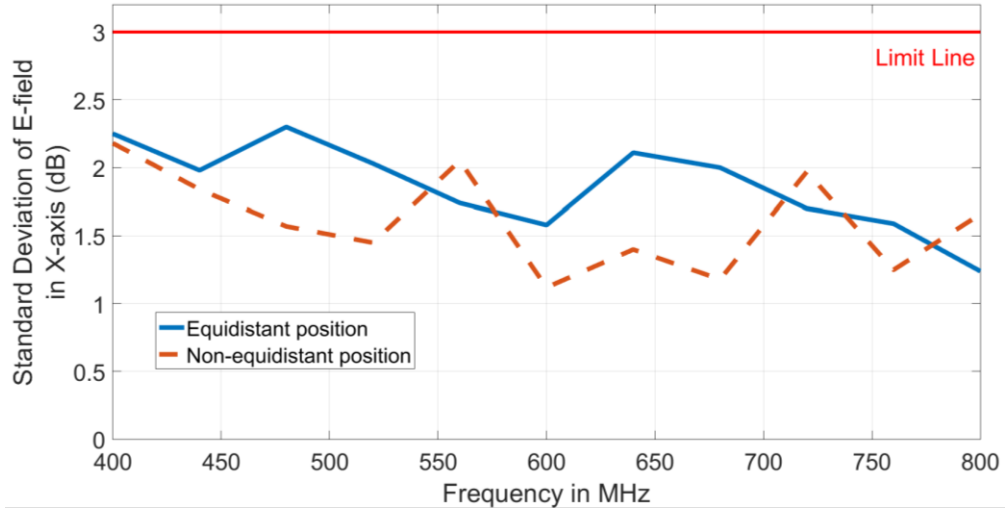
The simulation results have been verified in the RC, as presented in Fig. 2.5. The chamber size is 2.25 x 1.95 x 2.03 m, with a working volume of 0.8 x 0.8 x 0.8 m. Chamber validation has been conducted using the theories and equations as provided in Chapter 2 in terms of chamber loading, field uniformity, and  $Q$  factor. The transmitting antenna is mounted on the chamber wall and pointed directly to the tuner. The probe is placed at eight corner positions of the working volume to collect the

electric field strength data. The testing procedures strictly follow those mentioned in [36]. During the testing in each corner position, both the probe and the receiving antenna are placed in a new location (the receiving antenna is always placed within the working volume). The tuner positions are selected as described in Section 3.2.2.1. Similar to the simulation procedures, the measured results are processed and presented in the form of standard deviations of the three axes and the total data set.

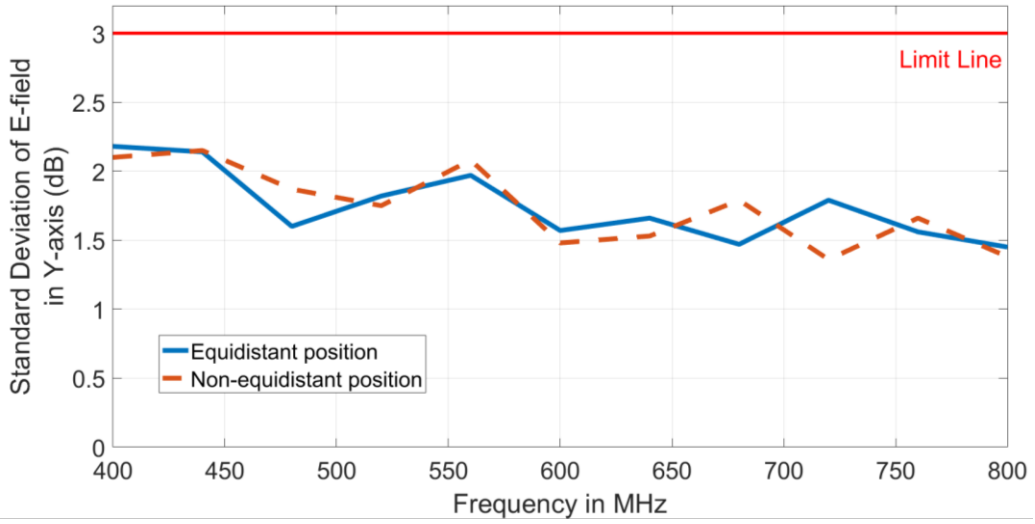
Fig. 3.8 illustrates the consistency between the simulation and measurement results. The standard deviations of the electric field of the three axes and total data set are below the required 3 dB for both equidistant and non-equidistant methods at 440 MHz. It is worth noting that, during the actual measurement, the standard deviation of the total data set is below 3 dB for the non-equidistant method at 400 MHz, in contrast to the simulation result.

On the other hand, even though the standard deviation of the total data set exceeds the limit at 400 MHz using equidistant tuner positions, the chamber validation is still considered as passed. The requirement in [36] indicates that a maximum of three frequencies per octave may exceed the allowed standard deviation by an amount not exceeding 1 dB of the required tolerance. The transmitting antenna orientation and non-equidistant tuner positions selected for the experiment have been validated with the measurement results, and it is observed that this set of parameters could eventually improve the chamber performance in the LUF range as compared to its performance using the conventional equidistant tuner positions.

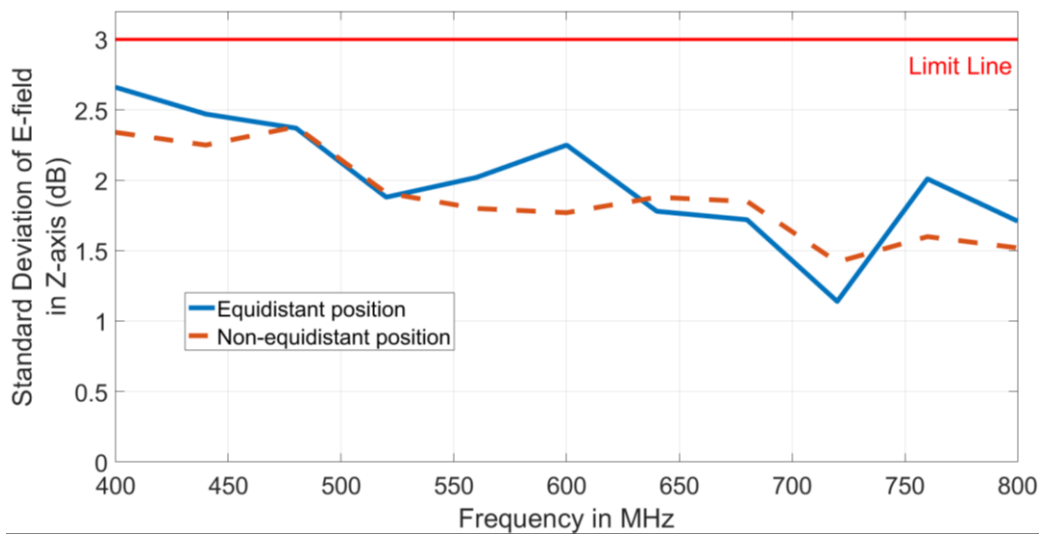
Another observation is that, during the actual measurement, tuner rotation control for the non-equidistant method is not optimised as a longer time was taken for the measurement to be completed. Further work on rotation control should be carried out if the non-equidistant method is to be implemented.



(a)



(b)



(c)

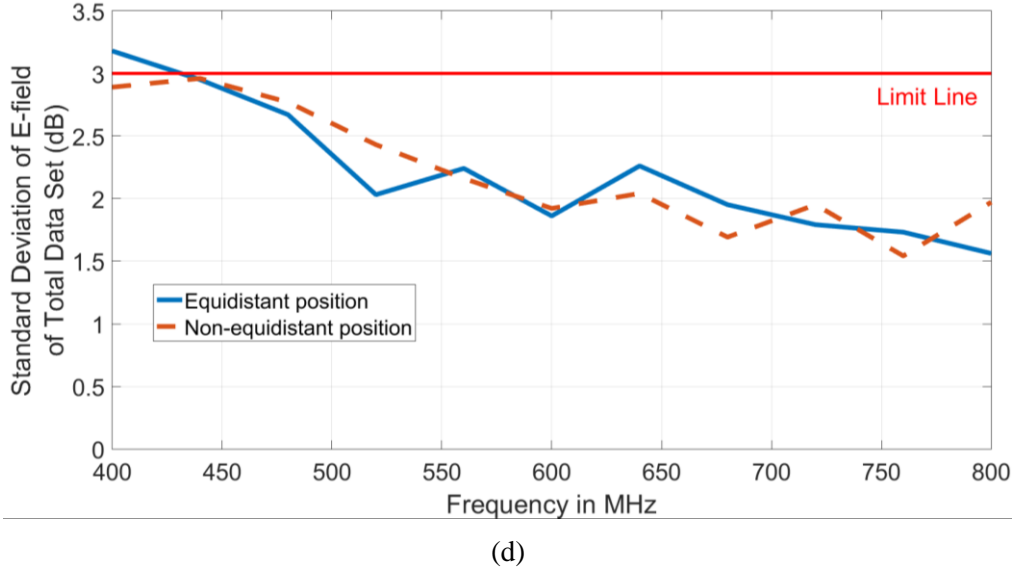


Fig. 3.8 Measurement results of standard deviation for E-field components of eight probes for: (a) x-axis; (b) y-axis; (c) z-axis; and (d) total data set, with transmitting antenna rotated 45 degrees clockwise.

### 3.3 Conclusion

This chapter investigates the use of non-equidistant tuner positions in an RC. The main focus is to determine the chamber performance, in terms of electric field uniformity and tuner efficiency, using non-equidistant tuner positions as compared to the conventional equidistant tuner positions. Both simulation and measurement results have been discussed, and it is observed that better field uniformity at LUF can be achieved using non-equidistant tuner positions. The standard deviations of the electric field in  $x$ ,  $y$ , and  $z$  directions and the total data set have been calculated, and are below the required limit of 3 dB using the parameters proposed in Section 3.2.2.1, with Set 2 non-equidistant tuner positions and 45 degrees clockwise-rotated transmitting antenna. The chamber performance is thus improved and more independent samples can be generated at frequencies near LUF. The MU in the RC is substantially dependent on the IFU, which is inversely proportional to the square root of the independent samples generated by the stirrer. This implies that the MU has been reduced; thus reproducibility is improved using the non-equidistant method.

## CHAPTER 4 CHARACTERISATION OF MEASUREMENT

### UNCERTAINTY IN A RADIATED EMISSION SYSTEM

#### 4.1 Background

The major MU contributions in a radiated emission test system are presented in Fig. 4.1. A number of research works have been carried out on radiated emission tests during the past decade to identify MUs associated with:

- 1) antenna design and parameters (e.g., the antenna pattern influence [19], uncertainty due to different types of receiving antenna [63-65], the ground plane effect [66], and uncertainty related to antenna calibration [18, 67]);
- 2) receiving apparatus (e.g., uncertainty evaluation for digital test receivers [68, 69], optical link based receivers [70], uncertainty of measurement time [71], and test receiver uncertainty overview [17]); and
- 3) uncertainty related to an open area test site [72, 73] or anechoic chamber [74], site imperfections [72-75], and test processes [11, 76, 77].

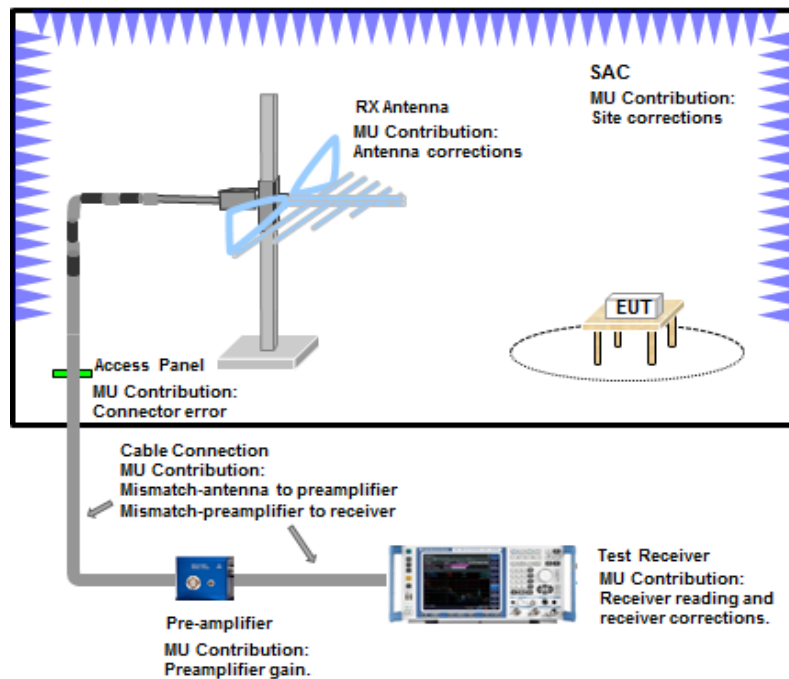


Fig. 4.1 Measurement uncertainty contributions in a typical radiated emission system



However, certain practical considerations in relation to the individual component level are absent from the existing literature. For instance, the performance of RF adapters is often neglected in measurements; however these adapters are likely to introduce unexpected errors (high insertion loss, etc.) due to manufacturing defects, and improper or prolonged use.

During most calibration processes, the entire cable path, together with all the connectors, is calibrated so that insertion loss of the RF connectors can be properly compensated. However, if a defective RF connector is used between the reference cable and the cable under calibration, the resulting errors will be mistakenly counted as part of the total cable path loss and compensated for when every real measurement is subsequently performed. Therefore, final measurement results will be affected. Thus, a proper characterisation, for instance, using a vector network analyser to verify the performance of an RF connector, should be carried out before it is used for any connection purpose. Alternatively, at least a few properly working connectors should be maintained for connecting the reference cable and the cable under calibration during the calibration process.

Lately, EMI test receivers have been recommended by CISPR, FCC, MIL-STD, EN, and all other standard-issuing bodies for EMC/EMI applications and tests. These test receivers usually consist of superheterodyne equipment which has been carefully designed to accurately measure the amplitude of CW or impulse signals [78]. The necessary requirements of the radio disturbance and immunity measuring apparatus and relevant methods have been well defined in CISPR 16-1-1 [79]. Most of the test receiver-related MU contributions can be retrieved from the test receiver's calibration report, e.g., sine wave voltage variation  $\sigma V_{SW}$ , noise floor proximity, and  $\sigma V_{nf}$ .

However, some sources of uncertainties remain which have not been identified in the measurement standards. For instance, signal synchronisation is often neglected

when using the signal generator together with the test receiver for cable calibration. It may sometimes be assumed that, by performing the normalisation process prior to a cable calibration, any error caused by the signal generator and the test receiver can be eliminated as both the normalisation and cable calibration processes are using the same settings. However, since the filter window of the test receiver may capture the wrong position for a given resolution bandwidth (RBW), the normalisation process is not able to eliminate this error. This can lead to either missing the peak value, or capturing the wrong peak value, with a given RBW setting. In a worst case scenario, the cable attenuation measurement results can have a difference of more than a few dB, with and without reference signal synchronisation between the signal generator and the test receiver. Thus, it is important for test laboratories to ensure that the reference signal is synchronised between the signal generator and the test receiver before both instruments are used for cable path attenuation measurement.

In addition to the aforementioned suggestions for RF adapters and reference signal synchronisation, it is the purpose of this chapter to provide further important insight into the characterisation of uncertainties, of which some aspects are either absent from or not practically considered in the actual measurements. The results obtained in this chapter are intended to supplement the existing standard for the industry.

## **4.2 RF Adapter**

As outlined in Section 4.1, when an RF adapter is used to connect the reference cable and the cable under calibration, the characteristic of the adapter may not be properly compensated for in the system. Furthermore, in [6], the uncertainty contributed by the RF adapter is not practically considered. Thus, in addition to the suggestion made in Section 4.1, it is of interest in this section to characterise the typical MU contribution of the RF adapter and to make necessary recommendations to the

existing standard when the adapter is used connect the reference cable and the cable under calibration.

The MU of a widely used, high precision N-type to N-type RF connector (working frequency from DC to 18 GHz) manufactured by SRI Connector Gage Company, is evaluated. The insertion loss of this RF connector is measured (using a vector network analyser (VNA) from Rohde & Schwarz, model ZVA 40) in the frequency range from 10 MHz to 40 GHz through R&S Network Analyser Measurement Uncertainty Calculation software. Thus, the MU of the network analyser is included in the measurement. The measurement is conducted in a controlled environment at a temperature of 25 °C and a humidity level of 55% RH.

To obtain the measurement uncertainty associated with the insertion loss, the measurement is repeated twenty times. The mean value of the insertion loss  $\bar{x}$  is recorded, and the standard uncertainty  $\mu_s$  which is equivalent to the standard deviation at different frequencies can be calculated using the following formula [80]:

$$\mu_s = \sqrt{\frac{\sum_{i=1}^n (x_i - \bar{x})^2}{n - 1}} \quad (23)$$

where  $n$  is the number of measurements,  $x_i$  is the result of the  $i$ th measurement; and the results are presented in Table 4.1. It can be seen that, as expected, the standard uncertainty increases with an increase in frequency. The value of the standard uncertainty changes markedly from 13 GHz to 18 GHz. This suggests that the performance of the adapter is less stable at higher frequencies. The maximum standard uncertainty occurs at 18 GHz, which is around 0.077 dB; thus the expanded uncertainty with 95% confidence interval can be obtained as:

$$U_{\text{adapter}} = 2\mu_s \approx 0.15 \text{ dB} \quad (24)$$

It is suggested that the regulatory authority consider including the  $U_{\text{adapter}}$  in the current MU budget tables as stated in [6]. Typically, the MU budget tables for EMI

tests are segmented into different frequency ranges: for instance, 30 MHz to 1 GHz; 1 GHz to 6 GHz; and 6 GHz to 18 GHz. The expanded uncertainties of the RF adapter calculated from Table 4.1 for 30 MHz to 1 GHz, and for 1 GHz to 6 GHz, are only 0.004 dB and 0.008 dB, which are negligible. Thus, it is recommended that the  $U_{\text{adapter}}$  be included in the MU budget table from 6 GHz to 18 GHz, and that the overall expanded MU limit for this frequency range be increased by 0.15 dB for the worst case consideration.

Table 4.1 The measured insertion loss, standard deviation and standard uncertainty of an N-type to N-type RF adapter

<b>Frequency (GHz)</b>	<b>Mean Insertion Loss (dB)</b>	<b>Standard Uncertainty (dB)</b>
1	0.040	0.002
2	0.039	0.002
3	0.045	0.003
4	0.072	0.004
5	0.082	0.004
6	0.082	0.004
7	0.089	0.005
8	0.092	0.007
9	0.094	0.007
10	0.096	0.009
11	0.096	0.014
12	0.106	0.019
13	0.102	0.025
14	0.110	0.030
15	0.131	0.039
16	0.146	0.051
17	0.164	0.063
18	0.188	0.077

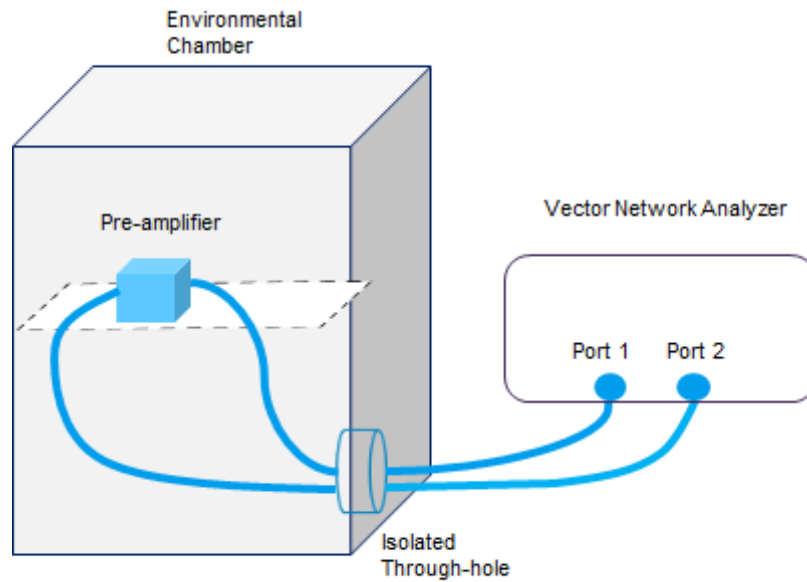
### 4.3 Pre-Amplifier Gain Variation

Typically, the pre-amplifier shall be calibrated by the manufacturer, and the necessary data, such as the instability of the amplifier gain, shall be given in the calibration report. However, these given values are normally obtained at a single fixed temperature only. This potentially leads to a larger MU at test sites operating under different temperatures. It is recommended in the measurement standards that gain variations/instabilities due to temperature variations be taken into account; however detailed methods to identify the gain variations are not provided. To address this issue, measurement campaigns are conducted to characterise the standard uncertainty associated with gain variations, and a reasonable method is proposed to determine such uncertainty.

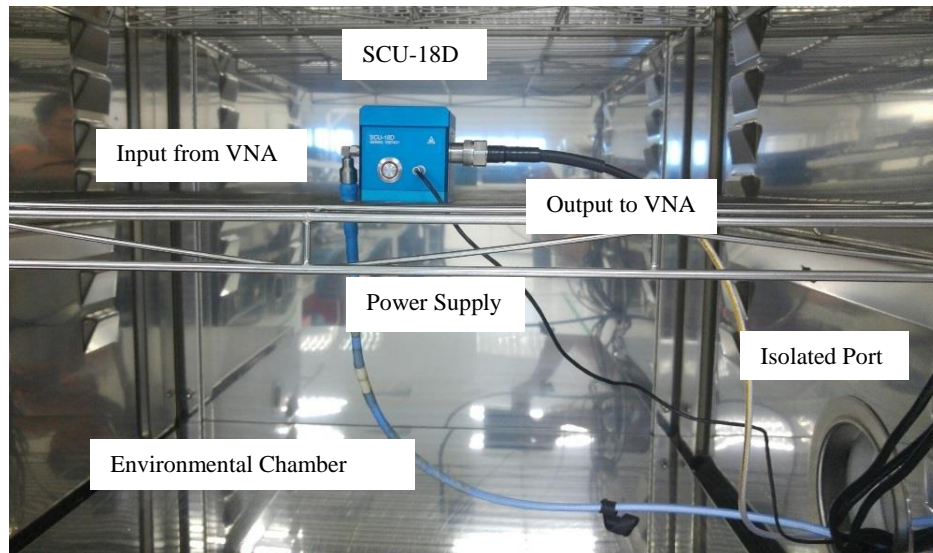
Similarly to the RF adapter measurement carried out in Section 4.2, an R&S® ZVA 40 network analyser is used in this experiment through the R&S Network Analyser Measurement Uncertainty Calculation software. The EUT used in the measurement is a pre-amplifier manufactured by R&S: model no. SCU-18D, serial no. 1747093, with an operating frequency from 1 GHz to 18 GHz, and a typical gain of 33 dB. The measurement set up is illustrated in Fig. 4.2.

A standard TOSM calibration is performed prior to the measurements, which are conducted inside an environmental chamber. The EUT (pre-amplifier) is first placed inside the environmental chamber at room temperature (23-25 °C) and is allowed to be powered on for at least 30 minutes to warm up completely. The test frequency range is set from 1 GHz to 18 GHz, the input power level is set at 0 dBm, and the bandwidth and number of sweep points are set to 10 kHz and 201 respectively. To protect the VNA as well as the pre-amplifier, the input and output attenuations of the VNA are set at 30 dBm and 10 dBm. The S-parameters are measured and recorded for room temperature. The temperature inside the environmental chamber is then set to 40 °C, and the pre-amplifier is given adequate time (>30 minutes) to stabilise after the

temperature becomes steady. Another standard TOSM calibration is then performed at 40 °C in order to eliminate the uncertainties contributed, due to the temperature change, by the part of the cable inside the environmental chamber. The S-parameters are again recorded. Similar procedures are also carried out at other temperatures.



(a)



(b)

Fig. 4.2 The measurement set up: (a) overview; and (b) inside the temperature chamber, for the characterisation of the measurement uncertainty associated with the pre-amplifier gain under different environmental temperatures.

The measured gain variations at different temperatures are presented in Fig. 4.3. The pre-amplifiers are mostly designed using discrete components with a different number of stages depending on the gain. The gain temperature coefficient of an amplifier is generally about 0.01~0.02 dB/stage/°C [81]. However, a properly designed temperature compensation circuit should be able to limit such gain variation to a certain value (for instance, 2 dB) over the operating temperature range.

As expected, the gain decreases when the temperature increases. To further analyse the pre-amplifier gain variation, the maximum gain at different temperatures with reference to the gain at room temperature (25 °C) is shown in Table 4.2. These results were obtained by taking the maximum difference throughout the frequency range from 1 GHz to 18 GHz, at different operating temperatures, using data obtained from Fig. 4.3. This table shows that, at 0 °C, the maximum gain variation of 1.277 dB is the largest compared to those measured at other temperatures.

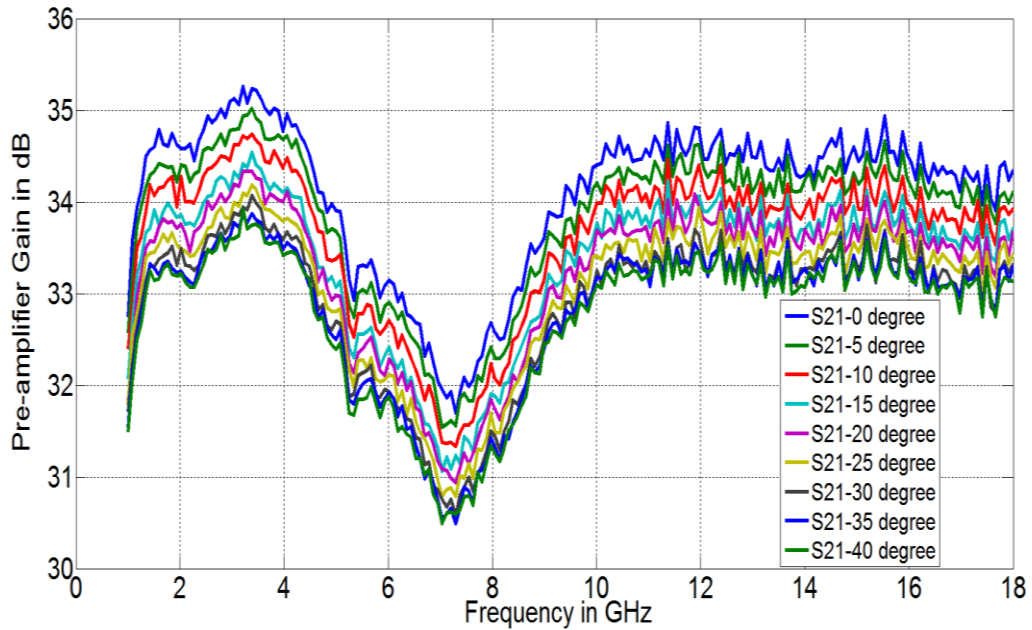


Fig. 4.3 The measured pre-amplifier gains at different temperatures from 0 to 40 °C

Table 4.2 The maximum gain variations at different temperatures with reference to the values at room temperature

Temperature (Celsius)	Maximum Gain Variation (dB)	Occurred Frequency (GHz)
0	+1.277	2.96
5	+0.961	1.17
10	+0.793	1.94
15	+0.467	12.14
20	+0.406	11.88
30	-0.391	11.71
35	-0.469	11.97
40	-0.505	11.63

In addition to the pre-amplifier model which supports 1 GHz to 18 GHz, similar evaluations are conducted for four other models: SCU01D, SCU08D, SCU26D, and SCU40D. The respective frequency ranges of these pre-amplifier models are: 1 kHz - 1 GHz; 100 MHz - 8 GHz; 18 GHz - 26.5 GHz; and 26 GHz - 40 GHz. The maximum gain deviations of these four pre-amplifiers have been measured and calculated based on the measurement results, as shown in Table 4.3. The results show that all four models have a similar gain variation, with a maximum value of 1.327 dB for model SCU40D. This further implies that, regardless of the frequency which the pre-amplifier supports, careful measurement is required of the maximum gain variation of the pre-amplifier as a  $\pm 1$  dB difference can significantly affect the measurement accuracy.

Table 4.2 indicates that for operating temperatures of 15 °C or 35 °C, at which many chambers may often operate, the absolute gain variation is already above 0.4 dB. The measurement accuracy will be greatly affected by this uncertainty contribution. Due to the significant parameter variations with temperature (for the pre-



Table 4.3 Maximum gain variation of pre-amplifiers of different frequency ranges with reference to room temperature

<b>Pre-amplifier model</b>	<b>Frequency Range</b>	<b>Maximum Gain Variation (dB)</b>
SCU01D	1 kHz – 1 GHz	0.968
SCU08D	100 MHz - 8 GHz	1.133
SCU26D	18 GHz – 26.5 GHz	1.076
SCU40D	26 GHz – 40 GHz	1.327

amplifier gain), larger measurement discrepancies are expected at different temperatures. Thus, to improve the reproducibility of the measurement results obtained in different climate regions, measurements must be performed in the specific temperature environment. Since not all chambers are operating in strictly controlled environments, according to ISO/IEC 17025 [82] and especially those located in cold regions, it is important that the pre-amplifier gain variation is properly characterised if the tests are not performed at room temperature.

Detailed procedures for the characterisation of pre-amplifier gain variation have been provided in this section. The investigation process is expected to serve as a guideline for the industry to characterise the pre-amplifier gain variation due to temperature change. The measurement results presented in this section provide necessary insight to the existing standard. Meanwhile, based on the results provided in this section, it is recommended that the regulatory authority consider adding to its standards the necessary details of characterising gain variations due to temperature changes. In this way, the MU contributed by pre-amplifier gain variation can be properly characterised by the industry, and measurement results across different test sites can be correlated.

#### 4.4 Impedance Mismatch

Impedance mismatch is considered to be one of the largest contributors to the entire uncertainty budget table. In the previous section, pre-amplifier gain variation due to temperature change is characterised. This section will further analyse the mismatch uncertainty contributions, between the pre-amplifier and the rest of the system, due to the fluctuation of the pre-amplifier's S-parameters at different operating temperatures.

A typical radiated emission test set up with pre-amplifier in place is illustrated in Fig. 4.4. The semi-anechoic chamber connection panel (CP) connector, access panel (AP) connector, cables, and pre-amplifier, are considered to form the two port network, and their S-parameters can be measured. As shown in Fig. 4.4, the S-parameter of the entire signal path from the antenna to the test receiver can be broken down into individual cascading matrices, which are those of the CP connector, AP connector, Cables 1-4, and the pre-amplifier. Note that the length of Cable 1 is around 50 cm. Cables 2, 3 and 4 have comparable lengths of approximately 8.0 m.

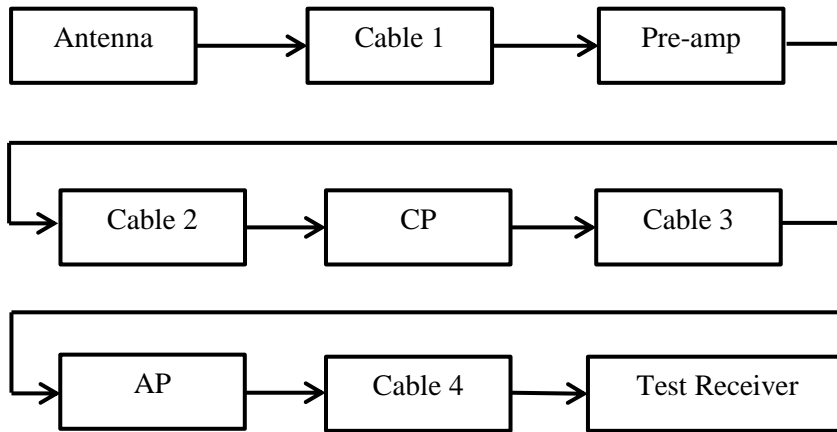


Fig. 4.4 Block diagram of a typical radiated emission test system with external pre-amplifier.

The mismatch uncertainty can be obtained from the S-parameter of the two port network defined above. Specifically, the following formula [6] for the mismatch uncertainty  $\delta M$  is used:

$$\delta M^{\pm} = 20\log_{10}[1 \pm (|\Gamma_a||S_{11}| + |\Gamma_r||S_{22}| + |S_{12}||S_{21}||\Gamma_a||\Gamma_r| + |\Gamma_a||\Gamma_r||S_{21}|^2)] \quad (25)$$

where  $\delta M^{\pm}$  is the extreme value of  $\delta M$  which considers the worst case impedance mismatch quantity.  $\Gamma_a$  and  $\Gamma_r$  are the reflection coefficients of the antenna and test receiver respectively. Note that the S-parameters in (25) are the conjugate S-parameters for the signal path from the antenna output to the input of the test receiver.

Several measurements have been carried out to obtain the individual S-parameters of the components which form the two port network. The same EUT (pre-amplifier SCU-18D) as mentioned in Section 4.3 is used for the investigation. The input and output VSWRs of the pre-amplifier are measured at different operating temperatures. The results are presented in Fig. 4.5 and Fig. 4.6; and it can be seen that neither the input nor the output VSWRs vary to any large degree at different operating temperatures. Generally, the variations are found to be larger at higher frequencies, with the maximum VSWR variation being only about 0.1. For mismatch uncertainty calculation, the S-parameters of the pre-amplifier measured at different temperatures are obtained from the gain measured in the previous section, as well as from the input and output VSWRs measured in Fig. 4.5 and Fig. 4.6.

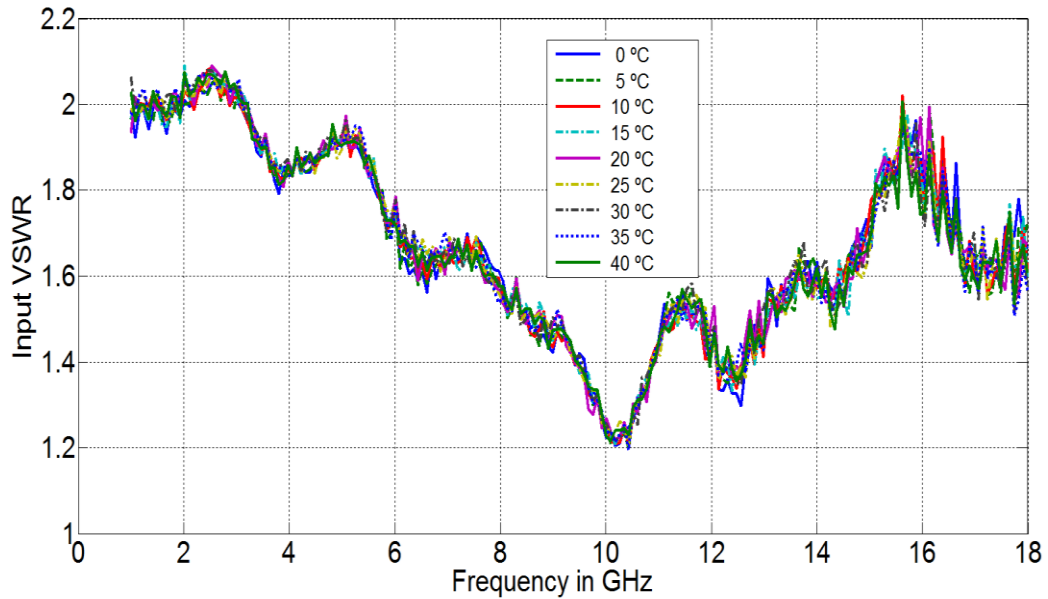


Fig. 4.5 The measured input VSWR of the pre-amplifier at different temperatures from 0 °C to 40 °C.

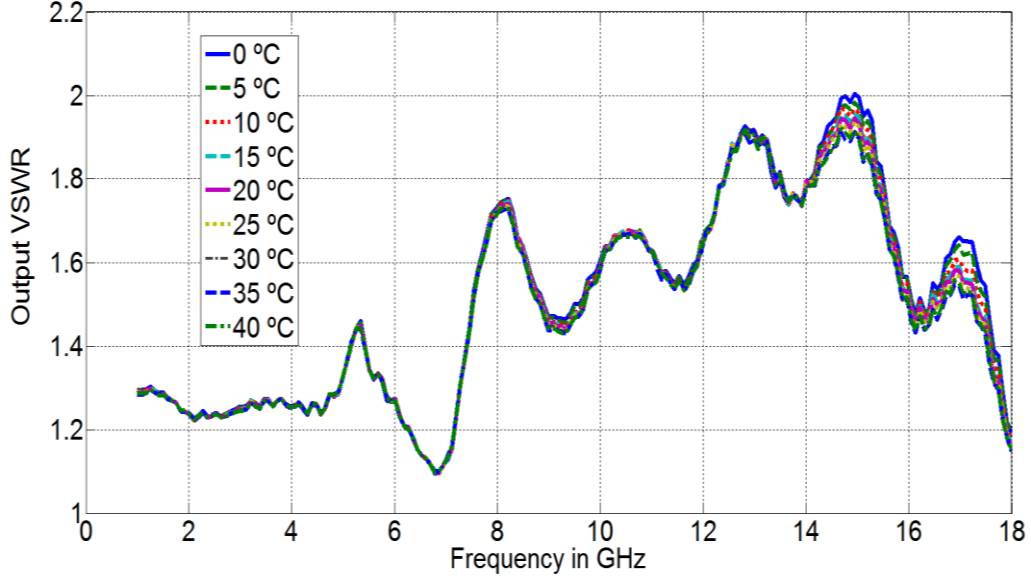


Fig. 4.6 The measured output VSWR of the pre-amplifier at different temperatures from 0 °C to 40 °C.

Most EMC laboratories typically operate at a temperature range from 15 °C to 35 °C. Thus, it is more practical to focus on how the pre-amplifier gain variation will affect the mismatch uncertainty in this temperature range. Since all the S-parameters (except for  $S_{12}$  which is negligible for a pre-amplifier) increase with a decrease in temperature, and the maximum gain variation is almost the same when the temperature changes from 25 °C to 15 °C or 35 °C, pre-amplifier S-parameters are selected from the measurement results at 15 °C and 12.14 GHz, which corresponds to the conditions for the maximum gain variation in the fourth row of Table 4.2:

$$S_{\text{pre-amp}}^{15} = \begin{bmatrix} 0.152 + j0.05 & -27.7 - j41.08 \\ 0 & 0.245 - j0.05 \end{bmatrix} \quad (26)$$

A further reason for selecting S-parameters at 15 °C is that, based on the observations, the chamber temperature control is often not properly implemented when ambient temperature is cool (15 °C ~ 20 °C), as it is comfortable to perform tasks at such temperatures. Similarly, with the aforementioned conditions, the other S-parameters of the individual components which form the two port network are measured as:

$$S_{\text{Cable1}_15} = \begin{bmatrix} 0.039 + j0.007 & 0.598 + j0.69 \\ 0.598 + j0.69 & 0.039 + j0.007 \end{bmatrix} \quad (27)$$

$$S_{\text{Cable234}_15} = \begin{bmatrix} 0.047 - j0.016 & 0.779 + j0.026 \\ 0.779 + j0.026 & 0.047 - j0.016 \end{bmatrix} \quad (28)$$

$$S_{\text{cp}_15} = S_{\text{ap}_15} = \begin{bmatrix} 0.006 + j0.008 & 0.21 + j0.956 \\ 0.21 + j0.956 & 0.006 + j0.008 \end{bmatrix} \quad (29)$$

Similarly, the pre-amplifier S-parameters at 25 °C can be obtained as:

$$S_{\text{Cable1}_25} = \begin{bmatrix} 0.038 + j0.01 & 0.548 + j0.73 \\ 0.548 + j0.73 & 0.038 + j0.01 \end{bmatrix} \quad (30)$$

$$S_{\text{Cable234}_25} = \begin{bmatrix} 0.048 - j0.013 & 0.776 + j0.08 \\ 0.776 + j0.08 & 0.048 - j0.013 \end{bmatrix} \quad (31)$$

$$S_{\text{cp}_25} = S_{\text{ap}_25} = \begin{bmatrix} 0.006 + j0.008 & 0.146 + j0.969 \\ 0.146 + j0.969 & 0.006 + j0.008 \end{bmatrix} \quad (32)$$

$$S_{\text{pre-amp}}^{25} = \begin{bmatrix} 0.138 + j0.06 & -22.04 - j41.45 \\ 0 & 0.235 - j0.05 \end{bmatrix} \quad (33)$$

The above S-parameter matrices can be converted into ABCD transmission matrices, which can be cascaded together, and the result is converted back to a congruent S-parameter matrix. The result is shown below:

$$S_{15} = \begin{bmatrix} 0.045 + j0.18 & 1.958 + j21.40 \\ 0 & 0.237 - j0.058 \end{bmatrix} \quad (34)$$

$$S_{25} = \begin{bmatrix} 0.008 + j0.11 & -8.548 + j18.06 \\ 0 & 0.233 - j0.056 \end{bmatrix} \quad (35)$$

Substituting (34) and (35) into (25), and assuming that  $\Gamma_a = \Gamma_r = 0.2$  (VSWR of 1.5), the worst case mismatch uncertainties at 15 °C and 25 °C are calculated to be 0.49

dB and 0.43 dB, respectively. The difference in the mismatch uncertainties at these two temperatures is only 0.06 dB. This shows that mismatch uncertainty in the system is not largely affected by the gain variation, but rather affected by the values of the congruent S-parameters, especially  $S_{11}$  and  $S_{22}$ . It is found that if both  $|S_{11}|$  and  $|S_{22}|$  increase by 0.1 dB in (34), the mismatch uncertainty will increase to 0.98 dB, which is 0.55 dB higher than the uncertainty at 25 °C.

In conclusion, therefore, to minimise the MU contributed by mismatch, it is necessary to ensure that the signal path (from the antenna to test receiver) input and output reflection coefficients do not vary greatly at different operating temperatures. This can be achieved by using a properly designed pre-amplifier with minimum  $|S_{11}|$  and  $|S_{22}|$  fluctuation due to temperature change, and coaxial cables with excellent temperature stability.

#### **4.5 Measurement Uncertainty Calculation Software**

As mentioned in respect to the original contributions of this thesis in Section 1.4, some of my research results have been adopted by Rohde & Schwarz Asia, and the development of “Measurement Uncertainty Calculation Software” (MUCS) has been proposed to their software development team. The MUCS serves as a complete solution for MU calculation and will be the first MU calculation-aided software in the market based on CISPR standards. The software will have the graphical user interface (GUI) of the MU budget table according to [6], and intensive calculation-aided tools can be triggered from individual uncertainty contributions within the main GUI. The main GUI of MUCS is presented in Fig. 4.7. Further verification and accreditation of the software will be carried out by the respective authorities once its development is complete.

Input Quantity $X_i$		Input Uncertainty $U_i$ [dB]	Probability of $x_i$	Distribution $k$	Standard Uncertainty $u(x_i)$ [dB]	Sensitivity Coefficient $c_i$	Uncertainty contribution $u_i(y)$ [dB]
Receiver reading	$V_f$	0.000	N1	1.000	0.000	1	0.000
Attenuation: AMN-receiver	$a_c$	0.000	N2	2.000	0.000	1	0.000
AMN voltage division factor	$F_{AMN}$	0.000	N2	2.000	0.000	1	0.000
Receiver corrections:							
Sine wave voltage	$\delta V_{sw}$	0.000	N1	1.000	0.000	1	0.000
Pulse amplitude response	$\delta V_{pa}$	0.000	N1	1.000			
Pulse repetition rate response	$\delta V_{pr}$	0.000	N1	1.000			
Noise floor proximity	$\delta V_{nf}$	0.000	RECT	1.732			
Mismatch: AMN-receiver	$\delta M$	0.000	U	1.414			
AMN VDF frequency interpolation	$\delta F_{AMNF}$	0.000	RECT	1.732			
AMN impedance	$\delta Z_{AMN}$	0.000 0.000	TRI	2.450	0.000	1	0.000
Effect of mains disturbance	$\delta D_{mains}$	-	-	-	-	-	-
Effect of the environment	$\delta V_{env}$	-	-	-	-	-	-

**Budget Table Interface.**  
All uncertainty quantities and corresponding uncertainty value are listed here.

Combined Standard Uncertainty 0.000 dB

Coverage Factor 2.000

Expanded Uncertainty 0.00 dB

**Budget Table Interface.**  
All uncertainty quantities and corresponding uncertainty value are listed here.

Fig. 4.7 Illustration of main user interface of MUCS

#### 4.5.1 AMN Impedance Uncertainty Calculation

Some selected features of MUCS are introduced in section, as the development of the software is bound by intellectual property restrictions. An example, as mentioned in Section 1.4, is the calculation of AMN impedance  $\delta Z_{AMN}$ . In CISPR 16-1-2 [83], it is stated that all AMN shall have the impedance (magnitude and phase) versus frequency characteristics required in the standard (nominal impedance), with tolerance of  $\pm 20\%$  for the magnitude and  $\pm 11.5^\circ$  for the phase. Thus, MU occurs when the actual AMN impedance deviates from the nominal impedance due to the tolerance. However, the detailed treatment of this uncertainty is not described in [6]. Some background information has been provided in [84], and a circuit illustration has been presented in Fig. 4.8.  $Z_{nom}$  will be replaced by  $Z_{amn}$  for a real AMN. For calculation, reflection coefficients  $\Gamma$  relative to a normalised impedance  $Z_0$  (50 ohm for instance) are used [84]:

$$\Gamma_{\text{nom}} = \frac{Z_{\text{nom}} - Z_0}{Z_{\text{nom}} + Z_0}, \quad \Gamma_{\text{eut}} = \frac{Z_{\text{eut}} - Z_0}{Z_{\text{eut}} + Z_0}, \quad \Gamma_{\text{amn}} = \frac{Z_{\text{amn}} - Z_0}{Z_{\text{amn}} + Z_0} \quad (36)$$

where  $Z_{\text{amn}} = Z_{\text{nom}} + \alpha|Z_{\text{nom}}|e^{j\theta}$  with  $0 \leq \alpha \leq 0.2, 0 \leq \theta \leq 2\pi$ . Thus, as shown in Fig. 4.8, the voltage across the AMN using nominal and actual impedance can be obtained as:

$$V_{\text{nom}} = \frac{Z_{\text{nom}}}{Z_{\text{nom}} + Z_{\text{eut}}} V_0 = \frac{(1 + \Gamma_{\text{nom}})(1 - \Gamma_{\text{eut}})}{2(1 - \Gamma_{\text{nom}}\Gamma_{\text{eut}})} V_0 \quad (37)$$

$$V_{\text{amn}} = \frac{Z_{\text{amn}}}{Z_{\text{amn}} + Z_{\text{eut}}} V_0 = \frac{(1 + \Gamma_{\text{amn}})(1 - \Gamma_{\text{eut}})}{2(1 - \Gamma_{\text{amn}}\Gamma_{\text{eut}})} V_0 \quad (38)$$

The AMN impedance uncertainty will be described as the deviation from  $V_{\text{amn}}$  to  $V_{\text{nom}}$ , which can be written as [84]:

$$\left| \frac{V_{\text{amn}}}{V_{\text{nom}}} \right| = \left| \frac{1 + \Gamma_{\text{amn}}}{1 - \Gamma_{\text{amn}}\Gamma_{\text{eut}}} \frac{1 - \Gamma_{\text{nom}}\Gamma_{\text{eut}}}{1 + \Gamma_{\text{nom}}} \right| \quad (39)$$

$Z_{\text{eut}}$  is often unknown, thus the value of  $\Gamma_{\text{eut}}$  is difficult to obtain. However, it is clear that the magnitude of  $\Gamma_{\text{eut}}$  cannot be greater than unity. Thus,  $\Gamma_{\text{eut}}$  can be written as:

$$\Gamma_{\text{eut}} = \rho e^{j\varphi} \quad (40)$$

where  $0 \leq \rho \leq 1, 0 \leq \varphi \leq 2\pi$ . It is suggested that the extreme values of (39) are likely to be obtained when  $\rho = 1$  and  $\alpha = 0.2$  from physical consideration [84].

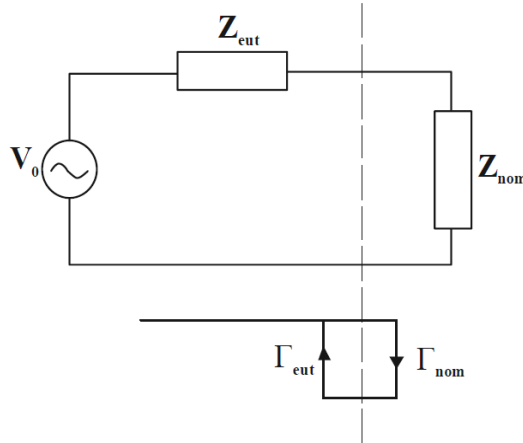


Fig. 4.8 Circuit illustration of EUT and ideal AMN connection



Even though some detailed background information has been provided in [84], an important consideration remains absent from the existing literature. It is known that the actual AMN impedance magnitude and phases calibrated by the manufacturers are associated with MUs (calibration uncertainty); however these MUs are not considered in the standard or in other literature. Thus, it is important to provide a solution to the industry with an appropriate model of treating the MUs associated with AMN impedance magnitude and phase calibration.

Based on the analysis described above, an AMN impedance uncertainty calculator (Microsoft Excel-based) has been developed to perform the computational intensive calculation as shown in Fig. 4.9. In addition to the information provided in [6], [83] and [84], a model has been developed for the treatment of the calibration uncertainty stated in the AMN impedance magnitude and phase calibration reports, which are discussed and considered in this calculator.

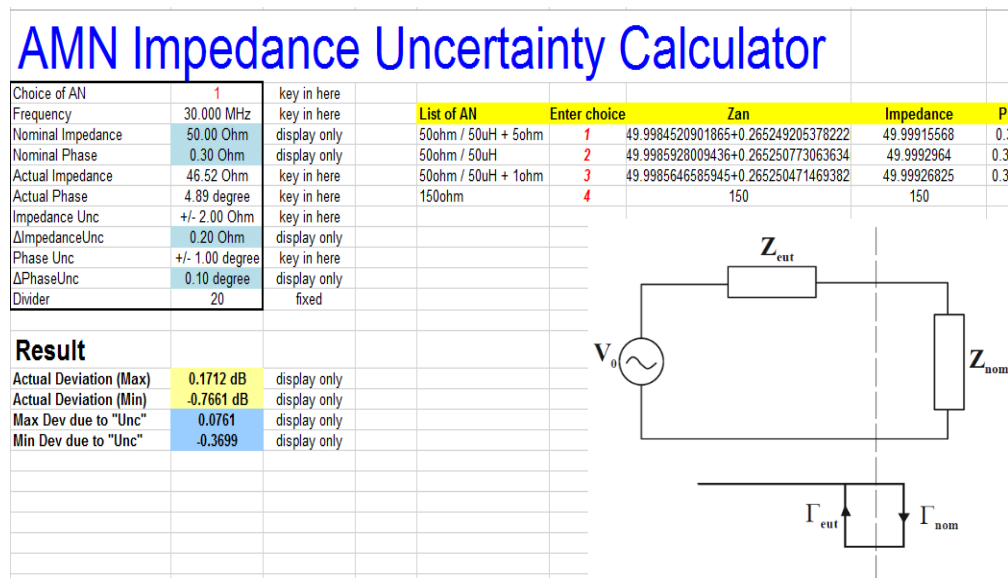


Fig. 4.9 AMN impedance uncertainty calculator main GUI (Microsoft Excel-based)

The actual AMN impedance deviation and calibration uncertainty are separately considered in the model. First, the actual impedance magnitude and phase deviation need to be calculated according to equations (37), (38) and (39) for all the frequency

points stated in the calibration report, as shown in Fig. 4.10.  $Z_{\text{out}}$  can be obtained from  $\Gamma_{\text{out}}$  in equation (40), with  $\rho = 1$  and  $0 \leq \varphi \leq 2\pi$ . The absolute value of  $V_{\text{amn}}/V_{\text{nom}}$  is calculated for  $\varphi = 0, 1^\circ, 2^\circ \dots 359^\circ$ , and converted into dB format. The maximum and minimum values provided in Fig. 4.10 are obtained by comparing all 360 values and used as the two extremes of the actual AMN impedance deviation.

Next, the worst case calibration uncertainty associated with the actual AMN impedance uncertainty is determined. In the calibration report, different frequency points are associated with different magnitude and phase uncertainty, and the calibration uncertainty must be evaluated for all frequency points in order to obtain the worst case value. For instance, the uncertainty of  $\pm 2.0$  ohm and  $\pm 1^\circ$  for actual AMN magnitude of 46.52 ohm and phase of  $4.89^\circ$  at 30 MHz is selected as an example for the selected AMN, as shown in Fig. 4.9. All the different combinations of magnitude and phase with consideration of the associated uncertainty are evaluated, using the nominal magnitude and phase of 50 ohm and  $0.3^\circ$  at 30 MHz [83] as the reference value. For instance, a division factor of 20 is used for the AMN shown in Fig. 4.9. Thus, the step size of the magnitude and phase will be 0.2 ohm and  $0.1^\circ$  when the MU of  $\pm 2.0$  ohm (magnitude) and  $\pm 1^\circ$  (phase) is considered.

Ideally, a larger division factor is always preferred since a smaller step size will ensure more combinations and have a higher probability of finding the largest uncertainty value. However, the computational work will be much more intensive. With the selected division factor of 20, the magnitude will vary from 48 ohm to 52 ohm, with a step size of 0.2 ohm. Similarly, the phase varies from  $-0.7^\circ$  to  $1.3^\circ$  with a step size of  $0.1^\circ$ , and both magnitude and phase have a total of 21 values. An example of the magnitude and phase combination evaluation is provided in Table 4.4.



Table 4.4 An example of the evaluation of AMN impedance magnitude and phase with consideration of uncertainty at 30 MHz

Nominal Impedance (Ohm)	Nominal Phase (degree)	Nominal Impedance (ohm) (cont'd)	Nominal Phase (degree) (cont'd)
48.0	-0.70	48.0	0.4
48.0	-0.60	48.0	0.5
48.0	-0.50	48.0	0.6
48.0	-0.40	48.0	0.70
48.0	-0.30	48.0	0.80
48.0	-0.20	48.0	0.90
48.0	-0.10	48.0	1.0
48.0	0	48.0	1.1
48.0	0.1	48.0	1.2
48.0	0.2	48.0	1.3
48.0	0.3		

Calculate Deviations	Actual Deviations (max, dB)	Calibration Uncertainty (max, dB)										
	0.4840	0.8609										
Frequency (MHz)	Impedance (Ω)	Uncertainty - Impedance (Ω)	Phase (°)	Uncertainty - Phase (°)	LISN Type	Actual Deviations (max, dB)	Actual Deviations (min, dB)	Uncertainty (max, dB)	Uncertainty (min, dB)	Mean: Actual Deviations (dB)	Mean: uncertainty deviations (dB)	
0.009	5.64	0.3	29.93	3.0	1	0.9621	-0.0059	0.7412	-0.7427	0.484	0.74195	
0.015	6.24	0.3	38.40	3.0	1	0.0262	-0.0037	0.7935	-0.7764	0.01495	0.78495	
0.02	7.24	0.3	45.01	2.5	1	0.0069	-0.0162	0.7480	-0.7299	0.01155	0.73895	
0.025	8.39	0.4	48.89	2.5	1	0.0205	-0.0971	0.8709	-0.8508	0.0588	0.86085	
0.03	9.59	0.4	51.74	2.5	1	0.0325	-0.1195	0.8728	-0.8429	0.076	0.85785	
0.05	14.66	0.5	55.39	2.0	1	0.1526	-0.2299	0.7790	-0.7531	0.19125	0.76605	
0.07	19.10	0.5	54.05	2.0	1	0.0487	-0.3087	0.6821	-0.6550	0.1787	0.66855	
0.08	21.32	0.6	52.73	2.0	1	0.0689	-0.3138	0.6795	-0.6552	0.19135	0.66735	
0.1	25.11	0.7	49.70	1.5	1	0.0413	-0.3214	0.5325	-0.5236	0.18135	0.52805	
0.15	32.43	0.9	41.85	1.5	1	0.0205	-0.3060	0.4562	-0.4515	0.16325	0.45385	
0.17	34.44	1.0	38.94	1.5	1	0.0110	-0.3428	0.4444	-0.4413	0.1769	0.44285	
0.2	37.02	1.1	35.16	1.5	1	0.0081	-0.3389	0.4243	-0.4226	0.1735	0.42345	
0.25	40.09	1.3	30.14	1.5	1	0.0033	-0.3166	0.4156	-0.4165	0.15995	0.41605	
0.3	42.15	1.3	26.20	1.5	1	0.0016	-0.3030	0.3835	-0.3844	0.1523	0.38395	
0.35	43.64	1.4	23.07	1.5	1	0.0015	-0.2818	0.3794	-0.3814	0.14165	0.3804	
0.4	44.55	1.4	20.59	1.0	1	0.0004	-0.2933	0.3239	-0.3291	0.14685	0.3265	
0.5	45.84	1.4	16.88	1.0	1	0.0002	-0.2847	0.3070	-0.3119	0.14245	0.30945	
0.7	47.11	1.4	12.43	1.0	1	0.0001	-0.2665	0.2903	-0.2951	0.1333	0.2927	
0.9	47.64	1.4	9.85	1.0	1	0.0006	-0.2644	0.2824	-0.2872	0.1325	0.2848	
1	47.81	1.5	8.92	1.0	1	0.0007	-0.2621	0.2959	-0.3017	0.1314	0.2988	
1.5	48.23	1.5	6.20	1.0	1	0.0025	-0.2548	0.2888	-0.2946	0.12865	0.2917	
2	48.39	1.5	4.85	1.0	1	0.0045	-0.2521	0.2857	-0.2915	0.1283	0.2886	
2.5	48.49	1.5	4.06	1.0	1	0.0065	-0.2475	0.2840	-0.2898	0.127	0.2869	
3	48.53	1.5	3.54	1.0	1	0.0083	-0.2485	0.2829	-0.2887	0.1284	0.2858	
4	48.58	1.5	3.00	1.0	1	0.0145	-0.2515	0.2816	-0.2875	0.133	0.28455	
5	48.61	1.5	2.74	1.0	1	0.0216	-0.2557	0.2809	-0.2867	0.13865	0.2838	
7	48.63	1.5	2.55	1.0	1	0.0363	-0.2685	0.2800	-0.2860	0.1524	0.283	
10	48.57	1.5	2.65	1.0	1	0.0608	-0.3033	0.2795	-0.2854	0.18205	0.28245	
15	48.47	1.5	3.09	1.0	1	0.1030	-0.3602	0.2790	-0.2850	0.2316	0.282	
20	48.30	1.5	2.98	1.0	1	0.0990	-0.3877	0.2788	-0.2848	0.24335	0.2818	
30	46.52	2.0	4.89	1.0	1	0.1712	-0.7661	0.3579	-0.3699	0.46865	0.3639	

Fig. 4.11 Complete AMN impedance uncertainty presentation with actual impedance deviation and calibration uncertainty

maximum and minimum uncertainties respectively, and the largest mean is used as the final actual deviation and calibration uncertainty. The completed AMN impedance uncertainty  $\delta Z_{AMN}$  will be the root sum square of the actual AMN impedance deviation and calibration uncertainty.

The calculator developed and based on Microsoft Excel has been adopted by R&S, and will be a plug-in of MUCS. The actual impedance, actual phase, and their respective uncertainties for each frequency point from the AMN calibration report, can be imported into the calculator. Final AMN impedance uncertainty can be immediately obtained with the backend processing of the data. Thus, tremendous effort can be saved while using the software to obtain an accurate MU result. An AMN calculator plug-in prototype has been developed by me based on the Microsoft Excel version, and the GUI is shown in Fig. 4.12.

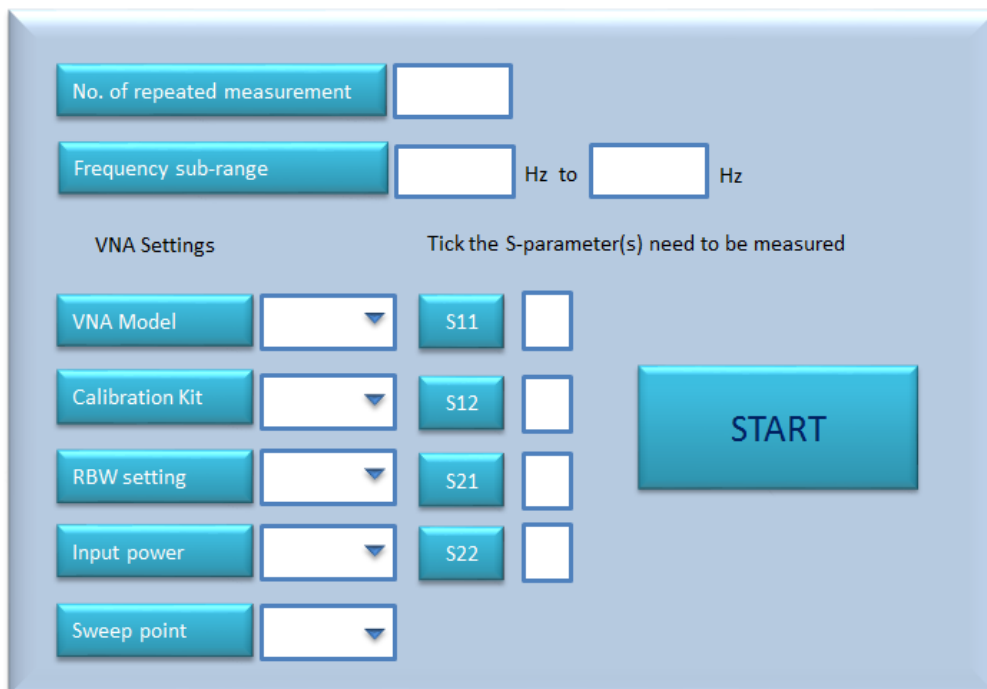
The screenshot shows a software window titled "Artificial Mains Network (AMN)". Inside, there are three main panels. The top panel has a radio button labeled "ENV" which is selected. The middle panel, titled "Input Values (AMN Impedance)", contains three input fields: "Frequency" with the value "0.15" and unit "MHz", "Magnitude" with the value "39.26" and unit "Ω", and "Phase" with the value "54.85" and unit "deg". The bottom panel, titled "Results", contains two output fields: "Maximum Deviation" with the value "3.61" and unit "dB", and "Phase of EUT" with the value "268.14" and unit "deg". At the very bottom of the window are three buttons: "Calculate", "Import", and "Exit".

Fig. 4.12 Prototype GUI of AMN impedance calculator plug-in

#### 4.5.2 Mismatch Uncertainty Calculation

Impedance mismatch is considered one of the biggest contributions towards the entire uncertainty budget table. It is quite computation-intensive, however, for the industrial laboratories to obtain this contribution. Thus, it is desirable to have an automated calculator which can provide all required quantities for the calculation, with minimal effort required from the laboratory end.

Fig. 4.13 shows the GUI of the automated impedance mismatch calculator. S-parameters of the entire cable path (from antenna to the test receiver) can be obtained using this calculator with the VNA MU associated by correctly selecting the VNA settings. The impedance mismatch can then be calculated using the measured S-parameters and the reflection coefficients of the antenna and test receiver, according to equation (25). A number of repeated measurements are also supported by the calculator, with the repeated measurements able to be individually processed. The final mismatch uncertainty will be the average of all the repeated measurement results.



The GUI is a light blue rectangular window with a 3D effect. It contains several input fields and buttons. At the top left, there is a button labeled 'No. of repeated measurement' followed by a text input box. Below this is a button labeled 'Frequency sub-range' followed by two text input boxes separated by 'Hz to'. In the center, there are two columns of settings. The left column is titled 'VNA Settings' and contains five rows: 'VNA Model' with a dropdown arrow, 'Calibration Kit' with a dropdown arrow, 'RBW setting' with a dropdown arrow, 'Input power' with a dropdown arrow, and 'Sweep point' with a dropdown arrow. The right column is titled 'Tick the S-parameter(s) need to be measured' and contains four rows, each with a button labeled S11, S12, S21, or S22, followed by a checkbox. A large blue 'START' button is positioned to the right of these settings.

Fig. 4.13 Prototype GUI of automated impedance mismatch calculator

## 4.6 Conclusion

The measurement uncertainties and possible errors associated with the RF connectors, test receivers, and pre-amplifiers, have been investigated in a radiated emission test which provides additional knowledge on the existing measurement standards used in the industry. It is suggested that the uncertainty of the RF connector used to connect the reference cable and the cable under calibration be considered for inclusion in the existing standard, since the uncertainty is not compensated for in the system. The MU associated with the pre-amplifier gain variation is found to be as large as 0.47 dB when the temperature changes from room temperature (25 °C) to 15 °C; therefore it is important for EMC laboratories to ensure that the tests are performed in the controlled environment according to ISO/IEC 17025 [82].

Furthermore, it is recommended that test laboratories obtain characteristics of the pre-amplifier gain under the actual operating temperature instead of using the pre-amplifier gain specified in the manufacturer's datasheets directly. The investigation procedures stated in Section 4.3 may be considered for inclusion in the existing standard as a guideline for the industry. Mismatch uncertainty of the radiated emission test system is also determined when the pre-amplifier is operating at different temperatures. It is shown that, as long as the input and output reflection coefficients of the pre-amplifier do not vary greatly with temperature changes, the mismatch uncertainty of the entire system will not alter significantly.

The development of the MUCS has been proposed to software team of Rohde & Schwarz Asia with the adoption of some of my research results. Some features of the software have been introduced in Section 4.5. The MUCS serves as a complete solution for MU calculation and will be the first MU calculation-aided software in the market based on CISPR standards.

The results obtained in this chapter have important implications for practical measurements and proper interpretation of measurement standards. Table 4.5 presents

the summary of the MU contributions discussed in this chapter, together with their impacts and possible treatments.

Table 4.5 Summary of MU contributions, their impact and treatments discussed in this section

<b>Error or MU contribution</b>	<b>Impact</b>	<b>Treatment</b>
RF adapter	Uncertainty contributed by RF adapters used to connect normalisation cable and cable under calibration is not compensated for in the system.	It is recommended that 0.15 dB uncertainty be considered for inclusion in the existing standard.
Pre-amplifier gain variation due to temperature change	Large measurement uncertainty due to pre-amplifier gain variation will occur at test sites operating under different temperatures.	The pre-amplifier gain variation shall be characterised and accounted for at different operating temperatures. Detailed characterisation procedures shall be included in the current standard.
Mismatch uncertainty due to pre-amplifier S-parameter fluctuation	Significant mismatch uncertainty will occur if there is a large fluctuation of the pre-amplifier's S-parameters at different operating temperatures.	To minimise the measurement uncertainty contributed by mismatch, it must be ensured that the signal path (from the antenna to test receiver) input and output reflection coefficients do not vary greatly at different operating temperatures.



## **CHAPTER 5 MEASUREMENT UNCERTAINTY AND ACCURACY USING TIME DOMAIN SCAN METHOD IN RADIATED SPURIOUS EMISSION MEASUREMENT**

### **5.1 Background**

There is a growing interest in the use of Fast Fourier Transform (FFT)-based time domain (TD) scan technique for radiated spurious emission (RSE) measurement in the industry [85-88]. This technique demonstrates an ability to perform measurements over a frequency range in just a few seconds, as compared to hours using the conventional sweep/stepped-frequency scan methods. With the publication of Amendment 1 to the third edition of CISPR 16-1-1 [79], the use of FFT-based measuring instruments has been permitted for EMI compliance measurements. Some product standards have included this method in their latest modifications, e.g., CISPR 13, 15 and 32 [89-91]. Other standards, such as CISPR 11, 12 and 25, will follow in 2016 [10, 92, 93]. Fundamental work on the use of TD and FFT regarding EMC emission, and compliance with the requirements of several standards, has also been reported by Braun and Russer [94].

Although the TD scan method has proved its capability to drastically reduce the test time, a practical comparison of accuracy and consistency using the TD scan method and the conventional sweep method in RSE measurement is not reported in the existing literature. It is important to determine the reliability of using the TD scan technique in the actual RSE tests. In this chapter, the performance of both methods is compared for GSM 900 and GSM 1800 tests, and the standard deviation of repeated measurements is calculated. This section investigates the measurement accuracy of the FFT-based TD scan in carrying out RSE measurements, while also exploring its MU. Meanwhile, the work undertaken in this section also serves the purpose of providing additional knowledge to the industry.

## 5.2 FFT-Based TD Scan

A block diagram of a typical test receiver with FFT-based TD scan [95] is provided in Fig. 5.1. The first stage is a pre-selector, which protects the input circuit of the receiver from overload or damage due to high out-of-band signals. The pre-selector also plays an important role in ensuring a correct measurement of weak disturbance signals in the presence of strong signals. The following stages of the receiver consist of a wideband IF filter, and an analogue to digital converter (ADC).

Typically, the IF filter bandwidth is limited to a maximum of 30 MHz, which helps to lower the analogue to digital conversion demands. Together with the first two stages, the ADC must provide an adequate dynamic range to fulfil the CISPR 16-1-1 requirement for quasi-peak measurements of pulse signals with low pulse repetition frequency (PRF). FFT computations are then performed to return the frequency spectra. Often, the FFT can be up to 16,384 frequency bins in length, which is written as 16k-FFT [95]. One of the biggest advantages of the test receiver equipped with the FFT function is that multiple frequencies scanning can be performed simultaneously at a given measurement time, as compared to the conventional test receiver which can only scan for a single frequency.

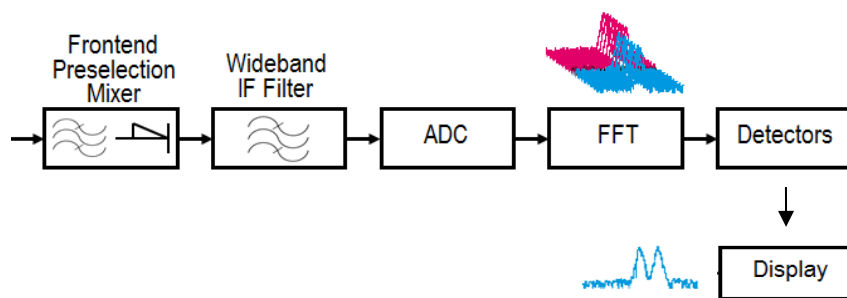


Fig. 5.1 Block diagram of using FFT-based TD scan for a test receiver [95]

Fig. 5.2 presents the concept of the TD scan based on the FFT technique [79]. The receiver can be illustrated to incorporate a filter bank, i.e., several thousand parallel filters. A large number of parallel measured values, covering the frequency range of

several thousand measurement bandwidths, can be obtained simultaneously. The total scan time can be estimated as:

$$T_{\text{scan}} = T_m N_{\text{segment}} \quad (41)$$

where  $T_m$  is the measurement time for each segment, and  $N_{\text{segment}}$  is the number of segments. For RSE measurements, the  $T_m$  selected must be the same as, or longer than, the measurement time/period as specified in the test standards, e.g., GSM, WCDMA, LTE.

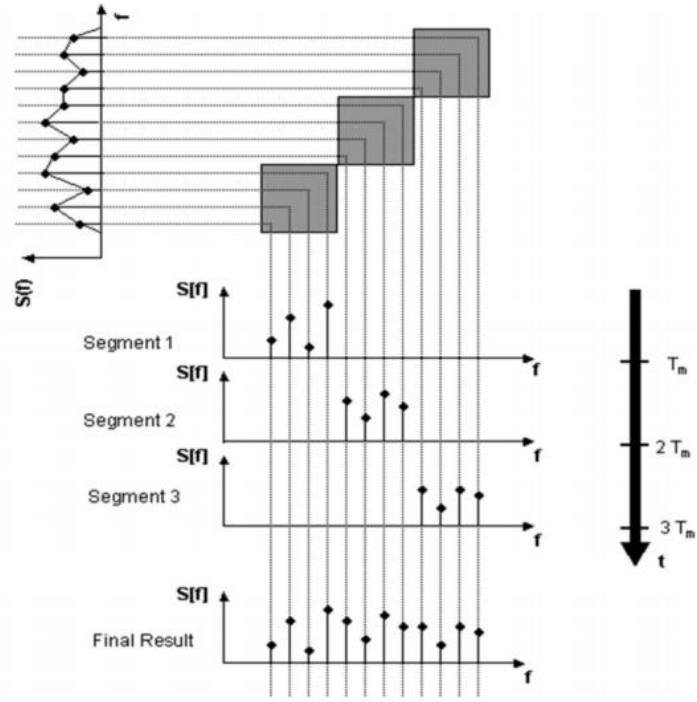


Fig. 5.2 Concept of FFT-based TD scan [79]

### 5.3 Test Set Up and Methodology

Fig. 5.3 shows the actual test set up for this investigation. The EUT, a test mobile phone, is subjected to RSE measurements based on relevant standards listed in ETSI EN 300607-1 Oct\_2000 V8.1.1 [96]. The chamber environment is well controlled at a temperature of 24 °C and a humidity level of 57% RH. An R&S® CMW500 Wideband Radio Communication Tester is used to establish a connection between the standard

signal source and the test mobile phone, i.e., uplink or downlink. Two types of RSE measurements are carried out for GSM 900 and GSM 1800 bands. The first measurement is based on the conventional frequency sweep, while the second measurement is carried out using the FFT-based TD scan.

In the sweep mode, a specific number of measurement points are defined for each frequency subrange to meet the RBW requirements. According to the standard ETSI EN 300607-1, the measurement time at any frequency shall be such that it includes the time during which the Mobile Station (MS) receives a TDMA frame containing the paging channel, i.e., 4.6 milliseconds. Hence, the sweep time of each subrange is set such that the measurement time of each frequency point is at least 4.6 milliseconds.



Fig. 5.3 Actual investigation set-up in a semi-anechoic chamber

In the TD scan mode, frequency segments are processed in parallel configuration, depending on the RBW of each subrange. Similarly to the conventional sweep method, the measurement time for each segment is set based on the test time requirements specified in the standards. In this investigation, the measurement time of each segment is set as 20 milliseconds. The tests performed are:

- auto-test using sweep for preview (R&S® FSV40) and single measurement in zero span mode (R&S® FSV40) for the final measurement.
- auto-test using TD scan for preview (R&S® ESR26) and stepped frequency scan (R&S® ESR26) for the final measurement.

The settings of both sweep and TD scan measurements (i.e., RBW, sweep time, etc.) are based on GSM 900 and GSM 1800 standards [96], as shown in Table 5.1 and Table 5.2.

Table 5.1 R&S® FSV40 parameter specifications in sweep mode

Frequency range	Frequency offset	Filter bandwidth	Approx video bandwidth
100 kHz to 50 MHz	-	10 kHz	30 kHz
50 to 500 MHz excl. relevant TX band: GSM 450: 450.4 to 457.6 MHz; GSM 480: 478.8 to 486 MHz; and the RX bands: 460.4 to 467.6 MHz; 488.8 to 496 MHz.	-	100 kHz	300 kHz
500 MHz to 12,75 GHz, excl. relevant TX band: P-GSM: 890 to 915 MHz; E-GSM: 880 to 915 MHz; DCS: 1710 to 1785 MHz; and the RX bands: 925 to 960 MHz; 1805 to 1880 MHz.	0 to 10 MHz ≥ 10 MHz ≥ 20 MHz ≥ 30 MHz  (offset from edge of relevant TX band)	100 kHz 300 kHz 1 MHz 3 MHz	300 kHz 1 MHz 3 MHz 3 MHz
relevant TX band: GSM 450: 450.4 to 457.6 MHz GSM 480: 478.8 to 486 MHz P-GSM: 890 to 915 MHz E-GSM: 880 to 915 MHz DCS: 1710 to 1785 MHz	1,8 to 6,0 MHz > 6,0 MHz  (offset from carrier)	30 kHz 100 kHz	100 kHz 300 kHz

Table 5.2 R&S® ESR26 parameter specifications in TD mode

<b>Sampling rate</b>	128M sample/s
<b>Resolution</b>	16 bit
<b>FFT length</b>	16 384
<b>FFT window</b>	Gaussian
<b>FFT overlap factor</b>	≥ 80 %
<b>Spectrum (FFT) processing rate</b>	250000/s (Span = 40 MHz)
<b>Minimum detectable signal duration</b>	25 ns (nom.) (span = 40 MHz, SNR > 60 dB)

## 5.4 Results and Discussions

### 5.4.1 GSM 900 Test Result

Fig. 5.4 and Fig. 5.5 present the RSE measurement results for GSM 900 (TX Mode) from 30 MHz to 6 GHz. Due to a change in receiving antenna set up, the measurements are divided into two different frequency ranges: 30 MHz to 3 GHz (using a hybrid BiConiLog antenna), and 3 GHz to 6 GHz (using a horn antenna). Table 5.3 presents two repeated final measurements for each test (Run 1 and Run 2). As shown in the table, the final measurement data of the two methods are comparable, with a maximum deviation of 2.42 dB at the first harmonics of the uplink frequency (i.e., 1804.8 MHz). The measurement deviations at other harmonics are within 1.5 dB. These deviations could be attributed to the sporadic nature of the emission signals at these harmonic frequencies. Further explanation is provided in Section 5.4.3.

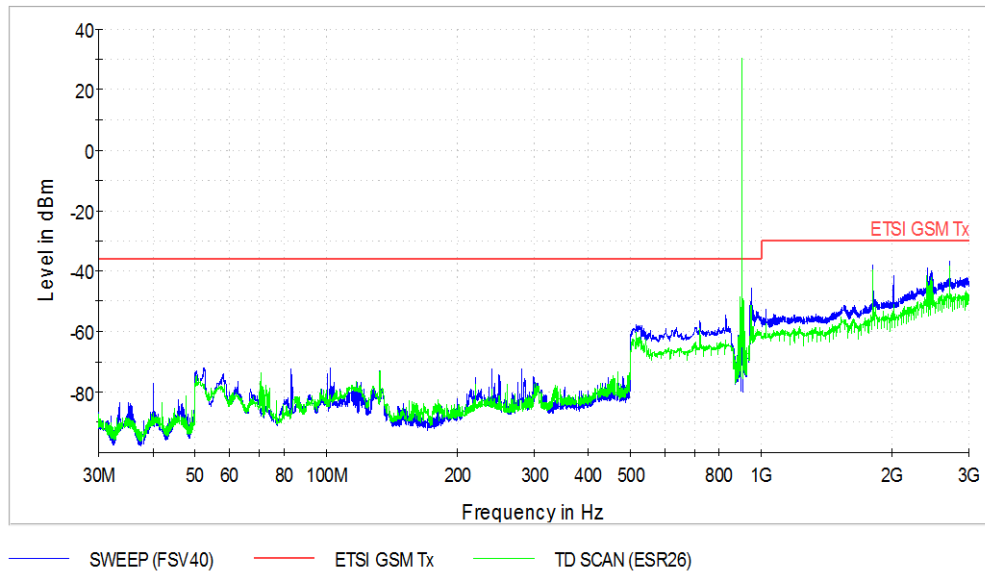


Fig. 5.4 RSE preview measurement for GSM 900 TX Mode (30 MHz to 3 GHz)

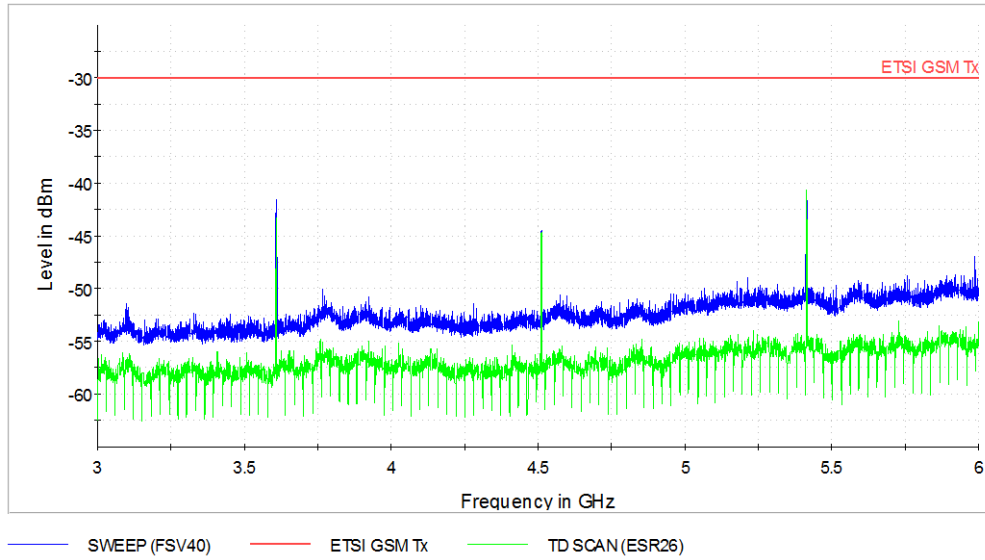


Fig. 5.5 RSE preview measurement for GSM 900 TX Mode (3 GHz to 6 GHz)

Table 5.3 Measurement data for GSM 900 RSE TX Mode

Run 1 (Sweep)		Run 2 (Sweep)	
Frequency (MHz)	Max Peak (dBm)	Frequency (MHz)	Max Peak (dBm)
1804.942	-38.61	1804.653	-37.09
2706.914	-36.45	2707.352	-36.63
3609.183	-39.65	3609.498	-39.52
4512.099	-42.57	4512.438	-43.65
5414.514	-38.30	5414.487	-39.54
Run 1 (TD Scan)		Run 2 (TD Scan)	
Frequency (MHz)	Max Peak (dBm)	Frequency (MHz)	Max Peak (dBm)
1804.639	-36.19	1804.993	-36.14
2706.575	-36.91	2707.576	-36.17
3609.977	-38.92	3609.298	-39.64
4511.667	-43.14	4511.805	-42.92
5414.208	-39.46	5413.977	-39.62

As shown in Fig. 5.6 to Fig. 5.10, the preview measurement results are comparable for the conventional and TD scan methods. It is noted that the noise floor of the sweep method is higher than that of the TD scan method at certain frequency ranges. This is primarily due to the different measurement bandwidths (IFBW) of the two methods. For instance, at frequencies between 500 MHz to 850 MHz, and between 945 MHz to 6000 MHz, the IFBW of sweep and TD scan methods are 3 MHz and 1 MHz, respectively.

In ETSI's GSM standard, an IFBW of 3 MHz is required to conduct the GSM 900's RSE measurements for the aforementioned frequency ranges. In this experiment, the maximum IFBW that an R&S® ESR26 can achieve when operating in the TD scan mode is 1 MHz. Nonetheless, the use of a smaller IFBW in the TD scan approach lowers the noise floor; thus increasing the measurement sensitivity for detecting lower spurious emissions of the signals.

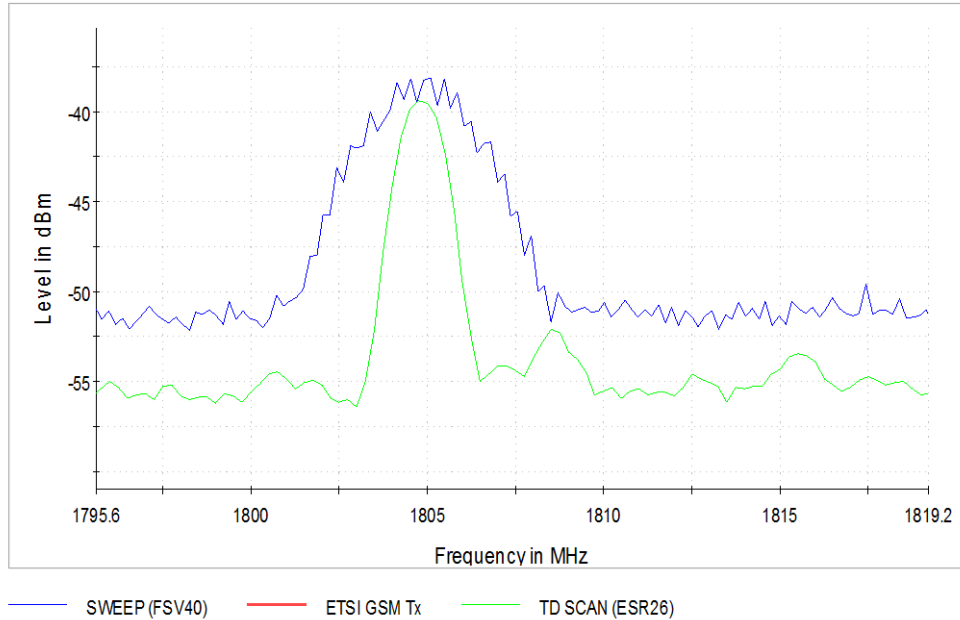


Fig. 5.6 RSE preview measurement for GSM 900 TX Mode (zoom at first harmonics of uplink frequency: 1804.8 MHz)



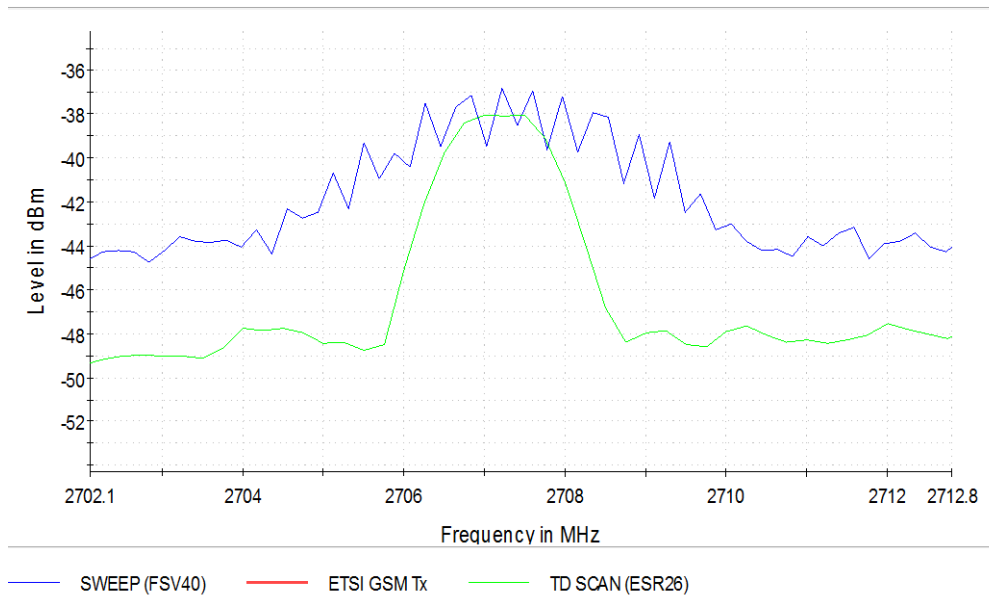


Fig. 5.7 RSE preview measurement for GSM 900 TX Mode (zoom at second harmonics of uplink frequency: 2707.2 MHz)

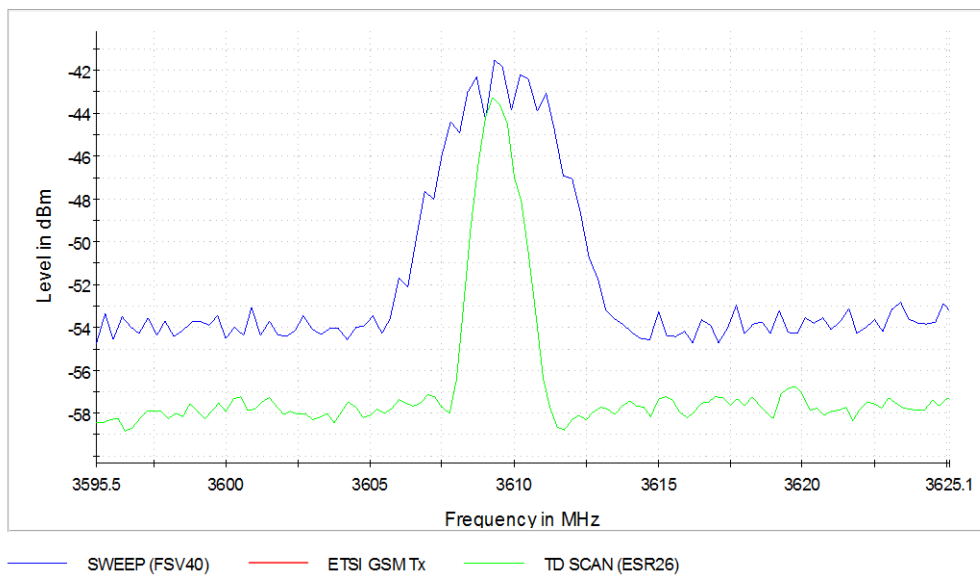


Fig. 5.8 RSE preview measurement for GSM 900 TX Mode (zoom at third harmonics of uplink frequency: 3609.6 MHz)

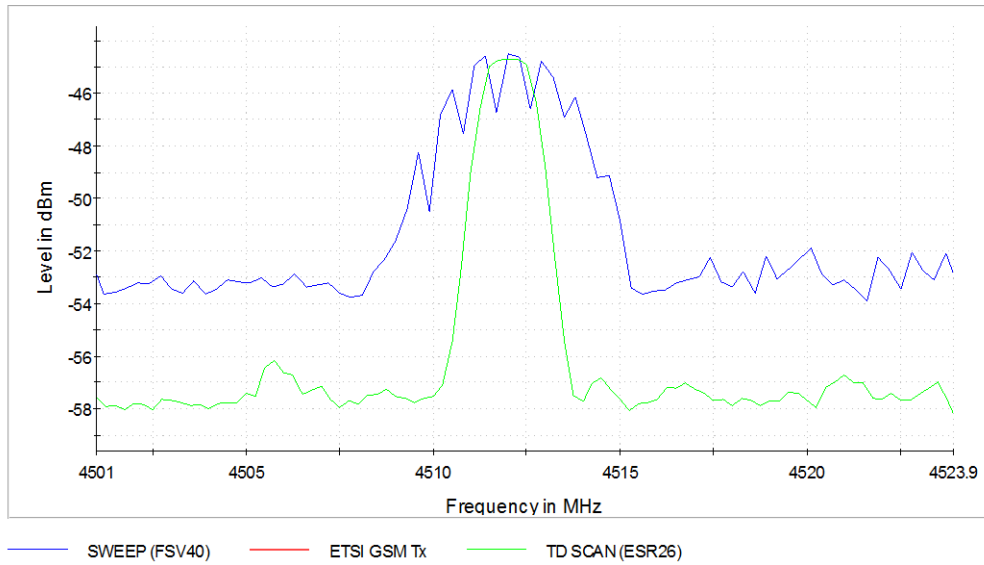


Fig. 5.9 RSE preview measurement for GSM 900 TX Mode (zoom at fourth harmonics of uplink frequency: 4512.0 MHz)

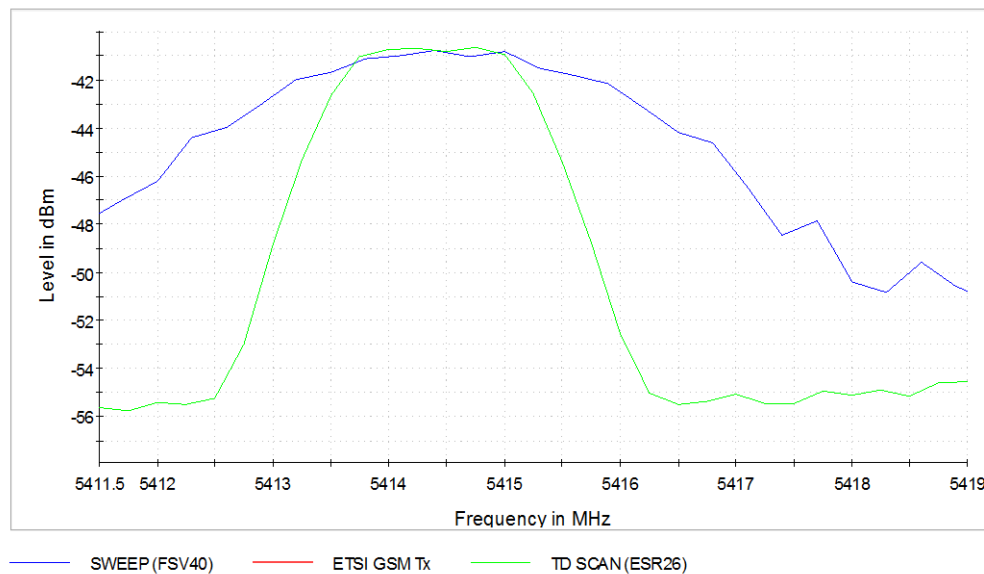


Fig. 5.10 RSE preview measurement for GSM 900 TX Mode (zoom at fifth harmonics of uplink frequency: 5414.4 MHz)

### 5.4.2 GSM 1800 Test Result

The RSE measurement results for GSM 1800 (TX Mode), from 30 MHz to 6 GHz, have been presented in Fig. 5.11 and Fig. 5.12. Similarly to GSM 900, the preview measurement results of GSM 1800 are comparable for the conventional and TD scan methods. For brevity, the zoom-in measurement results at each harmonic of the uplink frequencies of GSM 1800 are not provided.

Two repeated final measurement results (Run 1 and Run 2) are presented in Table 5.4. As illustrated in the table, the final measurement data of the two methods are comparable with a maximum deviation of 2.01 dB at the fourth harmonic of the uplink frequency (i.e., 10486 MHz). An exception is observed for the second harmonic, in which a deviation of 9 dB is observed in Run 1 of the TD scan compared to Run 1 of the sweep. It can be assumed that this measurement is a one-off reading due to the intermittent nature of the emission signals. To validate this assumption, further investigation is carried out using a stable noise source. Relevant details of this investigation are provided in Section 5.4.3.

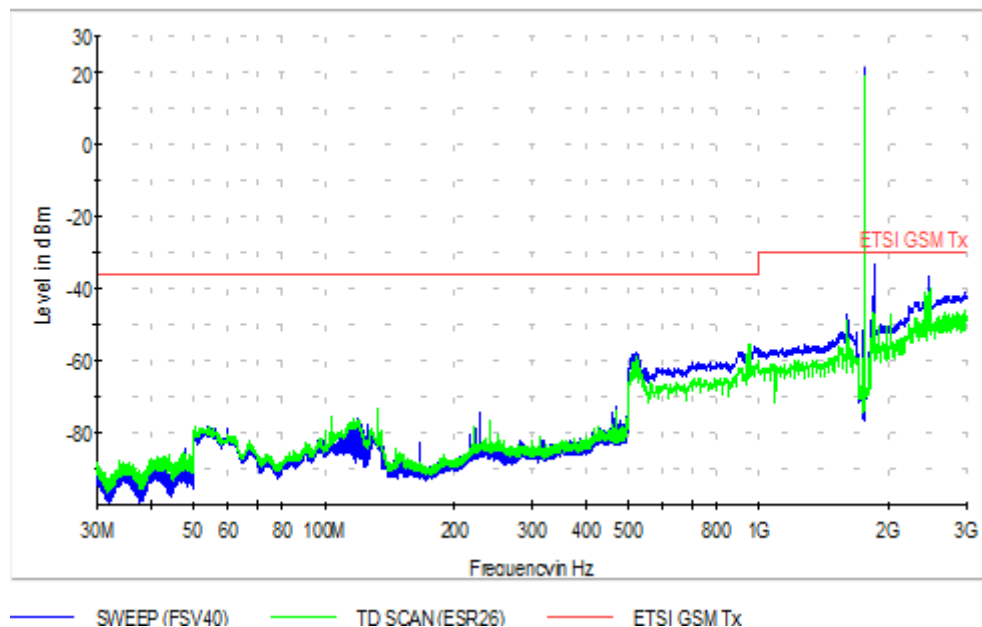


Fig. 5.11 RSE preview measurement for GSM 1800 TX Mode (30 MHz to 3 GHz)

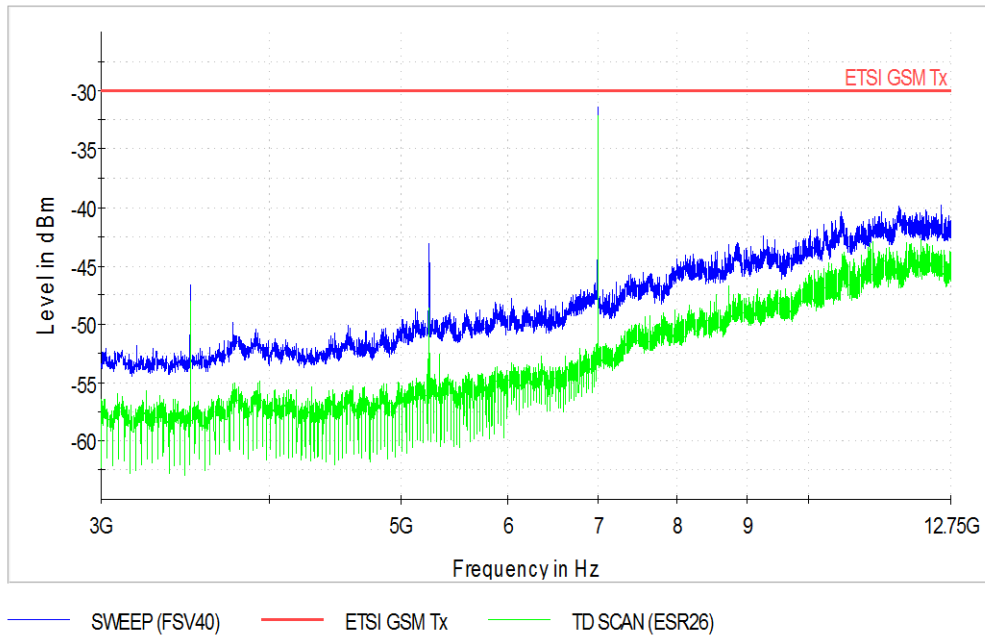


Fig. 5.12 RSE preview measurement for GSM 1800 TX Mode (3 GHz to 12.75 GHz)

Table 5.4 Measurement data for GSM 1800 RSE TX Mode

Run 1 (Sweep)		Run 2 (Sweep)	
Frequency (MHz)	Max Peak (dBm)	Frequency (MHz)	Max Peak (dBm)
3495.807	-45.32	3496.015	-46.02
5243.457	-37.57	5242.938	-43.21
6990.805	-30.35	6991.415	-30.19
10487.025	-41.60	10485.655	-39.59
Run 1 (TD Scan)		Run 2 (TD Scan)	
Frequency (MHz)	Max Peak (dBm)	Frequency (MHz)	Max Peak (dBm)
3495.730	-45.38	3495.784	-45.24
5242.753	-46.60	5243.523	-40.55
6991.290	-29.47	6991.030	-29.34
10486.475	-39.77	10486.681	-40.63

### 5.4.3 Result Verification using Stable Noise Source

In Section 5.4.1 and 5.4.2, it is postulated that the emission signals at the harmonics of uplink frequencies may be intermittent, and that this may cause certain deviations for the measurements using the sweep and TD scan methods. For verification purposes, additional RSE measurements are carried out using a stable noise source. The selected stable noise source is a comb generator emitter, model CGE01C, which has a step size of 50 MHz and operates from 50 MHz to 18 GHz. It is found that the measured signal levels using both methods are comparable, with a maximum deviation of around 0.5 dB. This minor deviation could be due to the different IFBW settings implemented by the two methods. Nonetheless, when the IFBW settings are the same for both methods, i.e., 1 MHz, the detected signal levels using the sweep and the TD scan methods are fairly consistent, as shown in Fig. 5.13 and Fig. 5.14.

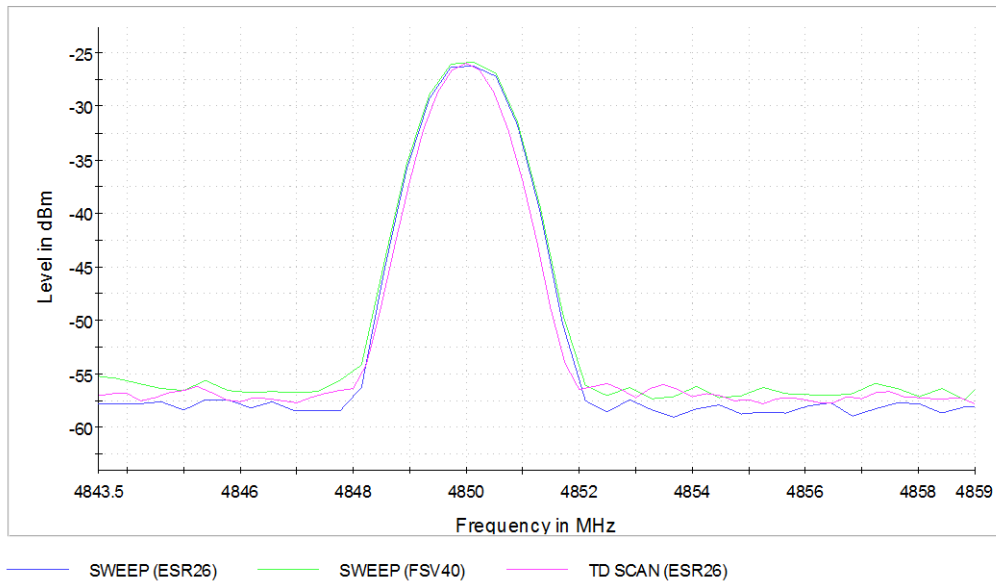


Fig. 5.13 RSE measurement using stable noise source based on IFBW of 1 MHz – zoom in measurement at 4850 MHz

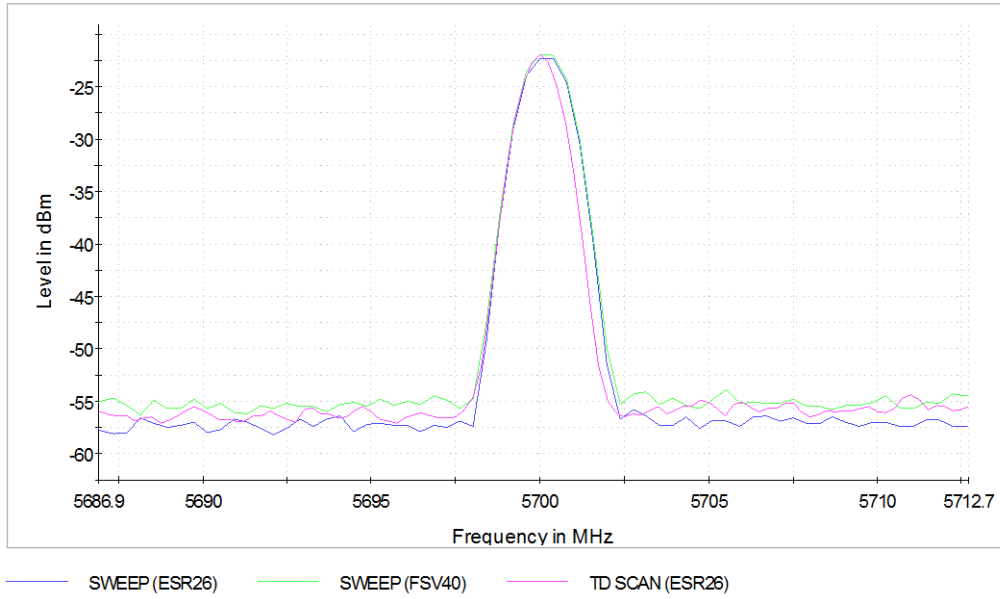


Fig. 5.14 RSE measurement using stable noise source based on IFBW of 1 MHz – zoom in measurement at 5700 MHz

Consistent with the results discussed in Section 5.4.1 and 5.4.2, the TD scan method is proven to be capable of achieving a degree of measurement accuracy which is comparable to the conventional sweep method. The IF bandwidth requirements for the measuring apparatus (e.g., test receiver) stated in [79] is often achieved using a Gaussian-type filter characteristic in the frequency domain. Consequently, the TD scan technique uses Gaussian-type windowing in the time domain when calculating the FFT, since the Fourier transform of a Gaussian function in the frequency domain is also a Gaussian function in the frequency domain. Thus, the IF bandwidth requirement in the frequency domain is perfectly met in the time domain. Furthermore, the leakage effect can be minimised to a negligible level [97].

The step size between two adjacent frequency bins in the TD scan method is selected to be one quarter of the IF bandwidth, which is the optimum value in terms of the amount of the sampled data and amplitude error due to the picket fence effect. Since the conventional sweep method typically uses a step size of one third of the IF bandwidth, the amplitude when using the TD scan method is often lower. The overlap of the Gaussian-type window in the TD could be as high as 90% for broadband-

impulsive or mixed signals. With the high degree of window overlap, only minimal measurement error is expected; and the worst case amplitude error is 0.4 dB between the lowest and highest points of the amplitude ripple [97]. For a minimal pulse width, the theoretical average amplitude error is only 0.09 dB. The practical error which depends on the pulse duration is typically even smaller.

#### **5.4.4 Uncertainty through Repeatability Study**

Another area which has been explored is the MU contribution by the FFT-based TD scan method, as compared to contribution by the conventional method through repeatability study. Both methods use the same set up and measuring equipment, with the exception of the receiver (i.e., spectrum analyser and EMI test receiver). MU using the TD scan method has been briefly discussed in [98]. The discussion reveals that the MU is substantially dependent on the overlapping of the window of single impulses during dwell time. A larger MU can be introduced if there is no overlapping in the measurement system.

In this section, a system level uncertainty comparison is conducted, through repeatability evaluation, between the TD scan method and the conventional sweep method. Repeated measurements are conducted using both methods for the GSM 900 and GSM 1800 band tests, using the same test set up. For the GSM 900 test, the average of the peak value, as well as the standard deviation of the peak value, for repeated measurements is presented in Table 5.5 and Table 5.6. Due to time constraints, only ten repeated measurements are conducted. If time had allowed, additional measurements could have been conducted in order to achieve a more accurate result.

It is observed that the average value (over ten repeated measurements) for the sweep and TD scan methods has a maximum deviation of approximately 1 dB at the first harmonic. This indicates that the TD scan method's accuracy is consistent with that of the conventional sweep method. Furthermore, the standard deviation of the TD scan

method is also comparable to that of the conventional sweep method. These results imply a comparable consistency and repeatability for both methods.

Table 5.5 Average peak value for ten repeated measurements for GSM 900 test

Sweep (ten repeated measurements)		TD Scan (ten repeated measurements)	
Frequency (MHz)	Average Peak (dBm)	Frequency (MHz)	Average Peak (dBm)
1804.942	-37.88	1804.653	-36.89
2706.914	-36.52	2707.352	-36.68
3609.183	-39.70	3609.498	-39.89
4512.099	-43.44	4512.438	-43.52
5414.514	-39.28	5414.487	-39.47

Table 5.6 Standard deviation of peak value for ten repeated measurements for GSM 900 test

Sweep (ten repeated measurements)		TD Scan (ten repeated measurements)	
Frequency (MHz)	Standard Deviation (dB)	Frequency (MHz)	Standard Deviation (dB)
1804.942	0.34	1804.653	0.10
2706.914	0.11	2707.352	0.19
3609.183	0.09	3609.498	0.22
4512.099	0.21	4512.438	0.08
5414.514	0.18	5414.487	0.12

A similar study is also carried out for the GSM 1800 test; with the average of the peak value of ten repeated measurements presented in Table 5.7, and the standard deviation of the peak value presented in Table 5.8. The same conclusion can be obtained for the GSM 1800 test as for the GSM 900 test; the accuracy when using the TD scan method is acceptable, with a maximum difference of 1.38 dB when compared to the sweep method.



Table 5.7 Average peak value for ten repeated measurements for GSM 1800 test

Sweep (ten repeated measurements)		TD Scan (ten repeated measurements)	
Frequency (MHz)	Average Peak (dBm)	Frequency (MHz)	Average Peak (dBm)
3495.807	-45.89	3495.730	-45.69
5243.457	-41.90	5242.753	-43.28
6990.805	-30.40	6991.290	-29.59
10487.025	-40.44	10486.475	-40.32

Table 5.8 Standard deviation of peak value for ten repeated measurements for GSM 1800 test

Sweep (ten repeated measurements)		TD Scan (ten repeated measurements)	
Frequency (MHz)	Standard Deviation (dB)	Frequency (MHz)	Standard Deviation (dB)
3495.807	0.29	3495.730	0.11
5243.457	0.49	5242.753	0.63
6990.805	0.11	6991.290	0.10
10487.025	0.18	10486.475	0.21

## 5.5 Conclusion

The data presented in this chapter provide important contributions to the industry by proving that measurement results obtained using the TD scan method are comparable to those of the conventional frequency sweep method, given the same IFBW settings for RSE measurement. For verification purposes, additional measurements are carried out using a stable noise source, and it is found that the measured signal levels using both methods are comparable. The reasons the received frequency spectrum in the TD scan method matches the spectrum detected with the

conventional method are briefly analysed and discussed, and the discussion supports the measurement results obtained in this chapter. Furthermore, it is demonstrated, through repeated measurements, that the consistency and repeatability of using the TD scan method are also comparable to those of the conventional method.

## CHAPTER 6 CONCLUSION AND FUTURE WORK

### 6.1 Conclusion

In the first part of the thesis, an RC is introduced as an alternative EMC test facility. Some important theories and parameters of the RC have been discussed to ensure the feasibility of using RC for EMC applications. These parameters are also important for the characterisation of measurement uncertainty in the RC. A new approach of using non-equidistant tuner rotation in an RC is also presented. The main focus is to find out the chamber performance in terms of electric field uniformity and uncertainties with reference to the conventional equidistant tuner rotation method. Simulation and measurement results have shown that better field uniformity at LUF can be achieved using non-equidistant tuner positions. The standard deviations of the electric field in  $x$ ,  $y$  and  $z$  directions as well as the total data set have been calculated which are smaller as compared to the conventional method. With the increased number of the independent samples generated by the stirrer at the frequencies near to LUF, the measurement uncertainty which substantially depends on IFU has been reduced thus reproducibility is improved. However, it is realised that there is a disadvantage using the proposed method in the industry as most of the system control software have yet to be optimized for ease of using non-equidistant tuner rotation as compared to the conventional method.

The measurement uncertainties and possible errors associated with the RF connectors, test receivers, and pre-amplifiers in a radiated emission test have been investigated. Additional knowledge has been provided to the existing measurement standards used in the industry. It is suggested that the uncertainty of the RF connector used to connect the reference cable and the cable under calibration be considered for inclusion in the existing standard, since the uncertainty is not compensated for in the system. The measurement uncertainty associated with the pre-amplifier gain variation is found to be as large as 1.277 dB when the temperature changes from the room

temperature (25 °C) to 0 °C. Mismatch uncertainty of the radiated emission test system is also determined when the pre-amplifier is operating at different temperatures. It is shown that as long as the input and output reflection coefficients of the pre-amplifier do not vary much with temperature, mismatch uncertainty of the entire system will not change significantly. The results obtained in this study have significant contributions to the industry by providing important implications for practical measurements and proper interpretation of measurement standards.

The development of “Measurement Uncertainty Calculation Software” has been proposed to the industrial partner Rohde & Schwarz Asia. The purpose for this software is to enable EMC labs which follow commercial EMC standards to calculate their MU, without the need for additional manpower from the labs. It will ensure that the test reports adhere to the standards’ requirements by appending the MU calculation to the EMC measurement results as a separate chapter or appendix. Important findings in my research work have been incorporated into the software, such as preamplifier gain variation due to temperature change, AMN impedance and the in-depth interpretation of the MU contributions from the standard. This software also serves a purpose of establishing a link between the research work and the industry application.

The use of an FFT-enabled TD scan method for RSE measurement has been discussed in this thesis. The comparison of accuracy and consistency using the TD scan method and the conventional sweep method is conducted for GSM 900 and GSM 1800 tests. It is proved that measurement results obtained using the TD scan method are comparable to that of the conventional frequency sweep given the same IFBW settings. The consistency and repeatability of using the TD scan method is also comparable to the conventional method through repeated measurements. This work serves a purpose to provide additional knowledge to the industry on the reliability and measurement uncertainty (through repeatability study) of the TD scan method.

## 6.2 Future Work

The results demonstrated in this thesis provide additional information for the characterisation measurement uncertainty to the industry. Some of the important parameters have been discussed which are not clearly defined in the standards. However, it is believed that there are still areas which need to be taken care of, such as uncertainty contributions which test labs are not familiarized with. In addition, automotive and military standards still have not yet adopted measurement uncertainty as part of the requirements. This could come from the below two factors: 1) there is less stringent requirement in some test equipment, e.g. transducers leads to bigger measurement uncertainty. Thus it is difficult to set an uncertainty budget. 2) Automotive and military tests are sometimes more complicated than commercial tests and tremendous effort is required to provide comprehensive coverage on the uncertainty contributions for the test standards. However, it is still of interest to look into these undefined areas and be able to provide some insightful knowledge to the industry and the regulatory authorities in my future works.

Furthermore, during my research work towards the uncertainty characterisation, certain limitations regarding workmanship, hardware and software capability has been identified. It is hoped the works done can further educate the lab operators so as to reduce the potential measurement errors and uncertainties in their day to day measurement routines. Meanwhile, it is hoped that further assistance can be rendered to the industry to improve some of the hardware and software limitations, thus adequate functions may be available in the tests. After all, it is the principle of the Industry Ph.D. Programme to solve the existing industry problem, provide in-depth knowledge to the industry and establish a link between the research works and industry applications.

As mentioned in Section 1.4, my research work has been adopted by Rohde & Schwarz Asia, and a new software named “Measurement Uncertainty Calculation Software” is in the midst of development. The software has adopted some of the results

and findings from this thesis as the foundation of the uncertainty database. It will greatly reduce the time and resources for the test houses to identify their measurement uncertainty. Future works are still needed to further interpret the standard and provide comprehensive information to the software development team.

## REFERENCES

- [1] H. W. Ott, *Electromagnetic compatibility engineering*: John Wiley & Sons, 2011.
- [2] C. R. Paul, *Introduction to electromagnetic compatibility*: John Wiley & Sons, 2006.
- [3] M. I. Montrose, and E. M. Nakauchi, *Testing for EMC compliance: approaches and techniques*: John Wiley & Sons, 2004.
- [4] I. BIPM, I. IFCC, and I. IUPAC, "OIML 1995 Guide to the Expression of Uncertainty in Measurement," *ISO, Geneva*, vol. 3, 1995.
- [5] CISPR 16-4-1 ed. 2.0: *Specification for radio disturbance and immunity measuring apparatus and methods - Part 4-1: Uncertainties, statistics and limit modelling - Uncertainty in standardized EMC tests*, 2009-02.
- [6] CISPR 16-4-2 ed. 2.0: *Specification for radio disturbance and immunity measuring apparatus and methods - Part 4-2: Uncertainties, statistics and limit modelling - Measurement instrumentation uncertainty*, 2011-06.
- [7] E. C. (EMC), "Part 4-3: Testing and measurement techniques - Radiated, radio-frequency, electromagnetic field immunity test", 3rd ed., Int Electrotech. Comm., IEC 61000-4-3, 2010.
- [8] E. C. (EMC), "Part 4-6: Testing and measurement techniques - Immunity to conducted disturbances, induced by radio-frequency fields", 4th ed., Int Electrotech. Comm., IEC 61000-4-6, 2013.
- [9] J. Medler, "New requirements in the treatment of measurement instrumentation uncertainty in accordance with CISPR 16-4-2 edition 2," in *Electromagnetic Compatibility (APEMC), 2012 Asia-Pacific Symposium on*, pp. 377-380, 2012.
- [10] CISPR 11 ed. 6.0: *Industrial, scientific and medical equipment - Radio-frequency disturbance characteristics - Limits and methods of measurement*, 2015-09.
- [11] M. Stecher, "Measurement uncertainty in EMI emission measurements," in *Electromagnetic Compatibility Proceedings, 1997 International Symposium on*, pp. 270-273, 1997.
- [12] M. Stecher, "A detailed analysis of EMI test receiver measurement uncertainty," in *Electromagnetic Compatibility, 2001 IEEE International Symposium on*, pp. 464-468 vol.1, 2001.
- [13] M. Bertocco, A. Sona, and P. Zanchetta, "An Improved Method for the Evaluation of Uncertainty of Channel Power Measurement With a Spectrum Analyzer," *IEEE Transactions on Instrumentation and Measurement*, vol. 56, no. 4, pp. 1165-1170, 2007.
- [14] J. Sroka, "Contribution of Impedance Imperfection of the T-type ISNs in Measurement Uncertainty of Conducted Disturbances," in *2009 20th International Zurich Symposium on Electromagnetic Compatibility, Zurich*, pp. 61-64, 2009.
- [15] M. Jun-Chul, L. Young-Chae, and K. Yung-Kyu, "The measurement uncertainty of electromagnetic conducted immunity test using CDN," in *2005 IEEE International Symposium on Microwave, Antenna, Propagation and EMC Technologies for Wireless Communications*. pp. 650-653 vol. 1, 2005.
- [16] M. Coenen, and A. v. Roermund, "Reducing compliance uncertainty with AMN measurements," in *2012 Asia-Pacific Symposium on Electromagnetic Compatibility*, pp. 517-520, 2012.
- [17] S. Chakrabarti, D. Dan, and G. Suresh, "Uncertainty analysis for conducted emission measurement," in *Electromagnetic Interference & Compatibility, INCEMIC 2008. 10th International Conference on*, pp. 251-254, 2008.

- [18] Z. Chen, "Measurement model based uncertainty evaluations for calibrations of dipole-like antennas," in *2013 Electromagnetic Compatibility (EMC), IEEE International Symposium on*, pp. 450-455, 2013.
- [19] A. Kriz, "Calculation of antenna pattern influence on radiated emission measurement uncertainty," in *2008 IEEE International Symposium on Electromagnetic Compatibility*, pp. 1-7, 2008.
- [20] D. Hamann, M. B. Konerding, and H. Garbe, "CISPR 16-4-2 Equivalent Measurement Uncertainty Analysis for TEM Waveguides," *IEEE Transactions on Electromagnetic Compatibility*, vol. 57, no. 4, pp. 616-622, 2015.
- [21] M. A. Azpurua, C. Tremola, and E. Paez, "Comparison of the gum and monte carlo methods for the uncertainty estimation in electromagnetic compatibility testing," *Progress In Electromagnetics Research B*, vol. 34, pp. 125-144, 2011.
- [22] J. Medler, "Reducing the standard compliance uncertainty by using ferrite type CMADs during radiated disturbance measurements acc. to CISPR 16-2-3," in *Electromagnetic Compatibility, Tokyo (EMC'14/Tokyo), International Symposium on*, pp. 247-250, 2014.
- [23] C. L. Holloway, H. A. Shah, R. J. Pirkl *et al.*, "Reverberation chamber techniques for determining the radiation and total efficiency of antennas," *IEEE Transactions on Antennas and Propagation*, vol. 60, no. 4, pp. 1758-1770, 2012.
- [24] M. L. Crawford, and G. H. Koepke, *Design, evaluation, and use of a reverberation chamber for performing electromagnetic susceptibility/vulnerability measurements*: US Department of Commerce, National Bureau of Standards, 1986.
- [25] P. Corona, J. Ladbury, and G. Latmiral, "Reverberation-chamber research-then and now: a review of early work and comparison with current understanding," *IEEE transactions on Electromagnetic Compatibility*, vol. 44, no. 1, pp. 87-94, 2002.
- [26] C. R. Dunlap, C. L. Holloway, R. Pirkl *et al.*, "Characterizing reverberation chambers by measurements of the enhanced backscatter coefficient," in *Electromagnetic Compatibility (EMC), IEEE International Symposium on*, pp. 210-215, 2012.
- [27] R. Heinrich, and U. Karsten, "Reverberation chambers—design and application for EMC," *SIGMA*, vol. 7, pp. 8, 2006.
- [28] D. A. Hill, *Electromagnetic fields in cavities: deterministic and statistical theories*: John Wiley & Sons, 2009.
- [29] P. Corona, G. Latmiral, E. Paolini *et al.*, "Use of a reverberating enclosure for measurements of radiated power in the microwave range," *IEEE Transactions on Electromagnetic Compatibility*, no. 2, pp. 54-59, 1976.
- [30] P. F. Wilson, M. T. Ma, and J. Adams, "Techniques for measuring the electromagnetic shielding effectiveness of materials. I. Far-field source simulation," *IEEE Transactions on Electromagnetic Compatibility*, vol. 30, no. 3, pp. 239-250, 1988.
- [31] Y. Huang, and D. Edwards, "A novel reverberating chamber: the source-stirred chamber," in *Electromagnetic Compatibility, Eighth International Conference on*, pp. 120-124, 1992.
- [32] D. A. Hill, "Spatial correlation function for fields in a reverberation chamber," *IEEE Transactions on Electromagnetic Compatibility*, vol. 37, no. 1, pp. 138, 1995.
- [33] L. Scott, "Mode-stir measurement techniques for EMC theory and operation," in *Antenna Measurements (Ref. No. 1998/254), IEE Colloquium on*, pp. 8/1-8/7.



- [34] T. Lehman, G. Freyer, M. Crawford *et al.*, “Recent developments relevant to implementation of a hybrid TEM cell/reverberation chamber HIRF test facility,” in *Digital Avionics Systems Conference, 16th DASC., AIAA/IEEE*, pp. 4.2-26-30 vol. 1, 1997.
- [35] M. Hatfield, M. Slocum, E. Godfrey *et al.*, “Investigations to extend the lower frequency limit of reverberation chambers,” in *Electromagnetic Compatibility, IEEE International Symposium on*, pp. 20-23, 1998.
- [36] E. C. (EMC), “*Part 4-21: Testing and Measurement Techniques—Reverberation Chamber Test Methods*”, 2nd ed., Int Electrotech. Comm., IEC 61000-4-21, 2011.
- [37] F. E. Borgnis, and C. H. Papas, *Electromagnetic waveguides and resonators*: Springer, 1958.
- [38] E. Argence, and T. Kahan, *Theory of waveguides and cavity resonators*: Blackie, 1967.
- [39] T. H. Lehman, “A statistical theory of electromagnetic fields in complex cavities,” *Interaction Notes, Note*, vol. 494, 1993.
- [40] D. A. Hill, “Electromagnetic theory of reverberation chambers,” *NIST Technical note*, no. 1506, 1998.
- [41] S. J. Boyes, and Y. Huang, *Reverberation Chambers: Theory and Applications to EMC and Antenna Measurements*: John Wiley & Sons, 2015.
- [42] D. A. Hill, M. T. Ma, A. Ondrejka *et al.*, “Aperture excitation of electrically large, lossy cavities,” *Electromagnetic Compatibility, IEEE Transactions on*, vol. 36, no. 3, pp. 169-178, 1994.
- [43] T. Chen, “On the definition of the effective aperture of antennas,” *IRE Transactions on Antennas and Propagation*, vol. 9, no. 2, pp. 224-225, 1961.
- [44] L. R. Arnaut, *Measurement uncertainty in reverberation chambers*: National Physical Laboratory, 2008.
- [45] L. R. Arnaut, “Time-Domain Measurement and Analysis of Mechanical Step Transitions in Mode-Tuned Reverberation: Characterisation of Instantaneous Field,” *Electromagnetic Compatibility, IEEE Transactions on*, vol. 49, no. 4, pp. 772-784, 2007.
- [46] L. R. Arnaut, “Effect of local stir and spatial averaging on measurement and testing in mode-tuned and mode-stirred reverberation chambers,” *IEEE transactions on electromagnetic compatibility*, vol. 43, no. 3, pp. 305-325, 2001.
- [47] D. A. Hill, “Electronic mode stirring for reverberation chambers,” *IEEE Transactions on Electromagnetic Compatibility*, vol. 36, no. 4, pp. 294-299, 1994.
- [48] V. M. Primiani, and F. Moglie, “Reverberation Chamber Performance Varying the Position of the Stirrer Rotation Axis,” *Electromagnetic Compatibility, IEEE Transactions on*, vol. 56, no. 2, pp. 486-489, 2014.
- [49] F. Moglie, and V. M. Primiani, “Analysis of the independent positions of reverberation chamber stirrers as a function of their operating conditions,” *IEEE Transactions on Electromagnetic Compatibility*, vol. 53, no. 2, pp. 288-295, 2011.
- [50] D. Zhang, and J. Song, “Impact of stirrers' position on the properties of a reverberation chamber with two stirrers,” in *Electromagnetic Compatibility, IEEE International Symposium on*, pp. 7-10, 2000.
- [51] N. Wellander, O. Lunden, and M. Backstrom, “Experimental Investigation and Mathematical Modeling of Design Parameters for Efficient Stirrers in Mode-Stirred Reverberation Chambers,” *Electromagnetic Compatibility, IEEE Transactions on*, vol. 49, no. 1, pp. 94-103, 2007.

- [52] M. Poci, I. Dotto, D. Festa *et al.*, "Improving the performances of a reverberation chamber: a real case," in *Electromagnetic Compatibility, 2009 20th International Zurich Symposium on*, pp. 53-56, 2009.
- [53] J. Clegg, A. C. Marvin, J. F. Dawson *et al.*, "Optimization of stirrer designs in a reverberation chamber," *IEEE Transactions on Electromagnetic Compatibility*, vol. 47, no. 4, pp. 824-832, 2005.
- [54] N. Wellander, O. Lundén, and M. Backstrom, "Experimental investigation and mathematical modeling of design parameters for efficient stirrers in mode-stirred reverberation chambers," *IEEE Transactions on Electromagnetic Compatibility*, vol. 49, no. 1, pp. 94-103, 2007.
- [55] J.-I. Hong, and C.-S. Huh, "Optimization of stirrer with various parameters in reverberation chamber," *Progress In Electromagnetics Research*, vol. 104, pp. 15-30, 2010.
- [56] X. Chen, "Experimental investigation of the number of independent samples and the measurement uncertainty in a reverberation chamber," *Electromagnetic Compatibility, IEEE Transactions on*, vol. 55, pp. 816-824, 2013.
- [57] R. J. Pirkel, K. A. Remley, and C. S. L. Patane, "Reverberation Chamber Measurement Correlation," *Electromagnetic Compatibility, IEEE Transactions on*, vol. 54, no. 3, pp. 533-545, 2012.
- [58] C. Lemoine, P. Besnier, and M. Drissi, "Estimating the Effective Sample Size to Select Independent Measurements in a Reverberation Chamber," *Electromagnetic Compatibility, IEEE Transactions on*, vol. 50, no. 2, pp. 227-236, 2008.
- [59] P. Hallbjörner, "Estimating the number of independent samples in reverberation chamber measurements from sample differences," *Electromagnetic Compatibility, IEEE Transactions on*, vol. 48, no. 2, pp. 354-358, 2006.
- [60] A. Adardour, G. Andrieu, and A. Reineix, "On the Low-Frequency Optimization of Reverberation Chambers," *Electromagnetic Compatibility, IEEE Transactions on*, vol. 56, no. 2, pp. 266-275, 2014.
- [61] M. Poci, I. Dotto, G. D'Abreu *et al.*, "Experimental definition of the lowest usable frequency (LUF) of an aluminum made reverberation chamber with reference to the IEC 61000-4-21 standard," in *Electromagnetic Compatibility, 2006 IEEE International Symposium on*, pp. 849-852, 2006.
- [62] H. G. Krauthauser, T. Winzerling, and J. Nitsch, "Statistical interpretation of autocorrelation coefficients for fields in mode-stirred chambers," in *Electromagnetic Compatibility, 2005 International Symposium on*, pp. 550-555, 2005.
- [63] N. van Dijk, "Uncertainties in 3-m radiated emission measurements due to the use of different types of receive antennas," *Electromagnetic Compatibility, IEEE Transactions on*, vol. 47, no. 1, pp. 77-85, 2005.
- [64] S. Blalock, and J. A. Fordham, "Antenna measurement uncertainty method for measurements in compact antenna test ranges," in *2016 10th European Conference on Antennas and Propagation (EuCAP)*, pp. 1-5, 2016.
- [65] M. Bittera, K. Kovac, V. Smiesko *et al.*, "Influence of Directivity Pattern of Bilog Antenna to Radiated EMI Measurement Uncertainty," in *Microwave Techniques, COMITE 2008. 14th Conference on*, pp. 1-4, 2008.
- [66] M. Bittera, V. Smiesko, K. Kovac *et al.*, "Interference between ground plane and bilog antenna and its effect on EMI measurement uncertainty," in *2008 Asia-Pacific Microwave Conference*, pp. 1-4, 2008.
- [67] C. Zhong, "Measurement uncertainties for biconical antenna calibrations using standard site method," in *Electromagnetic Compatibility (APEMC), 2013 Asia-Pacific Symposium on*, pp. 1-4, 2013.

- [68] M. Zingarelli, and R. Grego, "Improving EMC measurement uncertainty with digital EMI receivers & optical fiber technology from 10 Hz up to 6 GHz," in *10th International Symposium on Electromagnetic Compatibility*, pp. 26-30, 2011.
- [69] D. Festa, R. Grego, and M. Zingarelli, "Better measurement uncertainty using fully digital receivers in EMC emission tests," in *2008 Asia-Pacific Symposium on Electromagnetic Compatibility and 19th International Zurich Symposium on Electromagnetic Compatibility, Singapore*, pp. 299-302, 2008.
- [70] R. Azaro, and A. Gandolfo, "Optimizing radiated emission measurement uncertainty by using an optical link based receiver," in *Electromagnetic Compatibility (EMC EUROPE), 2013 International Symposium on*, pp. 1078-1081, 2013.
- [71] Y. Jing, Z. Lei, G. Yuan *et al.*, "Influence of uncertainty of measurement time on receiver's precision and assessment method," in *Radar Conference 2013, IET International*, pp. 1-5, 2013.
- [72] C. Christopoulos, and I. Argyri, "Measurement uncertainties in screened rooms and in open area test sites-a tutorial introduction," in *The Correlation Between Measurements in Screened Rooms and in Open Area Test Sites, IEE Colloquium on*, pp. 1/1-1/5, 1996.
- [73] K. Tae-Weon, and K. Hyo-Tae, "Reproducibility and uncertainty in radiated emission measurements at open area test sites and in semianechoic chambers using a spherical dipole radiator," *IEEE Transactions on Electromagnetic Compatibility*, vol. 43, no. 4, pp. 677-685, 2001.
- [74] C. F. M. Carobbi, M. Cati, and C. Panconi, "Reproducibility of Radiated Emissions Measurements in Compact, Fully Anechoic, Rooms-The Contribution of the Site-to-Site Variations," *Electromagnetic Compatibility, IEEE Transactions on*, vol. 51, no. 3, pp. 574-582, 2009.
- [75] T. Tze-Chuen, "Electromagnetic Interference Laboratory Correlation Study and Margin Determination," *Electromagnetic Compatibility, IEEE Transactions on*, vol. 51, no. 2, pp. 204-209, 2009.
- [76] N. van Dijk, "Numerical tools for simulation of radiated emission testing and its application in uncertainty studies," *Electromagnetic Compatibility, IEEE Transactions on*, vol. 44, no. 3, pp. 466-470, 2002.
- [77] E. L. Bronaugh, and J. D. M. Osburn, "A process for the analysis of the physics of measurement and determination of measurement uncertainty in EMC test procedures," in *Electromagnetic Compatibility, Symposium Record. IEEE 1996 International Symposium on*, pp. 245-249, 1996.
- [78] D. Morgan, *A handbook for EMC testing and measurement*: Iet, 1994.
- [79] CISPR 16-1-1 ed. 3.0: *Specification for radio disturbance and immunity measuring apparatus and methods – Part 1-1: Radio disturbance and immunity measuring apparatus – Measuring apparatus*, 2010-01
- [80] S. Bell, *A beginner's guide to uncertainty of measurement*: National Physical Laboratory, 1999.
- [81] I. Bahl, *Fundamentals of RF and microwave transistor amplifiers*: John Wiley & Sons, 2009.
- [82] E. ISO, IEC 17025, "General requirements for the competence of testing and calibration laboratories," pp. 05-15, 2005.
- [83] CISPR 16-1-2 ed. 1.2: *Specification for radio disturbance and immunity measuring apparatus and methods – Part 1-2: Radio disturbance and immunity measuring apparatus – Ancillary equipment-Conducted disturbances*, 2006-08.
- [84] M. Stecher, "Uncertainty in RF disturbance measurements: Revision of CISPR 16-4-2," in *Proceedings of the IEEE International Symposium on Electromagnetic Compatibility, Kyoto*, 2009.

- [85] F. Krug, and P. Russer, "The time-domain electromagnetic interference measurement system," *IEEE Transactions on Electromagnetic Compatibility*, vol. 45, no. 2, pp. 330-338, 2003.
- [86] H. Westenberger, "Use of time domain methods for CISPR16 compliant EMI measurements," in *Microwaves, Communications, Antennas and Electronics Systems, COMCAS 2009. IEEE International Conference on*, pp. 1-4, 2009.
- [87] F. Krug, and P. Russer, "Ultra-fast broadband EMI measurement in time-domain using FFT and periodogram," in *Electromagnetic Compatibility, EMC 2002. IEEE International Symposium on*, pp. 577-582 vol.2, 2002.
- [88] F. Krug, and P. Russer, "Time-Domain Broad-Band EMI Measurement Techniques," in *Microwave Conference, 32nd European*, pp. 1-4, 2002.
- [89] CISPR 13 ed. 5.1: *Sound and television broadcast receivers and associated equipment - Radio disturbance characteristics - Limits and methods of measurement*, 2015-01
- [90] CISPR 15 ed. 8.1: *Limits and methods of measurement of radio disturbance characteristics of electrical lighting and similar equipment*, 2015-03.
- [91] CISPR 32 ed. 2.0: *Electromagnetic compatibility of multimedia equipment - Emission requirements*, 2008-03.
- [92] CISPR 12 ed. 6.1: *Vehicles, boats and internal combustion engines - Radio disturbance characteristics - Limits and methods of measurement for the protection of off-board receivers*, 2009-10
- [93] CISPR 25 ed. 3.0: *Vehicles, boats and internal combustion engines - Radio disturbance characteristics - Limits and methods of measurement for the protection of on-board receivers*, 2008-03.
- [94] S. Braun, and P. Russer, "A low-noise multiresolution high-dynamic ultra-broad-band time-domain EMI measurement system," *IEEE Transactions on Microwave Theory and Techniques*, vol. 53, no. 11, pp. 3354-3363, 2005.
- [95] M. Keller, "Comparison of Time Domain Scans and Stepped Frequency Scans in EMI Test Receiver," *IEE24\_1E White Paper*, 2013.
- [96] E. ETSI, 300 607-1 V8.1.1, "Digital cellular telecommunications system (Phase 2+); Mobile Station (MS) conformance specification; Part 1: Conformance specification", 1999.
- [97] K.-H. Weidner, "Time-Domain Scan Increases Speed of CISPR 16 Compliant EMI Measurements," [http://www.rohde-schwarz-ad.com/docs/emc/WP\\_TimeDomainScan\\_ESU.pdf](http://www.rohde-schwarz-ad.com/docs/emc/WP_TimeDomainScan_ESU.pdf).
- [98] S. Braun, A. Frech, and P. Russer, "CISPR specification and measurement uncertainty of the time-domain EMI measurement system," in *2008 IEEE International Symposium on Electromagnetic Compatibility*, pp. 1-4, 2008.

## APPENDIX: Calibration Reports of Instrumentation Used in the Thesis



akkreditiert durch die / accredited by the

**Deutsche Akkreditierungsstelle GmbH**

als Kalibrierlaboratorium im / as calibration laboratory in the

**Deutschen Kalibrierdienst**



Kalibrierschein  
Calibration certificate

Kalibrierzeichen  
Calibration mark

0301
D-K- 15195-01-00
2013-06

Gegenstand  
Object **EMI Test Receiver**

Hersteller  
Manufacturer **Rohde & Schwarz**

Typ  
Type **ESR26**

Fabrikat/Serien-Nr.  
Serial number **101643**

Auftraggeber  
Customer **INSTITUTE FOR DESIGN OF ELECTRICAL  
MEASURING INSTRUMENTS  
SWATANTRAYAVEER TATYA TOPE MARG  
CHUNABHATTI, SION  
Swatantryaveer Taty Tope Marg,  
Chunabhatti, Sion,  
400022 MUMBAI  
INDIEN**

Dieser Kalibrierschein dokumentiert die Rückführung auf nationale Normale zur Darstellung der Einheiten in Übereinstimmung mit dem internationalen Einheitensystem (SI). Die DAkkS ist Unterzeichner der multilateralen Übereinkommen der European co-operation for Accreditation (EA) und der International Laboratory Accreditation Cooperation (ILAC) zur gegenseitigen Anerkennung der Kalibrierscheine. Für die Einhaltung einer angemessenen Frist zur Wiederholung der Kalibrierung ist der Benutzer verantwortlich.

*This calibration certificate documents the traceability to national standards, which realize the units of measurement according to the International System of Units (SI). The DAkkS is signatory to the multilateral agreements of the European co-operation for Accreditation (EA) and of the International Laboratory Accreditation Cooperation (ILAC) for the mutual recognition of calibration certificates.*

*The user is obliged to have the object recalibrated at appropriate intervals.*

Auftragsnummer  
Order No. **4971033978**

Anzahl der Seiten des Kalibrierscheines  
Number of pages of the certificate **37**

Datum der Kalibrierung  
Date of calibration **2013-06-21**

Dieser Kalibrierschein darf nur vollständig und unverändert weiterverbreitet werden. Auszüge oder Änderungen bedürfen der Genehmigung sowohl der Deutschen Akkreditierungsstelle GmbH als auch des ausstellenden Kalibrierlaboratoriums. Kalibrierscheine ohne Unterschrift haben keine Gültigkeit.

*This calibration certificate may not be reproduced other than in full except with the permission of both the Deutsche Akkreditierungsstelle GmbH and the issuing laboratory. Calibration certificates without signature are not valid.*

Datum  
Date

2013-06-21

Stellv. Leiter des Kalibrierlaboratoriums  
Vice Head of the calibration laboratory

Günther Jocham

Bearbeiter  
Person in charge

Robert Knobloch

Rohde & Schwarz Messgerätebau GmbH • Rohde-und-Schwarz-Str. 1 • 87700 Memmingen • Telephone national: 08331/10-80 International: 0049 8331/10-80  
Fax: 08331/10-811 24 • Managing Director: Jürgen Steigmüller • Chairman of the Supervisory Board: Manfred Fleischmann • Company's Place of Business: München  
Commercial Register No.: HRB 1 059 • VAT Identification No.: DE 811 190 745

akkreditiert durch die / accredited by the

**Deutsche Akkreditierungsstelle GmbH**

als Kalibrierlaboratorium im / as calibration laboratory in the

**Deutschen Kalibrierdienst**



Deutsche  
Akkreditierungsstelle  
D-K-15195-01-00

Kalibrierschein  
Calibration certificate

Kalibrierzeichen  
Calibration mark

0446
D-K- 15195-01-00
2014-03

Gegenstand  
Object **RF and Microwave Signal Generator**

Hersteller  
Manufacturer **Rohde & Schwarz**

Typ  
Type **SMB100A**

Fabrikat/Serien-Nr.  
Serial number **110092**

Auftraggeber  
Customer **INSTITUTE FOR DESIGN OF ELECTRICAL MEASURING INSTRUMENTS**  
  
**Swatantryaveer Taty Tope Marg,  
Chunabhatti, Sion,  
400022 MUMBAI  
IN**

Dieser Kalibrierschein dokumentiert die Rückführung auf nationale Normale zur Darstellung der Einheiten in Übereinstimmung mit dem Internationalen Einheitensystem (SI). Die DAkkS ist Unterzeichner der multilateralen Übereinkommen der European co-operation for Accreditation (EA) und der International Laboratory Accreditation Cooperation (ILAC) zur gegenseitigen Anerkennung der Kalibrierscheine. Für die Einhaltung einer angemessenen Frist zur Wiederholung der Kalibrierung ist der Benutzer verantwortlich.

*This calibration certificate documents the traceability to national standards, which realize the units of measurement according to the International System of Units (SI). The DAkkS is signatory to the multilateral agreements of the European co-operation for Accreditation (EA) and of the International Laboratory Accreditation Cooperation (ILAC) for the mutual recognition of calibration certificates. The user is obliged to have the object recalibrated at appropriate intervals.*

Auftragsnummer  
Order No. **4971033978**

Anzahl der Seiten des Kalibrierscheines  
Number of pages of the certificate **9**

Datum der Kalibrierung  
Date of calibration **2014-03-29**

Dieser Kalibrierschein darf nur vollständig und unverändert weiterverbreitet werden. Auszüge oder Änderungen bedürfen der Genehmigung sowohl der Deutschen Akkreditierungsstelle GmbH als auch des ausstellenden Kalibrierlaboratoriums. Kalibrierscheine ohne Unterschrift haben keine Gültigkeit.

*This calibration certificate may not be reproduced other than in full except with the permission of both the Deutsche Akkreditierungsstelle GmbH and the issuing laboratory. Calibration certificates without signature are not valid.*

Datum  
Date

Stellv. Leiter des Kalibrierlaboratoriums  
Vice Head of the calibration laboratory

Bearbeiter  
Person in charge

2014-03-30

Günther Jocham

Peter Hörmann

## Calibration Certificate

Certificate Number 20-352059

Kalibrierschein

Zertifikatsnummer

### Unit Data

Item  
Gegenstand  
**ESU26 EMI TEST RECEIVER**

Manufacturer  
Hersteller  
**ROHDE & SCHWARZ**

Type  
Typ  
**ESU26**

Material Number  
Materialnummer  
**1302.6005K26**

Serial Number  
Seriennummer  
**100367**

Asset Number  
Inventarnummer

This calibration certificate documents, that the named item is tested and measured against defined specifications. Measurement results are located usually in the corresponding interval with a probability of approx. 95% (coverage factor  $k = 2$ ). Calibration is performed with test equipment and standards directly or indirectly traceable by means of approved calibration techniques to the PTB/DKD or other national / international standards, which realize the physical units of measurement according to the International System of Units (SI). In all cases where no standards are available, measurements are referenced to standards of the R&S laboratories. Principles and methods of calibration correspond and are conformant with EN ISO/IEC 17025 and ANSI/NCSL Z540.1-1994. The applied quality system is certified to EN ISO 9001. This calibration certificate may not be reproduced other than in full. Calibration certificates without signatures are not valid. The user is obliged to have the object recalibrated at appropriate intervals.

### Order Data

Customer  
Auftraggeber

Order Number  
Bestellnummer  
**0000213777**

Date of Receipt  
Eingangsdatum  
**2013-09-19**

### Performance

Place and Date of Calibration  
Ort und Datum der Kalibrierung

**Memmingen, 2013-09-19**

Scope of Calibration  
Umfang der Kalibrierung

**Standard Calibration**

Statement of Compliance  
(Incoming)  
Konformitätsaussage  
(Anlieferung)

**New device**

Statement of Compliance  
(Outgoing)  
Konformitätsaussage  
(Auslieferung)

**Measurement results within specifications**

Extent of Calibration Documents

**2 pages  
39 pages test report**

Ref. No. 20-352059

Cal.  
2013-09-19

Custom. Due Date

ROHDE & SCHWARZ

Dieser Kalibrierschein dokumentiert, dass der genannte Gegenstand nach festgelegten Vorgaben geprüft und gemessen wurde. Die Messwerte lagen im Regelfall mit einer Wahrscheinlichkeit von annähernd 95% im zugeordneten Werteintervall (Erweiterte Messunsicherheit mit  $k = 2$ ). Die Kalibrierung erfolgte mit Messmitteln und Normalen, die direkt oder indirekt durch Ableitung mittels anerkannter Kalibriertechniken rückgeführt sind auf Normale der PTB/DKD oder anderer nationaler/internationaler Standards zur Darstellung der physikalischen Einheiten in Übereinstimmung mit dem Internationalen Einheitensystem (SI). Wenn keine Normale existieren, erfolgt die Rückführung auf Bezugsnormale der R&S-Laboratorien. Grundsätze und Verfahren der Kalibrierung beziehen sich auf und entsprechen EN ISO/IEC 17025 und ANSI/NCSL Z540.1-1994. Das angewandte Qualitätsmanagement-System ist zertifiziert nach EN ISO 9001. Dieser Kalibrierschein darf nur vollständig und unverändert weiterverbreitet werden. Kalibrierscheine ohne Signifizierungen sind ungültig. Für die Einhaltung einer angemessenen Frist zur Wiederholung der Kalibrierung ist der Benutzer verantwortlich.

### Rohde & Schwarz Messgerätebau GmbH

Date of Issue  
Ausstellungsdatum

Head of Laboratory  
Laborleitung

Person Responsible  
Bearbeiter

2013-09-19

Steigmüller

Winfried Gropper

Page 1/41  
ver0815/MB0705





**ROHDE & SCHWARZ**

**Calibration Certificate**

**Certificate No. 7150-308012003**

**Unit Data**

Item Vector Network Analyzer, 4 ports, 10MHz-40GHz  
Manufacturer ROHDE & SCHWARZ  
Type ZVA40  
Material No. 1145.1110K42 Serial No. 100118

This calibration certificate documents that the named item is tested and measured against defined specifications. Measurement results are located usually in the corresponding interval with a probability of approx. 95% (coverage factor k=2).

Calibration is performed with test equipment and standards directly or indirectly traceable by means of approved calibration techniques to the PTB/DKD or other national/international standards, which realize the physical units of measurement according to the International System of Units (SI). In all cases where no national standards are available, measurements are referenced to standards of the R&S laboratories. Principles and methods of calibration correspond with ISO /IEC 17025.

The applied quality system is certified EN ISO 9001.

This calibration certificate may not be reproduced other than in full. Calibration certificates without signatures are not valid.

The user is obliged to have the object recalibrated at appropriate intervals.

**Order Data**

Customer Rohde & Schwarz Asia Pte. Ltd.  
9 Changi Business Park Vista  
#01-01  
Singapore 486041

Order No.

Date of Receipt 2014-05-21

**Performance**

Place and Date of Calibration RS-RHQS - LOYANG, 2014-06-24

Scope of Calibration Standard Calibration

Statement of Compliance (Incoming) Defective

Statement of Compliance (Outgoing) One or more measured values are outside the data sheet specifications, marked as FAIL.

Extent of Calibration 45 Pages Calibration Certificate

Rohde & Schwarz Regional Headquarters Singapore Pte Ltd

Date of Issue  
(YYYY-MM-DD)

Head of Laboratory

Person Responsible

2014-06-24

BeeBee Woon

JunWei Zheng

Page 1/45  
PT 3583.9833.00

ROHDE & SCHWARZ Regional Headquarters Singapore Pte Ltd (RS-RHQS)  
Main Office: 9 Changi Business Park Vista #03-01, Singapore 486041 Tel: +65 6307 0000 Fax: +65 6307 0303  
Loyang Office: 4 Loyang Way 2, Singapore 507100 Tel: +65 6307 0000 Fax: +65 6307 0327





ROHDE & SCHWARZ

Calibration Certificate

Certificate Number 20-560013

Kalibrierschein

Zertifikatsnummer

Unit Data

Item Gegenstand **NRP-Z91 POWER SENSOR 6GHZ**

Manufacturer Hersteller **ROHDE & SCHWARZ**

Type Typ **NRP-Z91**

Material Number Materialnummer **1168.8004.02** Serial Number Seriennummer **103163**

Asset Number Inventarnummer

Order Data

Customer Auftraggeber

Order Number Bestellnummer **0000320107**

Date of Receipt Eingangsdatum **2015-09-17**

Performance

Place and Date of Calibration Ort und Datum der Kalibrierung **Memmingen, 2015-09-17**

Scope of Calibration Umfang der Kalibrierung **Standard Calibration**

Statement of Compliance (Incoming) Konformitätsaussage (Anlieferung) **New device**

Statement of Compliance (Outgoing) Konformitätsaussage (Auslieferung) **Measurement results within specifications**

Extent of Calibration Documents Umfang des Kalibrierdokuments **2 Pages incl. this**

This calibration certificate documents, that the named item is tested and measured against defined specifications.

Measurement results are located usually in the corresponding interval with a probability of approx. 95% (coverage factor  $k = 2$ ).

Calibration is performed with test equipment and standards directly or indirectly traceable by means of approved calibration techniques to the PTB/DKD or other national / international standards, which realize the physical units of measurement according to the International System of Units (SI).

In all cases where no standards are available, measurements are referenced to standards of the R&S laboratories.

Principles and methods of calibration correspond and are conformant with EN ISO/IEC 17025, ANSI/NCSL Z540.1-1994 and ANSI/NCSL Z540.3-2006. The applied quality system is certified to EN ISO 9001. This calibration certificate may not be reproduced other than in full. Calibration certificates without signatures are not valid. The user is obliged to have the object recalibrated at appropriate intervals.

Dieser Kalibrierschein dokumentiert, dass der genannte Gegenstand nach festgelegten Vorgaben geprüft und gemessen wurde. Die Messwerte lagen im Regelfall mit einer Wahrscheinlichkeit von annähernd 95% im zugeordneten Werteintervall (Erweiterte Messunsicherheit mit  $k = 2$ ).

Die Kalibrierung erfolgte mit Messmitteln und Normale, die direkt oder indirekt durch Ableitung mittels anerkannter Kalibriertechniken rückgeführt sind auf Normale der PTB/DKD oder anderer nationaler/internationaler Standards zur Darstellung der physikalischen Einheiten in Übereinstimmung mit dem Internationalen Einheitensystem (SI). Wenn keine Normale existieren, erfolgt die Rückführung auf Bezugsnormale der R&S-Laboratorien.

Grundsätze und Verfahren der Kalibrierung beziehen sich auf und entsprechen EN ISO/IEC 17025, ANSI/NCSL Z540.1-1994 und ANSI/NCSL Z540.3-2006.

Das angewandte Qualitätsmanagement-System ist zertifiziert nach EN ISO 9001. Dieser Kalibrierschein darf nur vollständig und unverändert weiterverbreitet werden. Kalibrierscheine ohne Signifizierungen sind ungültig.

Für die Einhaltung einer angemessenen Frist zur Wiederholung der Kalibrierung ist der Benutzer verantwortlich.

Rohde & Schwarz Messgerätebau GmbH

Date of Issue Ausstellungsdatum

Head of Laboratory Laborleitung

Person Responsible Bearbeiter

2015-09-17

Steigmüller

Franz Schragner

Page 1/2  
ver9815/MB0707

Rohde & Schwarz Messgerätebau GmbH · Postfach 1652 D-87686 Memmingen · Rohde-und-Schwarz-Str. 1 D-87700 Memmingen  
Telefon national: 08331/10-80; international: 0049 8331/10-80; Fax: 08331/10-811 24  
Geschäftsführer: Jürgen Steigmüller · Aufsichtsratsvorsitzender: Roland Steffen  
Sitz der Gesellschaft: München · Registertrag: Amtsgericht München HRB 1039



ROHDE & SCHWARZ

Calibration Certificate

Certificate Number 20-560014

Kalibrierschein

Zertifikatsnummer

Unit Data

Item  
Gegenstand  
**NRP-Z91 POWER SENSOR 6GHZ**

Manufacturer  
Hersteller  
**ROHDE & SCHWARZ**

Type  
Typ  
**NRP-Z91**

Material Number  
Materialnummer  
**1168.8004.02**

Serial Number  
Seriennummer  
**103164**

Asset Number  
Inventarnummer

Order Data

Customer  
Auftraggeber

Order Number  
Bestellnummer  
**0000320107**

Date of Receipt  
Eingangdatum  
**2015-09-17**

Performance

Place and Date of Calibration  
Ort und Datum der Kalibrierung  
**Memmingen, 2015-09-17**

Scope of Calibration  
Umfang der Kalibrierung  
**Standard Calibration**

Statement of Compliance  
(Incoming)  
Konformitätsaussage  
(Anlieferung)  
**New device**

Statement of Compliance  
(Outgoing)  
Konformitätsaussage  
(Auslieferung)  
**Measurement results within specifications**

Extent of Calibration Documents  
Umfang des Kalibrierdokuments  
**2 Pages incl. this**

This calibration certificate documents, that the named item is tested and measured against defined specifications. Measurement results are located usually in the corresponding interval with a probability of approx. 95% (coverage factor  $k = 2$ ). Calibration is performed with test equipment and standards directly or indirectly traceable by means of approved calibration techniques to the PTB/DKD or other national / international standards, which realize the physical units of measurement according to the International System of Units (SI). In all cases where no standards are available, measurements are referenced to standards of the R&S laboratories. Principles and methods of calibration correspond and are conformant with EN ISO/IEC 17025, ANSI/NCSL Z540.1-1994 and ANSI/NCSL Z540.3-2006. The applied quality system is certified to EN ISO 9001. This calibration certificate may not be reproduced other than in full. Calibration certificates without signatures are not valid. The user is obliged to have the object recalibrated at appropriate intervals.

Dieser Kalibrierschein dokumentiert, dass der genannte Gegenstand nach festgelegten Vorgaben geprüft und gemessen wurde. Die Messwerte liegen im Regelfall mit einer Wahrscheinlichkeit von annähernd 95% im zugeordneten Werteintervall (Erweiterte Messunsicherheit mit  $k = 2$ ). Die Kalibrierung erfolgte mit Messmitteln und Normen, die direkt oder indirekt durch Ableitung mittels anerkannter Kalibriertechniken rückgeführt sind auf Normale der PTB/DKD oder anderer nationaler/internationaler Standards zur Darstellung der physikalischen Einheiten in Übereinstimmung mit dem Internationalen Einheitensystem (SI). Wenn keine Normale existieren, erfolgt die Rückführung auf Bezugsnormale der R&S-Laboratorien. Grundsätze und Verfahren der Kalibrierung beziehen sich auf und entsprechen EN ISO/IEC 17025, ANSI/NCSL Z540.1-1994 und ANSI/NCSL Z540.3-2006. Das angewandte Qualitätsmanagement-System ist zertifiziert nach EN ISO 9001. Dieser Kalibrierschein darf nur vollständig und unverändert weiterverbreitet werden. Kalibrierscheine ohne Signifizierungen sind ungültig. Für die Einhaltung einer angemessenen Frist zur Wiederholung der Kalibrierung ist der Benutzer verantwortlich.

Rohde & Schwarz Messgerätebau GmbH

Date of Issue  
Ausstellungsdatum

Head of Laboratory  
Laborleitung

Person Responsible  
Bearbeiter

2015-09-17

Steigmüller

Franz Schragner

Page 1/2  
ver8815/MB0707

Rohde & Schwarz Messgerätebau GmbH · Postfach 1852 D-87686 Memmingen · Rohde-und-Schwarz-Str. 1 D-87700 Memmingen  
Telefon national: 08331/10-80; international: 0049 8331/10-80; Fax: 08331/10-811 24  
Geschäftsführer: Jürgen Steigmüller · Aufsichtsratsvorsitzender: Roland Steffen  
Sitz der Gesellschaft: München · Registeramt: Amtsgericht München HRB 1059



ROHDE & SCHWARZ

## Calibration Certificate

Certificate Number 17-548099

Kalibrierschein

Zertifikatsnummer

### Unit Data

Item **SMB100A SIGNAL GENERATOR**

Gegenstand

Manufacturer **ROHDE & SCHWARZ**

Hersteller

Type **SMB100A**

Typ

Material Number **1406.6000K02** Serial Number **110183**

Materialnummer

Seriennummer

Asset Number

Inventarnummer

### Order Data

Customer

Auftraggeber

Order Number **0000313779**

Bestellnummer

Date of Receipt **2015-06-29**

Eingangsdatum

### Performance

Place and Date of Calibration  
Ort und Datum der Kalibrierung

**Vimperk, 2015-06-29**

Scope of Calibration  
Umfang der Kalibrierung

**Standard Calibration**

Statement of Compliance  
(Incoming)  
Konformitätsaussage  
(Anlieferung)

**New device**

Statement of Compliance  
(Outgoing)  
Konformitätsaussage  
(Auslieferung)

**Measurement results within specifications**

Extent of Calibration Documents  
Umfang des Kalibrierdokuments

**2 Pages incl. this**

This calibration certificate documents, that the named item is tested and measured against defined specifications.

Measurement results are located usually in the corresponding interval with a probability of approx. 95% (coverage factor  $k = 2$ ).

Calibration is performed with test equipment and standards directly or indirectly traceable by means of approved calibration techniques to the PTB/DKD or other national / international standards, which realize the physical units of measurement according to the International System of Units (SI).

In all cases where no standards are available, measurements are referenced to standards of the R&S laboratories.

Principles and methods of calibration correspond and are conformant with EN ISO/IEC 17025, ANSI/NCSL Z540.1-1994 and ANSI/NCSL Z540.3-2006. The applied quality system is certified to EN ISO 9001.

This calibration certificate may not be reproduced other than in full. Calibration certificates without signatures are not valid.

The user is obliged to have the object recalibrated at appropriate intervals.

Dieser Kalibrierschein dokumentiert, dass der genannte Gegenstand nach festgelegten Vorgaben geprüft und gemessen wurde. Die Messwerte liegen im Regelfall mit einer Wahrscheinlichkeit von annähernd 95% im zugeordneten Wertintervall (Erweiterte Messunsicherheit mit  $k = 2$ ).

Die Kalibrierung erfolgte mit Messmitteln und Normen, die direkt oder indirekt durch Ableitung mittels anerkannter Kalibriertechniken rückgeführt sind auf Normale der PTB/DKD oder anderer nationaler/internationaler Standards zur Darstellung der physikalischen Einheiten in Übereinstimmung mit dem Internationalen Einheitensystem (SI). Wenn keine Normale existieren, erfolgt die Rückführung auf Bezugsnormale der R&S-Laboratorien.

Grundsätze und Verfahren der Kalibrierung beziehen sich auf und entsprechen EN ISO/IEC 17025, ANSI/NCSL Z540.1-1994 und ANSI/NCSL Z540.3-2006.

Das angewandte Qualitätsmanagement-System ist zertifiziert nach EN ISO 9001. Dieser Kalibrierschein darf nur vollständig und unverändert weiterverbreitet werden. Kalibrierscheine ohne Signifizierungen sind ungültig.

Für die Einhaltung einer angemessenen Frist zur Wiederholung der Kalibrierung ist der Benutzer verantwortlich.

Rohde & Schwarz závod Vimperk, s.r.o.

Date of Issue  
Ausstellungsdatum

Head of Laboratory  
Laborleitung

Person Responsible  
Bearbeiter

2015-06-29

Radek Bartusek

Tomas Rysanek

Page 1/2  
ver9815/RSVM0608

ROHDE & SCHWARZ závod Vimperk, s.r.o. - Špirova 49 - 38501 Vimperk, tel. 00420 388452 111, fax: 00420 388 452 113  
Obchodní vedení: Konrad Bartl, jednatel  
Daňové identifikační číslo (DIČ): CZ26034441 Identifikační číslo(IČ): 26 03 44 41  
Krajský soud v Českých Budějovicích oddíl C, vložka 9987



ROHDE & SCHWARZ

## Calibration Certificate

Certificate Number 20-548776

Kalibrierschein

Zertifikatsnummer

### Unit Data

Item  
Gegenstand **ESR26 EMI TEST RECEIVER  
26.5GHZ**

Manufacturer  
Hersteller **ROHDE & SCHWARZ**

Type  
Typ **ESR26**

Material Number  
Materialnummer **1316.3003K26** Serial Number  
Seriennummer **101361**

Asset Number  
Inventarnummer

### Order Data

Customer  
Auftraggeber

This calibration certificate documents, that the named item is tested and measured against defined specifications. Measurement results are located usually in the corresponding interval with a probability of approx. 95% (coverage factor  $k = 2$ ). Calibration is performed with test equipment and standards directly or indirectly traceable by means of approved calibration techniques to the PTB/DKD or other national / international standards, which realize the physical units of measurement according to the International System of Units (SI). In all cases where no standards are available, measurements are referenced to standards of the R&S laboratories. Principles and methods of calibration correspond and are conformant with EN ISO/IEC 17025, ANSI/NCSL Z540.1-1994 and ANSI/NCSL Z540.3-2006. The applied quality system is certified to EN ISO 9001. This calibration certificate may not be reproduced other than in full. Calibration certificates without signatures are not valid. The user is obliged to have the object recalibrated at appropriate intervals.

Dieser Kalibrierschein dokumentiert, dass der genannte Gegenstand nach festgelegten Vorgaben geprüft und gemessen wurde. Die Messwerte lagen im Regelfall mit einer Wahrscheinlichkeit von annähernd 95% im zugeordneten Werteintervall (Erweiterte Messunsicherheit mit  $k = 2$ ). Die Kalibrierung erfolgte mit Messmitteln und Normen, die direkt oder indirekt durch Ableitung mittels anerkannter Kalibriertechniken rückgeführt sind auf Normale der PTB/DKD oder anderer nationaler/internationaler Standards zur Darstellung der physikalischen Einheiten in Übereinstimmung mit dem Internationalen Einheitensystem (SI). Wenn keine Normale existieren, erfolgt die Rückführung auf Bezugsnormale der R&S-Laboratorien. Grundsätze und Verfahren der Kalibrierung beziehen sich auf und entsprechen EN ISO/IEC 17025, ANSI/NCSL Z540.1-1994 und ANSI/NCSL Z540.3-2006. Das angewandte Qualitätsmanagement-System ist zertifiziert nach EN ISO 9001. Dieser Kalibrierschein darf nur vollständig und unverändert weiterverbreitet werden. Kalibrierscheine ohne Signifizierungen sind ungültig. Für die Einhaltung einer angemessenen Frist zur Wiederholung der Kalibrierung ist der Benutzer verantwortlich.

Order Number  
Bestellnummer **0000313987**

Date of Receipt  
Eingangsdatum **2015-07-02**

### Performance

Place and Date of Calibration  
Ort und Datum der Kalibrierung

**Memmingen, 2015-07-02**

Scope of Calibration  
Umfang der Kalibrierung

**Standard Calibration**

Statement of Compliance  
(Incoming)  
Konformitätsaussage  
(Anlieferung)

**New device**

Statement of Compliance  
(Outgoing)  
Konformitätsaussage  
(Auslieferung)

**Measurement results within specifications**

Extent of Calibration Documents  
Umfang des Kalibrierdokuments

**2 Pages Calibration Certificate  
51 Pages Outgoing Results**

### Rohde & Schwarz Messgerätebau GmbH

Date of Issue  
Ausstellungsdatum

Head of Laboratory  
Laborleitung

Person Responsible  
Bearbeiter

2015-07-02

Steigmüller

Andreas Aumann

Page 1/53  
ver9815/MB0707

Rohde & Schwarz Messgerätebau GmbH · Postfach 1652 D-87666 Memmingen · Rohde und Schwarz-Str. 1 D-87760 Memmingen  
Telefon national: 08331/10-80; international: 0049 8331/10-80; Fax: 08331/10-811 24  
Geschäftsführer: Jürgen Steigmüller · Aufsichtsratsvorsitzender: Roland Steffen  
Sitz der Gesellschaft: München · Registeramt: Amtsgericht München HRB 1059

## LIST OF PUBLICATIONS

### Journal Publications:

1. J. Song, H. T. Hui, and Z. W. Sim, "Investigation of Measurement Uncertainties and Errors in a Radiated Emission Test System," *IEEE Transactions on Electromagnetic Compatibility*, vol. 57, pp. 158-163, 2015.
2. J. Song, and Y. X. Guo, "Characterisation of measurement uncertainties due to preamplifier gain variation," *Electronics Letters*, vol. 51, pp. 64-65, 2014.
3. J. Song, Y. X. Guo, H. T. Hui, H. Wang, and Z. W. Sim, "Reverberation chamber modeling based on proportional dimension," *Microwave and Optical Technology Letters*, vol. 57, pp. 838-841, 2015.
4. Z. W. Sim, and J. Song, "Radiated spurious emission measurements using fast Fourier transform-based time domain scan," *IET Science, Measurement & Technology*, vol. 9, pp. 882-889, 2015.
5. J. Song, H. Wang, Y. X. Guo, " Investigation of Field Uniformity and Uncertainties in Reverberation Chamber Using Non-Equidistant Tuner Position," *Microwave and Optical Technology Letters*, vol. 59, pp. 1190-1194, 2017
6. J. Song, Y. X. Guo, " Characterisation of Measurement Uncertainties of EMI System Using Time Domain Scan Receiver," – **In preparation**

### Conference Publications:

1. J. Song, and H. T. Hui, "Characterisation of uncertainties in RF adapters for EMC measurements," in *Electromagnetic Compatibility (APEMC), 2013 Asia-Pacific Symposium on*, Year, pp. 1-3.
2. J. Song, and Y. X. Guo, "Investigation of measurement uncertainties and errors in EMI measurement apparatus," in *2015 Asia-Pacific Symposium on Electromagnetic Compatibility (APEMC)*, Year, pp. 593-595.
3. J. Song, and A.T. Kuah, "Implementation of Harmonics Filter System for MIL and Automotive EMC Test," EDI CON 2016 – **Accepted**.

**Industry Achievement:**

My research work has been adopted by Rohde & Schwarz Asia, the proposal of the development for a new software named “Measurement Uncertainty Calculation Software” has been approved by the board of directors. The software currently is in the midst of development. I’m the project leader engineer (PLE) and currently leading the software development team to provide them with necessary information such as standard interpretation, uncertainty contribution formulation, uncertainty characterisation methods which are not stated in the standard in detail, etc. The software has incorporated some of the results and findings in my research work as the foundation of the uncertainty modelling as well as to enrich its database. With the availability of the software in the industry in the due time, it will greatly reduce the time and resources for the test houses to identify their measurement uncertainty. I am proud that the research work can be applied to the industry.